ProQuest LLC.
789 East Eisenhower Parkway
P.O. Box 1346
Ann Arbor, MI 48106 – 1346

The Potential Use of Three Photon Positron Annihilation in Positron Emission Tomography for Tumour Hypoxia Imaging

Mohammed A. Alkhorayef

A thesis submitted in fulfilment for the Degree of Doctor of Philosophy

Centre for Nuclear and Radiation Physics
Department of Physics
University of Surrey
Guildford, Surrey GU2 7XH, UK

May 2010

Abstract

Identifying and localising tumour hypoxia in cancer patients is a challenge in oncology imaging. There are many ongoing clinical trials using conventional positron emission tomography (PET) scans and PET agents as cellular markers for detection of tumour hypoxia depending on the concept of the basic physics of 2γ annihilation. However, Kacperski and Spyrou (2004) proposed, for the first time, to use 3γ annihilation as a new PET molecular imaging modality, where the positronium and its annihilation, could serve as an oxygen-sensitive marker. The effective yield of 3γ annihilation depends on the rates of formation and quenching. The formation of positronium is not only sensitive to the physics parameters, but also behaves as an active chemical particle. A hypoxic cell is a microenvironment which has an inadequate amount of oxygen. Oxygen is known to be a strong positronium quencher where 2γ annihilation replaces the 3γ process. It is thus possible for hypoxic cells to be characterised by higher 3γ rates than those cells which are well oxygenated.

The measurement of 3γ annihilation to differentiate between oxygenated and non-oxygenated biological samples in order to extract useful information in PET for oncology is a challenging project. It opens up very interesting applications in nuclear medicine imaging as the 3γ yield has not been measured before in biological tissue and in particular hypoxic tumour cells. The project is multidisciplinary involving physics, biology and chemistry. There are many factors which affect the dissolved oxygen in mineral water, defibrinated horse blood and serum samples. These factors and the challenges to prepare in-vitro hypoxic samples have been experimentally measured using polarography with different chemical reactions e.g. carbon dioxide, nitrogen and AnaeroGen™. Results have shown that polarography was more suitable than colorimetery in the measurement of dissolved oxygen in blood due to the high absorption characteristic of blood. AnaeroGen™ is the method of choice, unlike carbon dioxide or nitrogen treatment, for preparing hypoxic samples due to the good agreement of the behaviour of the oxygen reduction as in the oxyhaemoglobin dissociation curve which is caused by a decrease in pH, an increase in partial pressure of carbon dioxide and an increase in temperature.

The 3γ yield was measured in normoxic and hypoxic environments using the triple coincidence measurement of three high-energy resolution detectors (HPGe). The AnaeroGen™ was used to generate a hypoxic environment. The percentage of the coincidence events qualified as 3γ was 26.5% higher in the hypoxic environment. This reseach work is a step towards the application of the novel modality of 3γ PET which in conjunction with conventional 2γ PET could serve as a non-invasive oxygen sensitive marker. The combination of 3γ and 2γ coincidences in nuclear medicine imaging systems may contribute important information for the development and validation of appropriate hypoxia markers.

The relative 3γ/2γ yield was measured for a positron emitter ^{22}Na with the new generation of scintillator $LaCl_3$:Ce and $LaBr_3$:Ce detectors, which had been characterised together with NaI(Tl) and HPGe detectors. The experimental focus was on measuring the relative 3γ/2γ yield in different samples by applying the peak-to-peak and the peak-to-valley methods. The value of the ratio 3γ/2γ depends on the specimen and is of the order of 10^{-2}. The relative 3γ/2γ yields obtained for the peak to peak method in the silica sample were, for example, $(3.41\pm0.18)\times10^{-2}$, $(2.98\pm0.13)\times10^{-2}$, $(4.01\pm0.16)\times10^{-2}$ and $(2.12\pm0.14)\times10^{-2}$ for $LaBr_3$:Ce, $LaCl_3$:Ce, NaI(Tl) and HPGe detectors, respectively. The results show that the lanthanum based crystals, $LaBr_3$:Ce and $LaCl_3$:Ce, have the potential to replace NaI(Tl) and HPGe due to both good energy resolution and good detection efficiency and can be the scintillator of choice for determining the yield of 3γ. The peak-to-valley method was applied to measure the relative yield of 3γ/2γ positron annihilation using ^{18}F in 11 haematological samples of different oxygenation levels. The relative 3γ/2γ yield was found to vary as much as 11% between the components investigated.

بِسْمِ اللهِ الرَّحْمَـنِ الرَّحِيمِ

وَقَضَى رَبُّكَ أَلاَّ تَعْبُدُواْ إِلاَّ إِيَّاهُ وَبِالْوَالِدَيْنِ إِحْسَانًا إِمَّا يَبْلُغَنَّ عِندَكَ الْكِبَرَ أَحَدُهُمَا أَوْ كِلاَهُمَا فَلاَ تَقُل لَّهُمَآ أُفٍّ وَلاَ تَنْهَرْهُمَا وَقُل لَّهُمَا قَوْلاً كَرِيمًا وَاخْفِضْ لَهُمَا جَنَاحَ الذُّلِّ مِنَ الرَّحْمَةِ وَقُل رَّبِّ ارْحَمْهُمَا كَمَا رَبَّيَانِي صَغِيرًا

In the Name of Allah, the Most Beneficent, the Most Merciful.

Thy Lord hath decreed that ye worship none but Him, and that ye be kind to parents. Whether one or both of them attain old age in thy life, say not to them a word of contempt, nor repel them, but address them in terms of honour. And, out of kindness, lower to them the wing of humility, and say: "My Lord! bestow on them thy Mercy even as they cherished me in childhood."

To my parents and all members of my family

To those who are always there when I need them

Acknowledgements

I would like to take this opportunity to express my sincere gratitude to all those who have supported me to complete this thesis;

First of all, I would like to record my deepest sense of gratitude to Professor Nicholas M. Spyrou for his dedicated support and guidance from the early stage of this prototype research as well as giving me interesting experience throughout the work. It has been my great fortune to have him as an academic supervisor. He maintains close contact, weekdays and weekends, with this work. He always expressed concern about my health, above all and most importantly, he provides me with unflinching encouragement and support in various ways. His truly scientific background has made him a constant oasis of ideas and insights in science, which enrich my growth as a student, a researcher and the scientist I want to be.

I would also like to extend my thanks to the post doctoral fellows and my PhD research contemporaries, Dr. M. Chin, Dr. K. Kacperski, Dr. E. Abuelhia, Dr. M. Alnafea, Dr. C. Butler, Dr. N. Mohammed, Dr. M. Marouli, Dr. K. Alzimami, Dr. A. Alfuraih, Dr. A. Alsager, Mr. K. Alsafi, Mr F. Abolaban and others who worked with Professor Spyrou, for their encouragement, tremendous help, sharing ideas and advice throughout my research.

I would like to gratefully acknowledge all my friends, in the UK and Saudi Arabia, for the assist and encouragement given especially Dr. Mahboub, Dr. Alkhomashi, Dr. Aljarallah, Dr. Alhumam Dr. Alnasser, Dr. Butt, Mr. Alarifi, Dr. Alheymayed.

I am grateful to Mr. Brown, Mr. Wallbank and Mr. Baker for their assistance during the experimental part. I would also like to express thanks to the professional therapist K. Haynes and the chiropractors Dr. Weston, at the University Chiropractic Clinic Guildford, and Dr Vice, at the London Spine & Joint Clinic, for their help to overcome the tremendous pain particularly during the writing up stage.

Words would not be enough to thank all my family members, especially my parents who always pray for me. I owe more than I can say for the encouragement, continuous support and endless love that led me to successfully complete my PhD study in the United Kingdom.

Finally, I am grateful to my scholarship sponsor from the Applied Medical Sciences College, Radiological Sciences Department, King Saud University, Saudi Arabia, for financing and giving me the opportunity to pursue my higher education.

My apologies to anyone I have inadvertently omitted.

Table of Contents

List of Figures

List of Tables

Chapter 1

Introduction

The current incidence of cancer is increasing world-wide. Statistics in the UK show that one third of the population will at some stage of their life suffer from cancer and one quarter will eventually die from cancer [Cav99]. Around 293,601 new patients were diagnosed with malignant cancers in 2006 in the UK, which are about 800 cases a day [Nat10]. Table 1.1 shows the number of new cases and rates of all malignant neoplasms excluding non-melanoma skin cancer (NMSC) by cancer research UK in England, Wales, Scotland and N. Ireland for male and female patients. There are more than 200 different types of cancer, but breast, lung, large bowel (colorectal) and prostate cancers account for over half (54%) of all new cases. Figure 1.1 shows the 20 most commonly diagnosed cancers in the UK (2006) [Nat10]. The UK cancer mortality statistics in 2007 were 155,484 deaths from cancers of the lung, colorectal, breast and prostate. These four types accounts for 47% of all cancer deaths. The 20 most common causes of death from cancer are shown in Figure 1.2. More than 22% of all cancer deaths are from lung cancer. Around 10% and 8% of all cancer deaths in all persons are from colorectal and breast cancers, respectively. Therefore the treatment and diagnosis of cancer play an important role; accurate early diagnosis has shown to be crucial for patient outcome (improving mortality rates) and assessment of the treatment. A diagnostic test is required that is sensitive and specific for both the assessment and prognosis [Cav99]. A variety of imaging modalities have been used for cancer detection, among which is positron emission tomography (PET). PET has the potential of showing and assessing physiological function of individual organs in the body, which other imaging techniques cannot match or provide. PET scanning in oncology applications has been shown to change therapy regimes and help avoid unnecessary surgery in a significant number of patients [Sha05].

Table 1.1: Number of new cases and rates of all malignant neoplasms (exc. NMSC), UK, 2006 [Nat10].

	England	Wales	Scotland	N. Ireland	UK
Males	121564	8897	13072	3690	147223
Females	120620	8305	13794	3659	146378
Persons	242184	17202	26866	7349	293601

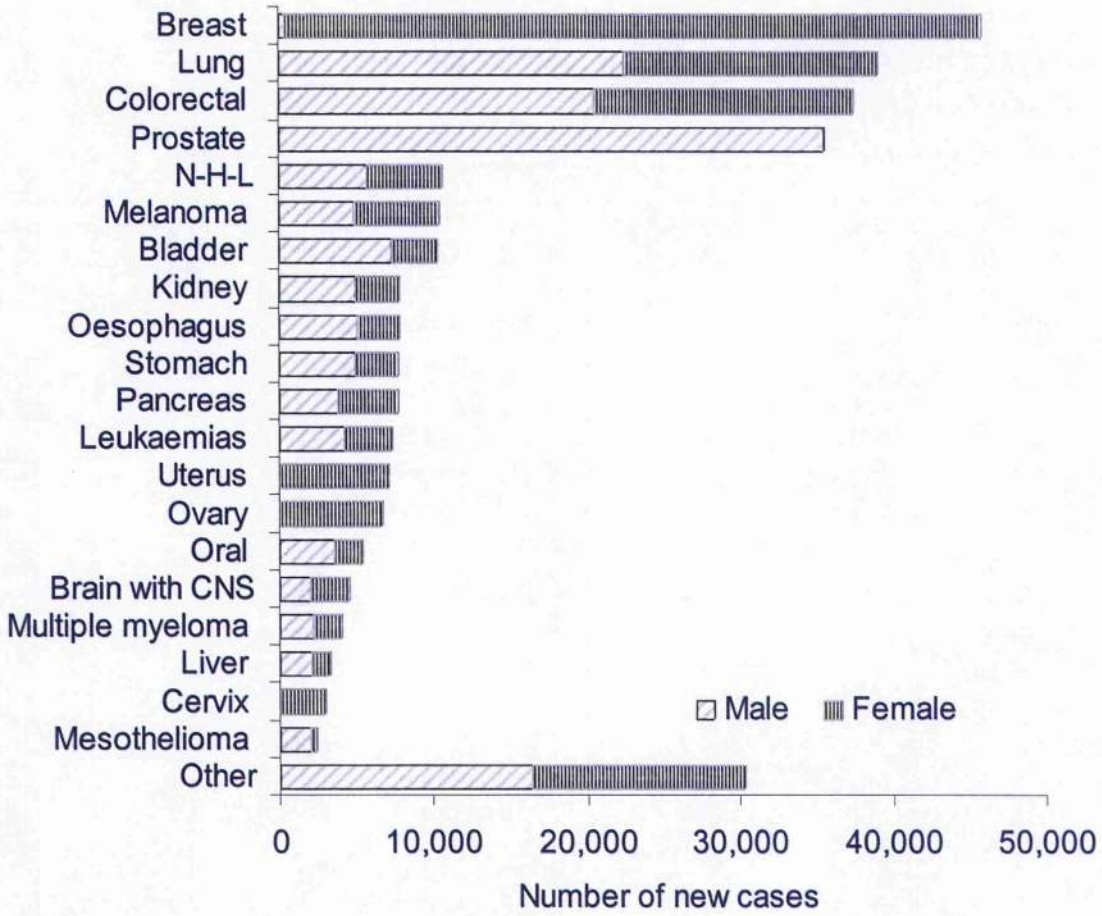

Figure 1.1: The 20 most commonly diagnosed cancers (exc. NMSC), UK, 2006 [Nat10].

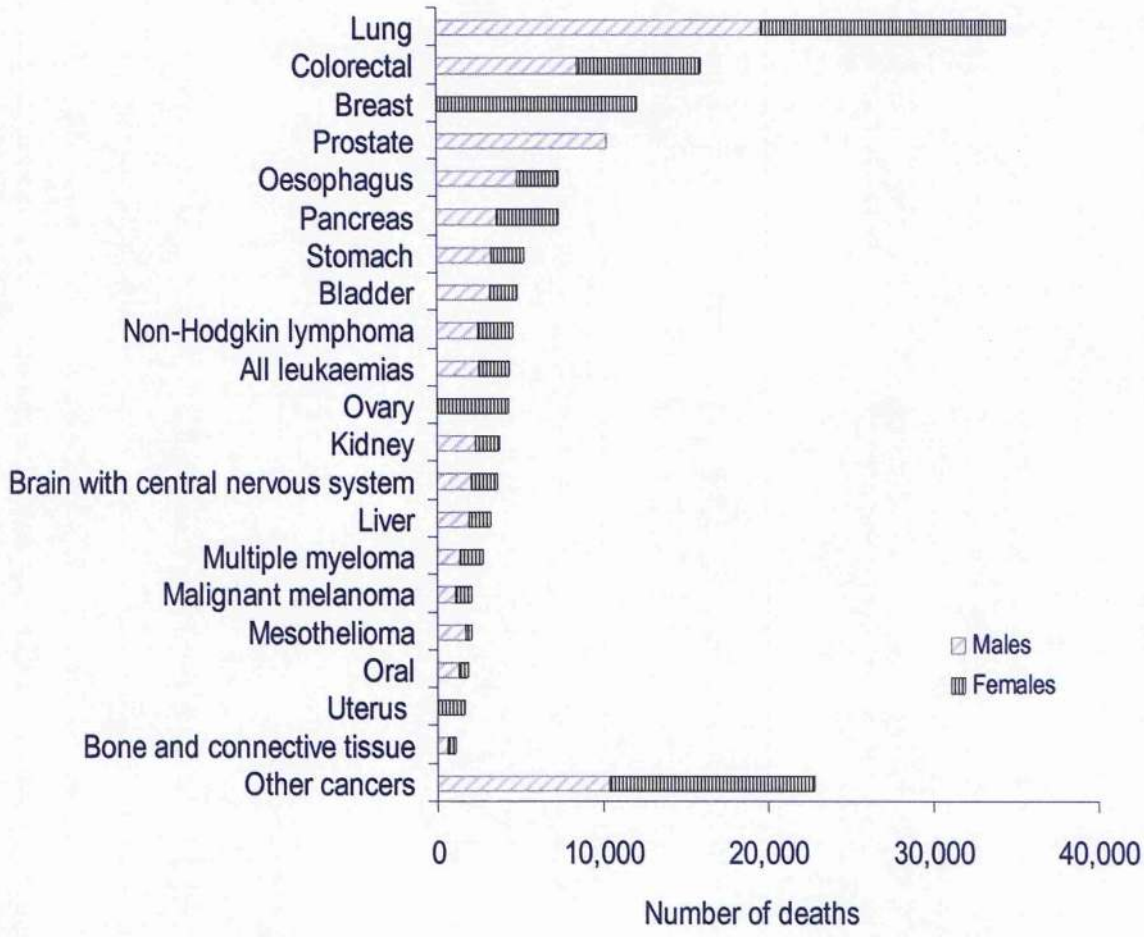

Figure 1.2: The 20 most common causes of death from cancer (exc. NMSC), UK, 2007 [Nat10].

PET is able to measure non-invasively the physiological quantities and the metabolic process *in vivo* owing this capacity to four of its features: 1) use of radiopharmaceuticals which resemble natural biological compounds, 2) quantification of tracer distribution, 3) rapid simultaneous volumetric acquisition and 4) whole body tomographic images. Indeed, it can measure tissue glucose metabolism, perfusion, amino acid uptake, receptor ligand mechanisms and drug kinetics [Sil98]. Such an approach can potentially detect subtle physiological abnormalities occurring at the cellular level, well before these become apparent in anatomy thereby improving disease management; detection of malignant tumours, differentiation of malignant

from benign tumours and staging of tumours. Recently PET has been increasingly used in planning and monitoring cancer therapy and not only in cancer diagnosis [Sha05]. Making the diagnosis of viable tumour tissue following chemotherapy is another application of PET. The sensitivity (the fraction of patients actually having the disease that is correctly diagnosed as positive) of ^{18}F- fluorodeoxyglucose (FDG) PET studies exceeds 80% [Sea07], dependent on tumour type, size, and location. PET can play a major role in the description of the extent and the spread of the tumour in the body via whole body scanning. Information gained through staging can be employed for determining the appropriate cause of treatment and eliminate many surgical investigating dissections and biopsies [Sil98, Str97, Sea07, Bin10].

The physics of PET scanning are predicated by the nuclei that emit the positron [Ter82]. A detail of the physics is given in Chapter 4 and is briefly given here. In clinical applications, a radiopharmaceutical or radiotracer is introduced into the patient intravenously. Then, after an appropriate uptake period, the concentration of tracer in tissue is measured by a PET scanner. During its decay process, the radionuclide emits a positron, when it reach thermal energies, after travelling a short distance (less than a few millimetres in tissue dependent on its energy and momentum), it encounters an electron from the surrounding environment. The two particles combine and annihilate resulting in the opposing emission at approximately 180 degrees of two gamma rays of 511 keV each. The image acquisition is based on the external detection in coincidence of the emitted γ-rays. A true or valid annihilation event must occur in coincidence within a short time interval ($\sim$ ns) between two detectors on opposing sides of the scanner. For the accepted coincidences, several lines of response (LOR) connecting the coincidence detectors are drawn through the object and used to reconstruct the image [Sha05, Ter82].

Kacperski and Spyrou (2004 and 2005), Kacperski et al (2004) and Spyrou et al (2005) proposed, for the first time, to use three gamma annihilation as a new imaging modality of PET, even though positron annihilation into three photons is quite a rare event [Kac04a,b, Kac05, Spy05]. The information gained with the three decay photons detected can be higher than in the case of two-gamma annihilation. This is due to the easy localisation of the point at which the three-gamma annihilation occurred with one measurement but also most importantly positronium can be an

indicator of the medium in which annihilation has taken place. Progress in the physics and technology of broad-band semiconductor materials and scintillation detectors has made possible a wider range of their application in medical imaging. Ideally, scintillation crystals or semiconductor materials used in medical imaging applications should have high detection and scintillation efficiency, good energy, time and spatial resolution, short dead time, fast scintillation response and mechanical and chemical stability. Unfortunately these requirements could not be met by any of the commercially available detectors. Thus there has been considerable research and development of new inorganic scintillators, (lanthanum bromide ($LaBr_3$:Ce) and lanthanum chloride ($LaCl_3$:Ce)), with enhanced performance [Dam06, Kuh04, Mos05]. Initial experiments using high-purity germanium (HPGe) detectors for PET increased the possibility of the use of three-gamma annihilation [Abu07]. It is important to clearly determine whether the new scintillator detectors can be used without the requirement for high resolution semiconductors.

Although ^{18}F- FDG has the status of being the standard tracer for PET oncology there is a need for markers of more specific tumour characteristics to novel treatment strategies e.g. tumour hypoxia. Assessment of tumour perfusion and hypoxia are likely to open new fields of interest for oncology and cardiology treatments specifically designed to attack poorly oxygenated (hypoxic) cells. The importance of hypoxia in solid tumours was linked to the fact that hypoxic cells are more resistant to both radiation therapies and chemotherapy [Sha04]. Hypoxia is also known to be a prognostic indicator, since hypoxic tumours are more biologically aggressive and are more likely to reoccur locally or metastasise [Cha83, Bri96]. The response of tumour cells to radiation therapy and resistant to chemotherapy increases further by their relative isolation from the blood supply. Three times more radiation is required to kill anoxic (absence of oxygen) than normally oxygenated cells. [Sha04, Vau01]. The degree of hypoxia in a tumour has been claimed to predict the efficacy of treatment being applied. It is vital to have accurate and reliable methods to measure the tumour oxygen concentration. The question arises here is how can tumour hypoxia be measured. A variety of physical and chemical methods has been proposed and employed to measure hypoxia in tumours. Two of these methods briefly discussed, are oxygen electrodes and the labelling agents for PET biomarkers.

Oxygenation levels in tumours have mostly been measured using polarographic oxygen electrodes [Nor94]. This is usually done by inserting the oxygen electrode through a small plastic tube into the tumour and the partial pressure of oxygen (PO_2) measurements is usually obtained along a track with the length depending on the tumour size and accessibility. The electrode would then be mechanically moved forward in steps of 1 mm followed by a retraction of 0.3 mm, giving a net step length of 0.7 mm between individual PO_2 measurements. In general, 2 to 4 insertions are obtained in the tumour and 1 to 3 tracks measured per insertion. Consequently, the median PO_2 and the fraction of PO_2 are produced [Nor01]. However, this method suffers from being restricted to accessible tumours, is extremely invasive and maybe contaminated from non-viable necrotic tissue. It mainly depends on a technically-skilled user and as a result there are many interlaboratory variations reported in oxygen tension measurement. Furthermore it does not distinguish between viable hypoxic cells, non-hypoxic cells, blood vessels. Moreover, the signal-to-noise ratio is low, especially at low oxygen tensions, and this can lead to uncertainties in the measurements [Nor03, Hoc93]. Implying alternative assays using hypoxia tracers in comparison with oxygen electrodes seem attractive.

The alternative may occur from PET imaging which was introduced as a non-invasive, in vivo method, to detect and quantify hypoxia by binding of ^{18}F-fluoromisonidazole (^{18}F-FMISO), ^{18}F-fluoroerythronitroimidazole (^{18}F-FETNIM), copper-diacetyl-bis (N^4-methylthiosemicarbazone) (Cu-ATSM) and [^{18}F]-fluoroazomycinarabinofuranoside (FAZA) [Kho92, Kho95, Lew99, Leh01, Lew01, Sor03, Gro04, Pad07]. It has been shown that ^{18}F-FMISO PET was able to discriminate between murine tumours treated with carbogen (95% oxygen, 5% CO_2) and control tumours. It is the most widely investigated tracer nowadays. It diffuses freely into cells and undergoes reduction where oxygen tension is low. ^{18}F-FMISO PET examination is followed by PO_2 measurements before both a diagnostic biopsy and the entire tumour is surgically removed. However, it has been investigated and found that [^{18}F]FAZA has better pharmacokinetics and cleared from normal tissue faster in comparison to [18F]FMISO [Pad07, Rei07].

Recently, efforts have been made to invent efficient non-invasive methods to assess the presence and extent of tumour hypoxia. Kacperski and Spyrou (2004) suggested that three-gamma images may provide more information about the concentration of oxygen in different types of malignant tumours, in comparison with the conventional two-gamma images. The use of three-gamma annihilation as a new PET molecular imaging modality, where the positronium and its annihilation, could serve as an oxygen-sensitive marker. The effective yield of three-gamma annihilation depends on the rates of positronium formation and quenching. The formation of positronium is not only sensitive to the physics parameters, but also behaves as an active chemical particle. Oxygen is known to be a strong positronium quencher where two-gamma annihilation replaces the three-gamma process. It is thus possible for hypoxic cells to be characterised by higher three-gamma rates than those cells which are well oxygenated.

This thesis describes the preparations and the methods employed to measure the oxygen level in biological and non biological samples. The major contribution of this project is its furthering of the understanding of the best methods that can be used to prepare biological samples with different concentrations of oxygen. This will help to investigate the probability of three-gamma positron annihilation with different concentrations of oxygen, imaging the oxygen levels in biological samples and develop more feasible methods for clinical use. Although there was a large diversity and several disciplines involved in this project efforts were made to highlight the advantages and disadvantages of each technique which may be applied. It was intended that this thesis provides the reader with sufficient background to be instrumental in the examination of the application in three gamma PET technique, and provide a non invasive method tested against existing oxygen measurement devices.

The second chapter discusses the physiological background of the transport of oxygen and carbon dioxide in blood as well as the structure and function of blood composition is presented. In chapter three a definition and causes of tumour hypoxia are highlighted with the measurement and assessment of tumour hypoxia by PET. In chapter four, a detailed discussion of the theory and the basic principle of two gamma

and three gamma PET is covered. The study of oxygen measurements in biological samples and the factors that affect dissolved oxygen in biological fluids are demonstrated in chapter five and six, respectively. Determination of the relative oxygenation of samples by ortho-positronium 3γ decay for future application in oncology is explained by the experimental results obtained from the triple coincidence measurement in chapter seven. Chapter eight explains the experimental comparison of the relative yield of $3\gamma/2\gamma$ positron annihilation using semiconductor and scintillation detectors by applying peak-to-peak and peak-to-valley methods. The final Chapter presents a summary and conclusion of the current work and a discussion of direction of the further work.

Chapter 2

Physiological Background

2.1 Oxygen cascade

It is surprising that over 90% of the human body is composed of just three elements; oxygen, carbon and hydrogen [Mad92]. Air consists mostly of oxygen, nitrogen and smaller quantities of argon and carbon dioxide. Gaseous exchange between the internal environment of the body and the atmosphere is achieved by the cardio-respiratory system. All gas exchanges are made according to the laws of diffusion, that is, movement occurs toward the area of lower concentration of the diffusing substance [Mar94]. At sea level, oxygen makes up about 21% of the inspired air and has atmospheric pressure of 760 mmHg. At this point, the oxygen starts to move down through the body to the cells. The driving force triggering diffusion of oxygen from the inspired air to its place of consumption, the cell mitochondria, is the partial pressure of oxygen (PO_2) gradient from air along the respiratory tract, alveolar gas, arterial blood, systemic capillaries and the tissue cells with PO_2 approximately 40 mmHg [Tre98, Kup03]. The process of declining oxygen tension from the atmospheric environment to the mitochondria in cells is known as the oxygen cascade.

2.2 Transport of oxygen and carbon dioxide in the blood

Blood accounts for approximately 8% of body weight and its volume in healthy adults is 5 to 6 litres. Among all of the body's tissues, blood is the only fluid tissue [Suk93]. Blood is a complex connective tissue in which living blood cells are suspended in a liquid called plasma. These cells represent about 45% of the blood volume and include red cells (erythrocytes), white cells (leucocytes) and platelets (thrombocytes). The remaining 55% is plasma, an aqueous suspension of proteins, salts and organic solutes. About 90% of the cells are red cells, and nearly 10% are white cells and platelets which are important in defence and blood clotting, respectively [Tor03, Mar94]. The haemoglobin molecule, inside the erythrocytes, is made up of an iron porphyrin compound (the haem group) and a protein (globin). The haem group

contains a ferrous iron atom, which is capable of carrying a single oxygen molecule. A single molecule of human haemoglobin has four haem groups. Therefore, it is capable of carrying four molecules of oxygen (Fig. 2.1) [Too95].

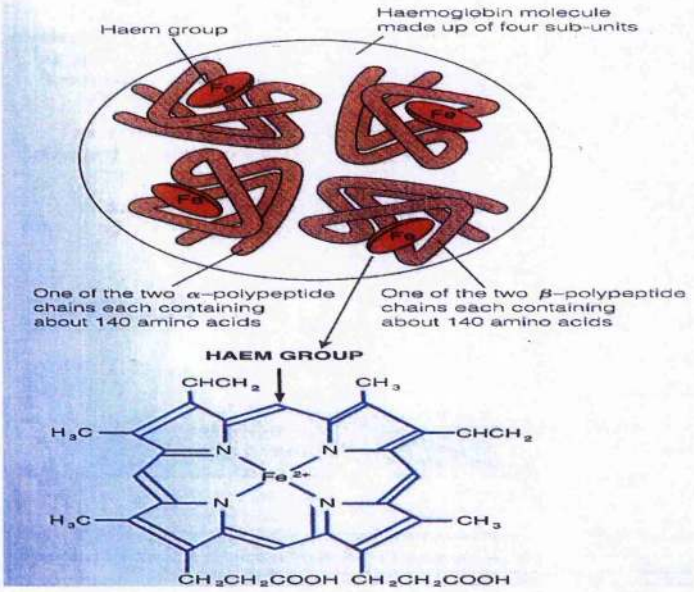

Fig. 2.1 : The structure of haemoglobin [Too95].

There are two ways of carrying oxygen in the blood; bound or dissolved. Approximately 97% of oxygen is transported from the lung to the tissue in chemical combination with the haemoglobin. About 3% of oxygen is carried in the dissolved state in the water of the plasma and blood cells. Thus, under normal conditions, oxygen is carried to the tissues almost entirely by haemoglobin [Tor03]. When PO_2 is high, as in the pulmonary capillaries, oxygen binds with the haemoglobin but when PO_2 is low, as in the tissue capillaries, oxygen is released from the haemoglobin. This is the basis for almost all oxygen transport from the lung to the tissues. Carbon dioxide (CO_2) is also carried in blood in three ways (Fig.2.2). (1) Approximately 10% of CO_2 is dissolved in plasma and combined with plasma proteins. (2) About 60% CO_2 enters the red blood cells and ends up as bicarbonate ion (HCO_3^-) in plasma as a result of reaction of CO_2 with water by the effect of a protein enzyme in the red blood cells called carbonic anhydrase, which catalyses the reaction. (3) About 30% of CO_2

binds to haemoglobin molecule to form carbaminohaemoglobin compounds ($HbCO_2$) [Tor03].

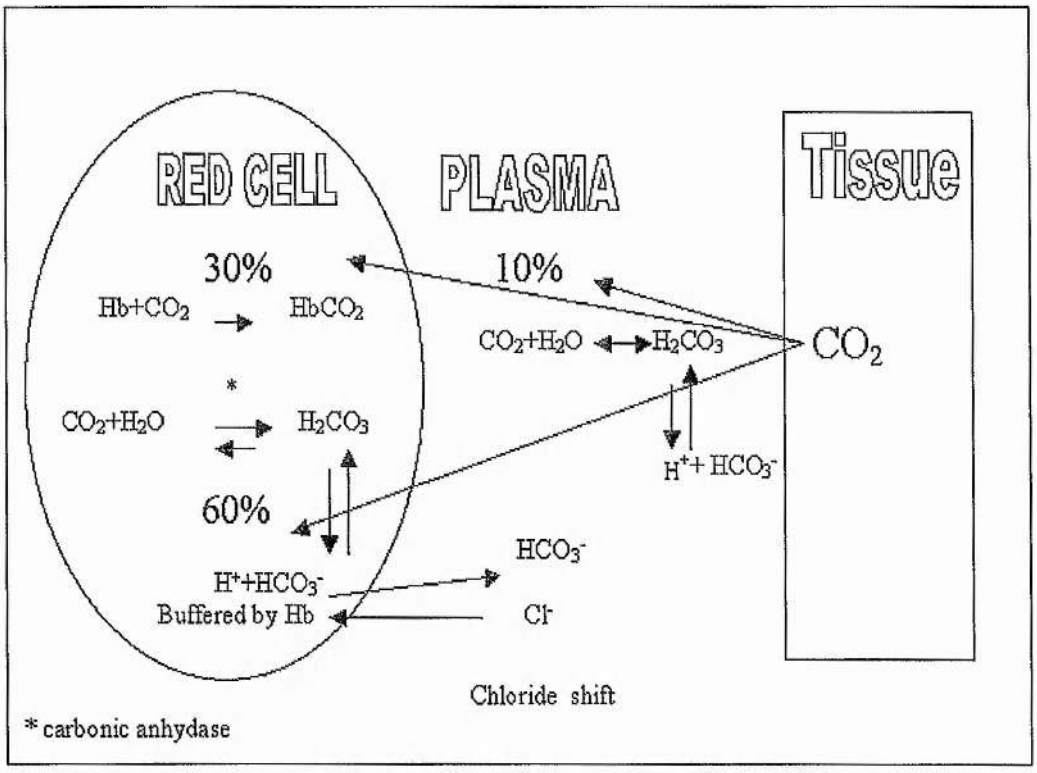

Fig. 2.2 : Transport of carbon dioxide in the blood, adapted from [Tor03].

2.3 Oxygen-haemoglobin dissociation curve

Dissolved oxygen obeys Henry's law, that is, the amount of oxygen dissolved is proportional to the partial pressure (P). In other words, the most important factor that determines how much O_2 or CO_2 combines with haemoglobin is the partial pressure of oxygen (PO_2) or partial pressure of carbon dioxide (PCO_2), respectively (Table 2.1) [Tor03,Guy06]. The higher PO_2 the more O_2 combines with haemoglobin. This relationship between the partial pressure of oxygen PO_2 and the saturation of haemoglobin is called the oxygen-haemoglobin dissociation curve (Fig.2.3) [Dav99]. In pulmonary capillaries, where PO_2 is high (100 mmHg) the haemoglobin is nearly 95–98% saturated, which means that a large amount of O_2 binds with haemoglobin. However, in tissue capillaries, where PO_2 is lower (40 mmHg) the haemoglobin does not hold as much oxygen, about 75% saturated, and the O_2 is unloaded via diffusion into tissue cells [Tor03, Guy06].

Table 2.1 : Partial pressure (P) of oxygen and carbon dioxide values (mmHg) [Tor03,Guy06].

	PO_2	PCO_2
Alveolar air	100	0.3
Arterial blood	95	40
Venous blood	40	45
Tissues	40	45

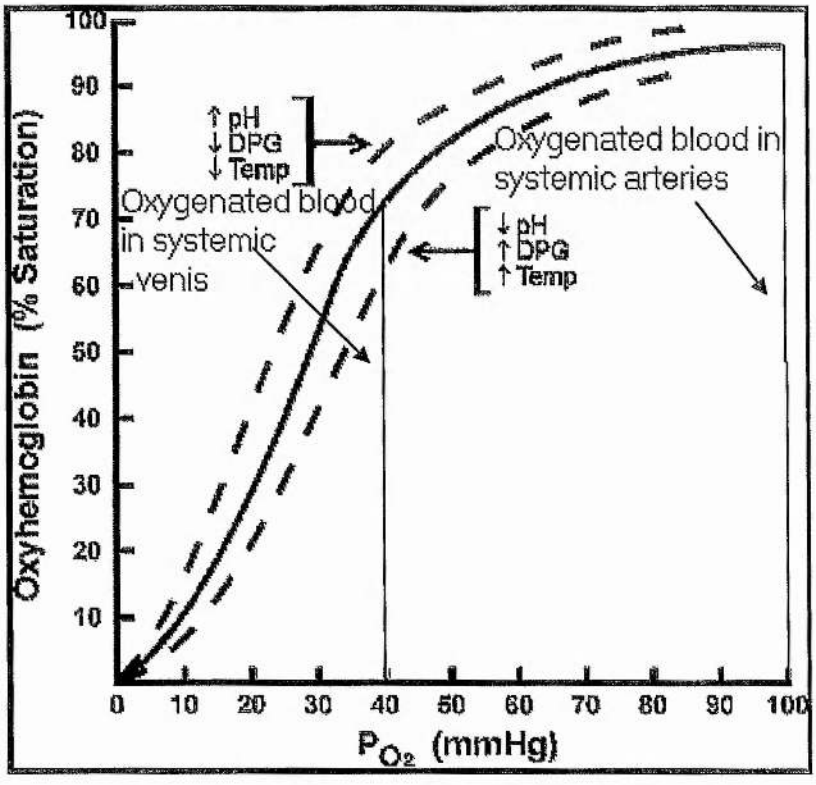

Fig 2.3 : The oxygen-haemoglobin dissociation curve.[Dav99]

2.3.1 Factors that shift the oxygen-haemoglobin dissociation curve

There are several factors that influence haemoglobin attraction to oxygen which can result in the curve being shifted to the right or left [Tor03, Guy06]. Several situations can increase haemoglobin affinity for oxygen, which result in a shift of the curve to the left and upward caused by a decrease in (1) hydrogen ion concentration (increase in pH), (2) carbon dioxide concentration, (3) blood temperature, (4) 2,3-diphosphoglycerate (DPG) concentration. On the other hand, the curve is shifted to the

right by an increase of these factors mentioned above which can be explained as follows:

An increase of carbon dioxide and hydrogen ion concentration in the blood causes oxygen to be displaced from the haemoglobin. As the blood passes through the tissues, CO_2 diffuses from the tissue cells into the blood. This increases the blood carbonic acid (H_2CO_3) and the hydrogen ion concentration. This is called the Bohr effect. This effect shifts the oxygen-haemoglobin dissociation curve to the right and downward allowing haemoglobin to easily off-load oxygen to the peripheral tissues. Exactly the opposite effect occurs in the lungs where CO_2 diffuses from the blood into the alveoli. Therefore, binding of oxygen with haemoglobin tends to displace CO_2 from the blood. This effect is called the Haldane effect.

In addition to CO2 and pH changes, an increase of diphosphoglycerate (DPG) concentration is also shifting the curve to the right. DPG is an organic phosphate, which is produced in erythrocytes during glycolysis. DPG is present in the blood in different concentrations under different metabolic conditions. The production of DPG increases when the peripheral tissue oxgyen's availability decreases, such as in the condition of hypoxia, chronic lung disease or anaemia. Therefore, under some conditions, the DPG mechanism can be important for adaptation to hypoxia, especially to hypoxia caused by poor tissue blood flow.

The temperature of the muscle during heavy exercise often rises 2° to 3°C, which can increase oxygen delivery to the muscle fibres. The exercising muscles, in turn, release large quantities of CO_2 and other acids which increase the hydrogen ion concentration in the muscle capillary blood. All these factors act together to shift the oxygen-haemoglobin dissociation curve to the right and downward forcing oxygen to be released from the haemoglobin to the muscles at the PO_2 levels as great as 40 mmHg.

2.3.2 Clinical uses of oxygen-haemoglobin dissociation curve

The role of haemoglobin as an oxygen carrier in the blood and the oxygen-haemoglobin dissociation curve are clinically important since they describe the relationship between the arterial oxygen saturation and the partial pressure of oxygen. It is considered as a good tool in understanding the influence of the factors that may

affect the standard dissociation curve or in other words the affinity of haemoglobin to oxygen. For example, it is useful in understanding the effect of carbon dioxide (CO2) with normal partial pressure of oxygen and haemoglobin saturation of oxygen. Furthermore, the changes of blood acidity during CO2 transport can be assessed. Carbonic acid formed when CO2 enters the blood in the peripheral tissues decreases the blood pH. In the hypoxic condition, high metabolic activity or when blood flow through the tissues is poor, the decrease in pH in the tissue blood causes significant tissue acidosis. Hypoxia and acidosis may promote tumour growth by recruiting blood vessels more effectively. A tumour can be more aggressive if either hypoxia or acidic pH induces genes such as vascular endothelial growth factor (VEGF). However, the relationship between tissue oxygen partial pressure, pH and VEGF transcription in vivo is not well understood [Fuk01, Gil01, Hel97].

2.4 Methods of measuring oxygen

The amount of dissolved oxygen in fluid plays a vital role in a wide range of biological and environmental processes. Therefore, measuring of dissolved oxygen has attracted many scientific efforts and still remains a research topic of great importance. When a liquid and gas such as oxygen in the alveoli and blood are at equilibrium, the amount of dissolved gas reaches its maximum value. However, the amount of a gas dissolving in a liquid is dependant mainly on three factors according to Henry's Law: the solubility of the gas in the fluid, the temperature of the fluid and the partial pressure of the gas [Hit78]. There are a number of methods and equipment that have been developed for oxygen measurement. At present, blood gas analysis and pulse oximeters are commonly used in hospitals, especially in clinical laboratories, critical care units and emergency departments.

2.4.1 Blood gas analysis

Blood gas analysis is a procedure to measure the partial pressure of oxygen (PO_2), carbon dioxide (PCO_2) and blood pH (concentration of hydrogen ions) in whole blood. It can also measure electrolytes like K^+ and Na^+ and metabolites; glucose and lactate. The haemoglobin saturation (HbO_2%) can also be calculated from the PO_2 using the oxygen dissociation curve. These values are used by clinicians to assess the extent of hypoxia and acid-base imbalance [Sha94].

Often blood gas analysis is called arterial blood gas analysis, since it requires a sample of arterial blood. This sample is usually collected from the radial, femoral or brachial artery. It is very important that air be excluded from the syringe both before and after the sample is collected. The syringe must be filled completely and never exposed to air. For transportation, the syringe should be capped with a blind hub, placed on ice, and immediately sent to the laboratory for analysis to guarantee the accuracy of the result obtained. The sample is inserted into an analytical instrument that uses PO_2, PCO_2 and PH electrodes to measure the concentrations. The oxygen electrode details are given below.

2.4.1.1 Oxygen electrode - Polarographic electrode

The oxygen electrode is employed in the clinical chemistry laboratory or in intensive care areas. It is also known as a Clark cell or polarographic electrode. It has a thin organic membrane covering a platinum cathode and a silver chloride anode which are immersed in an electrolyte solution of potassium chloride (Figure 2.4) [Pot01]. A constant voltage of 0.7 V is applied between the cathode and anode. At the anode, electrons are provided by the oxidation reaction of the silver with the chloride ions of the potassium chloride electrolyte to give silver chloride and electrons as in the following reactions;

i) $KCl + OH^- \rightarrow KOH + Cl^-$ (In the electrolyte)

ii) $Ag + Cl^- \rightarrow AgCl + e^-$ (At the anode)

At the cathode, when oxygen diffuses through the membrane it is electrochemically reduced, oxygen combines with the electrons and water giving rise to hydroxyl ions

iii) $O_2 + 2H_2O + 4e^- \rightarrow 4(OH)^-$ (At the cathode)

The principle of the probe works on the fact that the more oxygen is available, the more electrons can be taken up at the cathode and consequently the greater the current flow. The current flow through the cell is dependent on the oxygen concentration at the platinum electrode and therefore, directly proportional to the partial pressure of oxygen. All measurements, in the blood gas analyser, are performed at 37°C, the temperature of blood in the human body. In certain measurement systems the probe

employed in the experiment has temperature sensors built into the probe for temperature measurement and compensation [Sha94, Pot01].

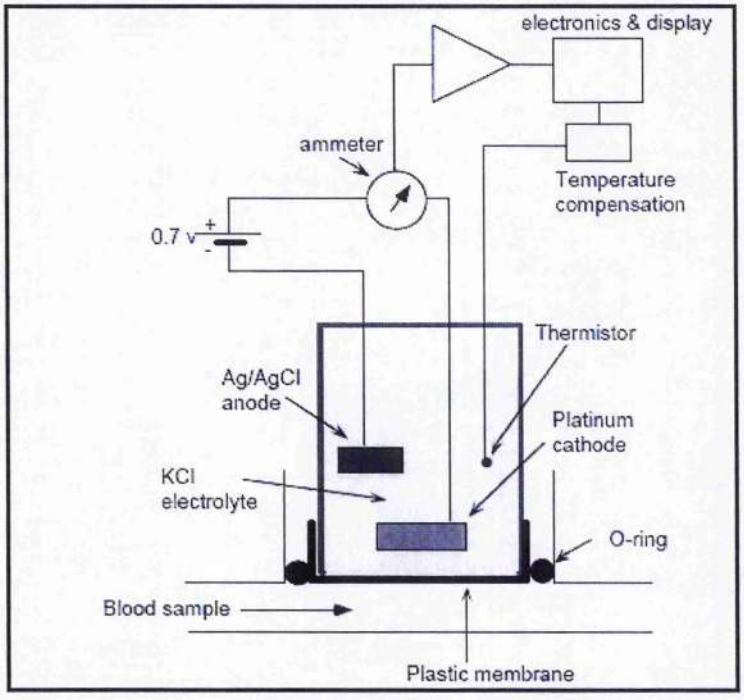

Fig. 2.4 Oxygen electrode [Pot01]

2.4.1.2 pH electrode

The H^+ electrode is an ion selective electrode dependent on the hydrogen ion sensitive glass at its tip. A potential develops across this glass is dependent on the difference of H^+ across it. The H^+ within the H^+ electrode is maintained at a constant value by the buffer solution so that the potential across the glass is dependent only on the H^+ in the blood sample channel. To measure the potential difference it is necessary to make an electrical contact with the blood and with the buffer solution. However in the case of the blood, a reference electrode is employed with a membrane at its tip to avoid contamination. Each electrode consists of two conductors; a metal component which conducts electrons and an electrolytic component to conduct ions. In both electrodes reference and H^+ electrode, the stability of the metal to solution is maintained through a special silver electrode in contact with its chloride which is in turn in contact with a solution of chloride ions. The silver/silver chloride connection in the H^+ electrode is in contact with the buffer solution while the silver/silver chloride reference electrode is linked to the membrane and the blood via a saturated solution of

potassium chloride which completes the electrical circuit (Figure 2.5). The potential difference between the electrodes is measured and converted into a direct reading of H^+ or pH. Temperature control is again important and the measurement is performed at 37°C.

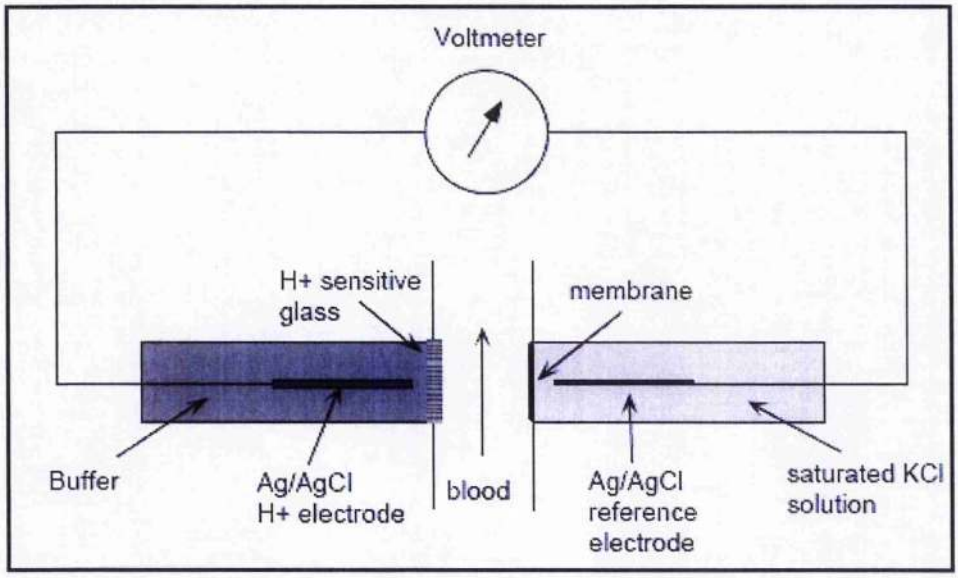

Fig. 2.5 pH electrode [Pot01]

2.4.1.3 CO_2 electrode

CO_2 electrode provides a direct method of CO_2 measurement from the H^+ change associated with the reaction of CO_2 with water.

$$i)\ CO_2 + H_2O \leftrightarrow H_2CO_3 \leftrightarrow H^+ + HCO_3^-$$

ii) The CO_2 is directly related to H^+ concentration

The electrode incorporates hydrogen ion sensitive glass with electrodes either side. The glass is in contact with a thin film of sodium bicarbonate solution in an nylon mesh which is fixed over the glass tip (Figure 2.6). The blood is separated from the nylon mesh and bicarbonate by a plastic membrane which is permeable to carbon dioxide. At the tip of the electrode, carbon dioxide diffuses through the plastic membrane into the mesh impregnated with the bicarbonate solution and combines with the water present producing hydrogen ions and bicarbonate. The resulting change

of hydrogen ion concentration is measured by the glass electrode then the analyser then calculates the CO_2.

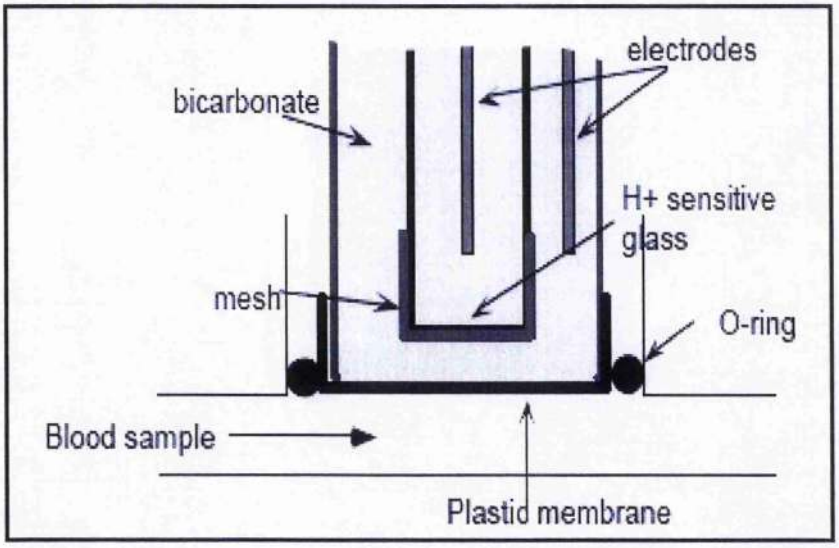

Fig. 2.6 CO2 electrode [Pot01]

2.4.2 Pulse oximeter

The pulse oximeter is a device to measure the rate and the amount of oxygen in the arterial blood. It measures the amount of oxygen as a percentage of haemoglobin molecules that are oxygenated versus the total amount of haemoglobin molecules. Most pulse oximeters display pulse heart rate (beats per minute, BPM). A pulse oximeter probe consists of: two low power light emitting diodes (infra red 940 nm & red light 660 nm) and a photodetector. The infrared and red light is shone alternatively through some tissue (finger, foot, toe, earlobe or nose). As the light is passed through the tissue some of it is absorbed. The amount of light absorbed changes every time the heart beats as the blood pulses past the sensor. The light is absorbed differently by haemoglobin and oxyhaemoglobin. The light intensity of the infrared and red light is measured by the photodetector after it has passed through the finger. The pulse oximeter calculates the percentage of haemoglobin which is oxygenated. The typical values for adults are 95-100% of oxygen-haemoglobin saturation and 50-90 BPM. For neonates are 90-98% of oxygen-haemoglobin saturation and 120-180 BPM [Sin99].

2.4.3 Colorimetric method

Dissolved oxygen can be measured by the colorimetric method which is commonly applied in the field of dilute solutions. For the colorimetric method to be quantitative, it must form a compound with a distinct colour with characteristics which are directly proportional to the concentration of the oxygen in the sample. Colorimetry relies on Lambert's and Beer's Laws. Lambert's law relates to the absorption of light to the depth within the coloured liquid. Lambert's law states that each layer of equal thickness absorbs an equal fraction of the light that traverses it. Therefore when applying a ray of monochromatic light through an absorbing medium its intensity decreases exponentially as the length of the medium increases. Beer's law is concerned with light absorption in relation to solution concentration and it states that the intensity of a ray of monochromatic light decreases exponentially as the concentration of the absorbing medium increases [Saw94].

In the colorimetric method, the fluid sample is taken up into an ampoule under vacuum, and the chemical reagents which are present in the ampoule interact with oxygen to constitute a coloured product. This coloured product, which absorbs light with visible wavelength, has intensity proportional to oxygen concentration. Furthermore, the intensity of the colour is compared to a series of tubes with colour intensities that illustrate known concentrations of dissolved oxygen expressed in units of mg/L. Colorimetric kits are used to measure low oxygen levels, since it can measure 1 mg/L of dissolved oxygen. The active chemical components of ampoule reagent are Ethylene Diamine Tetraacetic Acid (EDTA), Tetrasodium salt, Hydroquinone, alph-(dinonylphenyl)-omega-hydroxy-poly(oxy-1,2-ethanediyl) and L-Lysine. These chemical reagents can cause eye, skin and respiratory tract irritation thus it is important to ensure the wearing of protective clothing, gloves, masks and goggles [Hac05].

2.5 Reactive oxygen species - Free radicals

A free radical is an atom or group of atoms that have one or more unpaired electrons in their outer orbital, indicated in formulae as [•]. As a consequence they have an increased reactivity with other molecules. This reactivity is determined by the ease with which a species can accept or donate electrons. They are highly reactive and vital

in a vast number of biological processes [Fre82]. The prevalence of oxygen in biological systems means that oxygen centered radicals are the most common type found. The term reactive oxygen species (ROS) rather than oxygen radicals is now generally the preferred term because singlet oxygen – superoxide $O_2^{\bullet -}$, hydrogen peroxide (H_2O_2), hydroxyl (•OH), nitric oxide (NO•) and hydroperoxide have chemically reactive and harmful oxygen containing functional groups. They can be grouped into superoxide and hydroxyl radicals [Coy93, Bea95, Kin06]. These reactive oxygen species are not allowed to accumulate in large amounts and removed by the body's defence system. Large amounts of these radicals could result in oxidative stress and could lead to permanent damage to cell tissue; therefore it is necessary to maintain a fine balance between the free radicals and the antioxidants that counteract these.

Free radicals can cause major damage in biological matter. The normal ageing process produces an increase in the amount of free radicals in the body but a decrease in the ability to fight against them; this will lead to cellular damage [Smi95]. Vitamin E and C used in the protection from free radicals. Vitamin E is the major lipid-soluble antioxidant and plays a vital role in protecting membranes from oxidative damage. Its primary activity is to trap peroxy radicals in cellular membranes. Vitamin C or ascorbic acid is a water-soluble antioxidant that can reduce radicals from a variety of sources [Kin06, Pec05].

Chapter 3

Tumour Hypoxia

3.1 Definition and causes

All cells need a sufficient supply of oxygen to perform their functions. Oxygen is used in aerobic metabolism, which turns carbohydrates into the energy needed to power essential cellular processes. However, when there is insufficient supply of oxygen to tissues, this case is called hypoxia. Hypoxia is a pathological condition that can be caused by a number of factors, such as: 1) low oxygen partial pressure, as a result of reduction in gas exchange area, exposure to high altitudes or pulmonary diseases, 2) reduced ability of blood to carry oxygen e.g. anaemia, 3) reduced tissue perfusion, generalized or local, circulatory or ischemic hypoxia, 4) inability of cells to use oxygen even with normal quantity of oxygen reaching the cells, because of intoxication (cytotoxic hypoxia) [Hoc01, Har04].

Hypoxic tissues are also defined as areas with oxygen tension values of 20 mmHg or lower (surrounding normal tissue between 24-66 mmHg) [Men05, Vau90]. Tumours grow possibly from a single cell, probably from not more than a few. An increase in cell number must mean a rise in the demand for oxygen [Har04]. Cells in tumours become hypoxic in either or both of two ways; first, the form of tumour growth may result in some cells lying so far from the capillaries that constitute their immediate source of oxygen that it is almost used up by the metabolism of the intervening cells. Secondly, the vascular system of the growing tumours may fail to deliver enough oxygen both because of inadequacies in the vessels themselves and in the quantity of blood that flows through them [Vau04]

The presence of hypoxic cells in tumours is of importance because it may affect the outcome of treatment by radiotherapy. Tumour hypoxia increases the malignant potential and reduces the sensitivity towards non-surgical treatment modalities (x- and γ-radiation), because the radiosensitivity is increasingly limited when the PO_2 in a

tumour is less than 25 mmHg. This is because of the fact that the presence of oxygen molecules increases DNA damage through the formation of oxygen free radicals, which occurs principally after the interaction of radiation with cells. As a result, the dose of ionizing radiation required to achieve the same cell survival fraction is about two to three times higher under hypoxic conditions than under normoxic conditions [Sha04, Vau01]. In other words, hypoxic cells are up to three times more resistant to ionizing radiation than normoxic cells.

3.2 Adaptation of tumour cells

Normal tissue function depends on sufficient supply of oxygen through blood vessels. In the case of a hypoxic tumour, a variety of specific adaptation mechanisms occur. These mechanisms are associated with physiological responses and genetic alterations that have two important consequences: 1) in order for tumour growth to occur, adequate oxygen delivery must be effected via the tumour vascularization that results from increased synthesis of angiogenic growth factors and decreased synthesis of anti-angiogenic growth factors. These allow the growth of new blood vessels from pre-existing vessels. 2) Tumour cells adapt their metabolism to inadequate supply of oxygen by increasing glucose transport and glycolysis (oxidation of glucose in the absence of oxygen) in order to maintain ATP production despite the reduced efficiency of anaerobic metabolism compared with oxidative metabolism [Kin06].

The key regulator of these processes is hypoxia-inducible factor 1 (HIF-1). HIF-1 is an important transcription factor that stimulates tumour growth through more than 40 target genes whose protein products play critical roles in each of the above processes. HIF-1 is composed of two subunits, an oxygen-sensitive HIF-1α subunit and a HIF-1β subunit. Under hypoxic conditions, these mechanisms combine to induce maximal HIF-1 activation. Under normal oxygen conditions, HIF-1α is maintained at low levels by rapidly oxidized hydroxylase enzymes, but when cells become hypoxic, HIF-1α escapes the degradation and starts to accumulate, triggering the activation of a large number of genes, like vascular endothelial growth factor (VEGF) and erythropoietin [Har02, Sem02].

3.3 Assessment of tumour hypoxia

In advanced tumours, oxygen delivery is often reduced or even abolished. The PO_2 values vary widely from study to study, this maybe due to the methods used for PO_2 level measurements, the difference in severity of cancers or the number of patients used in each study. The amount of partial pressure of oxygen in tumours is extremely variable, with the PO_2 generally less than 20 mmHg, in contrast to PO_2 of 40–80 mmHg in most normal tissues.

3.3.1 Head and neck cancer

The PO_2 value in patients with cancers of the head and neck was evaluated as less than 5 mmHg in most of the studies. Brizel et al. (1999) reported that the overall median PO_2 was 4.8 mmHg in a group of 63 patients with head and neck carcinomas [Bri99]. This level is in agreement with results reported by Chen et al. 2004, overall median PO_2 less than 5 mmHg in 101 patients with newly diagnosed head and neck carcinomas [Che04]. Nordsmark et al. (1994) also found the tumour oxygenation status measured by a polarographic needle electrode in 31 patients with carcinoma of the head and neck was less than 5 mmHg [Nor94]. In another study by Lehtio et al, (2004) both invasive polarographic PO_2 measurement and [^{18}F] FETNIM PET scanning were used to measure PO_2 [Leh04]. The results of these methods were in concordance and indicated that a high percentage of PO_2 values were less than 5 mmHg. In contrast, in a normal, non-cancerous head and neck, the PO_2 median value is approximately 43 mmHg [Tei95].

3.3.2 Breast cancer

Assaad et al. (2001) found that in 16 patients, the median PO_2 measurements varied between 1.6 mmHg and 49.4 mmHg with an overall mean of 22 mmHg, in contrast to PO_2 26-55 mmHg with an overall mean of 45 mmHg in normal tissue [Ass01]. Vujaskovic et al. (2003) reported that 11 (61%) of 18 patients with breast cancer had an overall median PO_2 = 3.2 mmHg, where the other seven patients had well oxygenated tumours (overall median PO_2 = 48.3 mmHg) [Vuj 03]. In another study by Vaupel et al., (1991) where polarographic needle electrode measurements were obtained without the use of general anaesthesia have revealed median PO_2 values of 30 mmHg for breast cancers, compared with 65 mmHg for normal tissue [Vau91].

However, Vaupel et al. in 2003 studied the tumour oxygenation in 37 women (12 premenopausal and 25 postmenopausal) with breast tumours using ultrasound guidance in collaboration with an oxygen microsensor. They found that 63% of the tumours were hypoxic ($PO_2 \leq 2.5$ mmHg). The mean PO_2 was found to be 6 mmHg [Vau03-].

3.3.3 Cervix cancer

Nordsmark et al. (2003) reported that the overall median PO_2 was less than 3 mmHg in 86 patients with primary carcinoma of the uterine cervix [Nor03]. This level is roughly compatible with results reported by Fyles et al. in 2002, the overall median PO_2 less than 5 mmHg in 106 patients [Fyl02]. However, in a group of 95 patients, Höckel et al. (2001) showed that the overall median PO_2 was less than 11 mmHg [Hoc01]. This level is in agreement with results reported by Wong et al. 1997, the overall median PO_2 less than 10 mmHg for 42 patients with newly diagnosed cervical carcinoma [Won97]. In contrast, in a normal, non-cancerous cervix, the PO_2 median value is approximately 48 mmHg [Tei95].

3.3.4 Prostate cancer

The first electrode studies in man with prostate cancer were carried out by Movsas et al. (1999) [Mov99]. In this study, 41 patients had oxygen measurements made during spinal anesthesia. Partial pressure of oxygen was measured within the prostate gland and from normal muscle. Hypoxia was found in a large proportion of these patients, with the average median PO_2 of only 9.9 mmHg, in contrast to a PO_2 median value of 28.6-42 mmHg in normal muscle. In another study, the incidence of hypoxia was analyzed in 12 patients with cancer of the prostate in 2000. This study found that the overall median PO_2 was less than 10 mmHg [Mov00]. However, Benjamin et al. in 2001 reported that the median PO_2 obtained from Fifty nine patients with prostate cancer was 2.4 mmHg, whereas in normal muscles it was 30 mmHg [Ben01]. In addition, Parker et al. (2004) reported that the median PO_2 was ranged from 0.2 to 57.3 mmHg in 55 patients with the overall median PO_2 was 4.5 mmHg [Par04].

3.3.5 Soft tissue sarcomas

Sarcomas strike people in all age ranges, but they are rare, accounting for only 1% of all cases of cancer [Bor03]. Soft tissue sarcomas, such as leiomyosarcoma,

chondrosarcoma, and gastrointestinal stromal tumour (GIST), are more common in adults than in children. GIST is the most common form of sarcoma. Brizel et al. (1995) found in fifteen patients who had soft tissue sarcoma, the overall median PO_2 was 18 mmHg [Bri95]. A year later, Nordsmark et al. also found in all of the 22 patients who had primary soft tissue sarcomas the overall median of PO_2 was 18 mmHg [Nor96]. However, Bentzen et al. (2003) reported that the overall median in 6 patients was 10 mmHg, the median PO_2 ranged from 1 to 34 mmHg [Ben03].

3.3.6 Malignant melanoma

Lartigau et al. (1997) reported that the overall median PO_2 was 11.6 mmHg found in 20 patients with past history of melanoma. PO_2 was measured using an Eppendorf probe [Lar97]. In 2004 Brurberg et al. found the mean PO_2 was less than 10 mmHg for those who had malignant melanoma [Bru04]. The median PO_2 for normal tissues, non-cancerous tissues, was 40.5 mmHg.

3.3.7 Pancreatic cancer

Koong et al. in 2000 characterised the oxygenation in human pancreatic and peripancreatic cancers using Eppendorf electrodes. The study involved seven patients having peripancreatic or pancreatic cancer. The results showed that the median PO_2 ranged from 0 to 6.2 mmHg. However, the median PO_2 in normal patients was ranged from 43.4 to 67.5 mmHg. Furthermore, the study also included patients with chronic pancreatitis with the median PO_2 was 24.3 mmHg [Koo00].

3.3.8 Lung cancer

Koong et al. in 2003 used the Eppendorf polarographic electrode to directly assess the tumour oxygenation in 25 patients with non-small cell lung cancers (NSCLC). In 11 patients, the median PO_2 ranged from 1.5 to 39.7 mmHg. However, the remaining 14 patients, the median PO_2 ranged from 23 to 143 mmHg involved in the study. Based on this study, it was concluded that tumour hypoxia exists in lung cancer disease but occurs less in comparison with other solid tumours [Koo03].

3.3.9 Summary

It can be seen from the previous studies that the PO_2 values vary from one study to another even though most of these values were evaluated using a similar method,

computerized polarographic electrode, to measure PO_2 values in normal and tumour tissues. It seems that the magnitude of the effect of the technique used for PO_2 level measurements is not only the reason for the discrepancy in the PO_2 values but also the clinical history or the stage of cancer could be other possible reasons. Unfortunately, the effect of this factor was not clear since some of the studies have not taken into account the relationship between the cancer severity and the PO_2 values. In addition, haemoglobin concentration could be another factor that affects the variations of PO2 measured. A reduction in haemoglobin level in blood will lead to the lack of oxygen delivery to tissues. Oxygen saturation and partial pressure decrease due to low haemoglobin levels, resulting in hypoxia. Therefore, one might expect to see that most of the anaemic patients may have poorly oxygenated tumours. Brizel et al. (1999) showed that when O_2 carrying capacity is below normal, a poorly oxygenated tumour will probably result. Normal O_2 carrying capacity does not, however, guarantee a well-oxygenated tumour [Bri99].

3.4 Measurement of tumour hypoxia

Reliable measurement of tumour oxygenation could potentially provide critical information for prognosis and treatment. There are direct invasive and direct non-invasive methods to measure tumour oxygen tension. The invasive technique of using computerized polarographic oxygen-sensitive electrodes is regarded to be the gold standard for measuring the hypoxic fractions in tumours. However, the search for a non-invasive approach to detect tumour hypoxia is still a challenge for medical imaging. The most encouraging results have been obtained using radiotracers that selectively accumulate in hypoxic tumours and which can be applied together with functional PET imaging [Sto93].

3.4.1 Direct invasive method polarographic technique

The direct invasive technique using computerized polarographic oxygen-sensitive electrodes has been considered to be the gold standard for measuring hypoxic fractions in tumours [Sto93]. Measurements with the polarographic needle electrode probe are made by implanted electrodes directly into tumours to measure oxygen concentration. Measurements are made upon retraction of the tip in order to reduce artefacts caused by fluid tissue pressure and localised bleeding. The increase in the clinical use of this technique did not come about until the development of the

Eppendorf Histograph oxygen electrode system, which has a very fast response time and can be moved quickly through a tumour under computer control to obtain large numbers of oxygen measurements [Nor01, Men05].

Although direct invasive measurement of oxygen levels in tumours using Eppendorf probes has been shown to allow prognostic stratification of various tumours, it has not been feasible to widely implement this technique in clinical practice. This is due to the logistic issues including inaccessibility of many tumour sites, dependence on a technically-skilled user, inter-observer variability, failure to distinguish hypoxic cells from blood vessels and inability to provide information regarding patterns of hypoxia. Therefore there has been significant interest in developing non-invasive imaging approaches to the detection and definition of tumour hypoxia [Men05, Sto93].

3.4.2 Direct non-invasive method

Ongoing research for a non-invasive approach to detect tumour hypoxia is still a challenge for medical imaging. A number of cross-sectional non-invasive imaging techniques have been recently developed. Magnetic resonance imaging (MRI) techniques such as blood oxygen level-dependent MRI (BOLD MRI) and dynamic contrast-enhanced MRI (DCE MRI) have been applied to inaccessible tumours to measure tumour oxygenation. BOLD MRI detects the relative changes in tumour deoxyhemoglobin concentration and blood flow before and after the intervention. DCE MRI has emerged as a promising method for measuring blood flow and volume in tumour tissue. However, the widespread use of DCE MRI is limited because it cannot provide a comprehensive picture of tumour oxygen status. Therefore it requires special purpose data acquisition techniques and analysis software [Lon02, Rob99, Haw98].

The most encouraging results have been obtained using radiotracers that selectively accumulate in hypoxic tumours and which can be applied together with functional positron emission tomography (PET) imaging. PET is an attractive method for assessing tumour hypoxia. It can provide an opportunity to study tumour metabolism by the in vivo detection of physiological processes through the use of short-lived positron emitting radiopharmaceuticals. For example the most extensively studied PET agent in the clinical setting of hypoxia is ^{18}F-fluoromisonidazole (^{18}F-FMISO). In

vitro and in vivo studies have shown that intracellular retention of ^{18}F-FMISO is dependent on oxygen concentration [Res01, Leo04].

3.5 Evaluation of tumour hypoxia by PET

Evaluation and measurement of tissue oxygenation is critically important because oxygen tension is considered to be the main modifier that specifies the radiotherapy outcome. In view of the fact that most cancers are hypoxic, it is difficult to treat them due to low tumour oxygenation, and therefore, high resistance to radiotherapy. For an imaging modality to be ideal in hypoxia investigation, it should distinguish between normoxia, hypoxia, and hyperoxia. Furthermore, it should be sensitive to even low oxygen levels and applicable to any tumour location with optimum regional assessment. From this point, it has become significant to assess tumour hypoxia either by the invasive or non-invasive techniques. Positron emission tomography is one of the non-invasive techniques to image and assess hypoxic tumours.

Rasey et al. (1987) found that very low oxygen levels were required for substantial uptake of [^{18}F]-fluoromisonidazole (FMISO) by cells, based on in vitro study. The oxygen level was inhibiting [^{18}F]FMISO binding by 50%, relative to binding under anoxic conditions, varied from 0.55 to 1.75 mmHg [Ras87]. Rasey et al. (1996) studied different types of cancers in 37 patients (21 lung cancer patients, 7 head and neck cancer patients, 4 prostate cancer patients, and 5 patients with other malignancies). They observed hypoxia in 36 (97%) of 37 patients and these results consistent with Eppendorf electrodes PO_2 measurements. They found that very low oxygen levels were necessary for FMISO accumulation in the tumour [Ras96]. However, Rasey et al. (2000) found a disagreement between results of [^{18}F]FMISO PET scanning and assessment of radiobiological hypoxic fraction in rats [Ras00]. They suggested that this could be due to failure of [^{18}F]FMISO to identify hypoxic cells at or above an oxygen level of 2–3 mmHg and that will still give substantial protection against radiation.

Bentzen et al. (2003) evaluated [^{18}F]FMISO PET in comparison with Eppendorf PO_2 measurements for assessment of tumour oxygenation status [Ben03]. This research involved using a [^{18}F]FMISO PET scanning and Eppendorf electrodes PO_2 measurements in the same soft tissue tumours. They found that the soft tissue tumours

in three patients were identified by the PET scanning but without obvious accumulation of radioactivity, except in one patient. They were large and very hypoxic with an overall median 3 mmHg, when measured with the Eppendorf PO_2 measurements. Furthermore the contrast between a tumour and its surrounding normal tissue was small in PET images. The study concluded that the [^{18}F]FMISO PET examination is not feasible for the detection of hypoxia in soft tissue tumours. Gagel et al. (2004), however, disagreed with this finding, arguing that the results from their [18F]FMISO PET research did show that PET scanning was highly feasible for the detection of hypoxia [Gag04]. This study found that there were correlations between the results of [^{18}F]FMISO PET scanning and Eppendorf electrodes PO_2 measurements in 16 patients with primary carcinoma of the head and neck. Lehti et al. (2004) found, similar results as Gagel et al., in 21 patients with carcinoma of the head and neck; the results of polarographic PO_2 measurement and [^{18}F]-fluoroerythronitroimidazole (FETNIM) PET scanning were in concordance [Leh04].

[^{18}F]FMISO PET tracer has a homogenous uptake in most normal tissues imaged by PET, however, Padhani et al (2007) reported that [^{18}F]FMISO has slow clearance kinetics from normal tissues, as a result affecting tumour-to-background ratio. They noticed that in early distribution of [^{18}F]FMISO (1 minute); there was a hyperperfusion in the area of the primary tumour and metastasis. However, after 240 minutes, PET images showed that only the left neck nodal metastasis is hypoxic [Pad07]. [^{18}F]-fluoroazomycin arabinoside (FAZA) is another new radiopharmaceutical used in hypoxia PET scanning. In a recent study, it has been investigated that [^{18}F]FAZA has better pharmacokinetics in comparison to [^{18}F]FMISO. This investigation is based on the fact that [^{18}F]FAZA is cleared from normal tissue faster than [^{18}F]FMISO; consequently, tumour-to-tissue background ratio will be more enhanced [Rei07].

Intensive research is ongoing in research institutions and pharmaceutical companies to develop radiotracers for imaging hypoxia. However Kacperski and Spyrou (2004) reported that when the three-gamma annihilations, which are simply ignored in the current PET scanners, are recorded, the positron itself, or more precisely the positronium, could serve as an oxygen-sensitive marker [Kac04a, Spy05]. The formation of positronium is not only sensitive to the physics parameters, but also

behaves as an active chemical particle. Oxygen is known to be a strong positronium quencher; therefore hypoxic regions should be characterized by higher three-gamma rates than those of well oxygenated regions. This can be obtained by measuring the variability of the three-gamma yield at a variety of different levels of oxygen concentration between hypoxia and normoxia in biological samples. Thus three-gamma images may provide more information about the concentration of oxygen in different types of malignant tumours, in comparison with the conventional two-gamma images.

Table 3.1 Comparison of techniques for evaluating human tumour hypoxia [Pad07]

Technique	Invasive investigation	Requires injection	Measures	Clinically Validated in RT	General availability (1-5; poor-wide)	Monitors changes in pO_2
^{18}F-MISO PET	No	Yes	Hypoxia	±	3	No
^{18}F-AZA PET	No	Yes	Hypoxia	No	2	No
^{18}F-EF5 PET	No	Yes	Hypoxia	±	2	No
^{64}Cu ATSM	No	Yes	Hypoxia	±	3	No
BOLD-MRI	No	No	[dHb] in RBCs	Yes	4	Yes
Polorographic electrode	Yes	No	pO_2	Yes	2	Yes

Chapter 4

Physics of positron emission and annihilation

4.1 Background and basic principles

4.1.1 Introduction

Positron Emission Tomography (PET) is a nuclear medicine procedure allowing biochemical processes to be investigated by in-vivo imaging. PET has the potential to play a major role in the emerging field of molecular imaging by enabling the study of molecular pathways and genetic processes in living bodies, non-invasively. Different positron emitters are used to label biochemical substances that are present in tissues and therefore their distribution within the body can be followed. The idea of using positron emitters for imaging was first investigated in the early 1950's [Wre51, Kou82, Val03]. In the 1960's the first PET scanners used single slices when performing tomographic studies with systems employing a ring of 32 NaI(Tl) detectors. The spatial resolution of the slice had a full width half maximum (FWHM) of at least 2 cm. The next generation of PET scanners reduced the detector size and added additional rings to improve the spatial resolution to less than 1 cm. As time progressed, more and smaller detectors using bismuth germanate (BGO), and appropriate photomultiplier tubes (PMTs) were added to these machines to increase their sensitivity and spatial resolution which typically was found to be 4-5mm [Tho90]. The current generation of dedicated PET scanners tend to use alternative crystal technologies e.g. lutetium oxyorthosilicate (LSO) or gadolinium oxyorthosilicate (GSO) [Hum03].

The ability of PET to utilise isotopes of elements naturally occurring in biological molecules is a distinct advantage of the technique. Elements such as carbon, nitrogen and oxygen are structural elements of all biological tissues and labelling of organic compounds with physiological affinity to the biological system becomes possible. Fluorine-18, which is also a positron emitter, can replace hydrogen in many important biological molecules without changing their function significantly; for example, ^{18}F-

deoxyglucose (^{18}FDG) can be used to measure glucose utilization rate by a tissue or organ such as brain. It also can be incorporated into many biological molecules such as amino acids and proteins. The use of positron emitting tracers with PET has found numerous applications in oncology, cardiology and neurology. Table 4.1 shows the most common PET medical imaging radionuclides and their properties.

Table 4.1: Physical properties of most commonly used radioisotopes in PET [Kou82, Hum03]

Nuclide	E_{max} (MeV)	E_{mean} (MeV)	Half-life (min)	Average range in water (mm)	Path length in water (mm)
^{11}C	0.96	0.38	20.4	1.7	4.1
^{13}N	1.20	0.49	10.0	2.0	5.1
^{15}O	1.74	0.74	2.0	2.7	7.3
^{18}F	0.63	0.24	109.8	1.4	2.4

4.2 Positron emission

Proton-rich radionuclides can decay mainly by two processes known as electron capture and positron emission (β^+ decay). Decay by electron capture and positron emission compete with each other. Electron capture is the dominant process in nuclides with high atomic number (Z) due to an increased amount of orbital electrons close to the nucleus. Most nuclides in living tissue are of low atomic number so the foremost process of decay for proton rich radionuclides is positron decay. The general form of the positron emission scheme is:

$$ {}^{A}_{Z}X \rightarrow {}^{A}_{Z-1}Y + \beta^+ + \nu $$

Where ${}^{A}_{Z}X$ is the original nucleus with an atomic number of Z and a mass number of A. The energy released is dependent on the nuclide and is shared between the positron and the neutrino. The neutrino is a particle of negligible mass and zero charge emitted sharing its energy with the positron. Positrons are therefore emitted with a range of energies, from zero up to a maximum endpoint energy E_{max}. This maximum energy is characteristic for the nucleus and the mean kinetic energy of the emitted positrons is approximately 40% of E_{max} [Hum03]. Decay of positron emission is the basis for PET imaging.

4.3 Positron annihilation

The positron that is ejected following β^+ decay has a very short lifetime when interacting with atomic electrons in the tissue. When the positron loses most of its kinetic energy and reaches thermal equilibrium, its collision with an electron results in annihilation, where the mass of the electron and the positron is converted into electromagnetic energy. Because the positron and electron are almost at rest when this occurs, the energy released comes largely from the mass of the particles and can be calculated from Einstein's mass-energy equivalence as:

$$E = mc^2 = m_e c^2 + m_p c^2$$

where m_e and m_p are the mass of the electron and positron, respectively (9.1×10^{-31} kg), and c is the speed of light (3×10^8 m/s). Using the conversion of Joules to eV (1 eV = 1.6×10^{-19} J), the energy released is 1022 keV.

The energy is released in the form of high-energy photons. As the positron and electron are almost at rest when the annihilation occurs, two photons are emitted simultaneously in opposite directions (180° apart), carrying an energy equal to $1022keV/2$, or 511 keV, ensuring that both energy and momentum are conserved. This process is shown schematically in Figure 4.1. The annihilation of these two photon process forms the basis for current PET imaging. However annihilation of a positron with an electron can proceed by multiphoton processes. Annihilation can also occur with the emission of three photons or more but their probabilities decrease strongly with the number of decay quanta involved. (see positronium formation section 4.7.1).

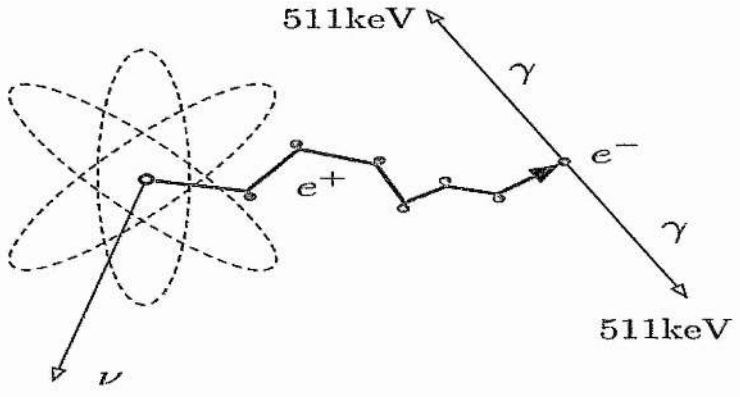

Figure 4.1: Schematic diagram of positron annihilation.

In some situations the positron may not come to complete rest before the annihilation process. In this case the photon pair may not be emitted at exactly 180°, to allow for conservation of energy and momentum. This effect results in an uncertainty in the localisation of the nuclear decay event of 0.5° FWHM from strictly 180°. The positron travels a finite range from the nucleus before it annihilates, and therefore the photons will originate a small distance from the nucleus. Both these factors add an error in the spatial resolution achieved by PET. The range of the positron is dependant on its energy and the electron density of the medium. Table 4.1 shows the numerical data for the average range and path length of the positrons emitted in water, which is the major component of biological tissue, for most commonly used radionuclides in PET [Kou82, Hum03]. As positrons do not move along a straight line in matter because of the high number of interactions with small energy exchange, their path length is always longer than their range.

4.4 Photon interactions in matter

Photons interact with matter via a number of mechanisms, depending on their energy and on the atomic number (Z) of the absorber materials. There are four prevailing mechanisms: photoelectric effect, Compton scattering, Rayleigh scattering and pair production. The relative importance of the dominating interaction for different absorbers (Z) and energies (hv) is shown in Figure 4.2. The curves represent the values of Z and hv for which the two neighbouring effects are equally probable. It can be seen that photoelectric absorptions are dominant at low energies (up to several hundred keV), pair production at high energies (more than 5MeV) and Compton scattering being most important in the mid-energy range.

For the photons produced by positron annihilation, Compton scattering and photoelectric effect are the most important interactions with materials of interest in PET such as human tissue, detector crystal and shielding. These are the main mechanisms involved both with the detection of the annihilation photons in PET as well as the problem of attenuation and scatter. To understand the response of the detector used, knowledge of the main processes by which a photon interacts with matter is essential.

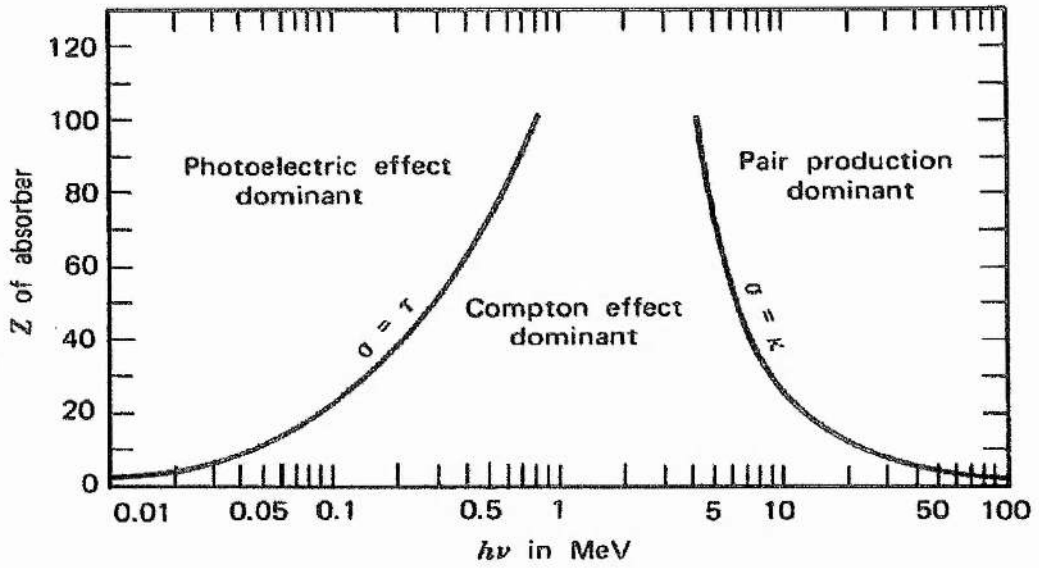

Figure 4.2: The relative importance of the three major types of photon interactions [Eva55, Kno00].

4.4.1 Photoelectric absorption

In the photoelectric process, absorption occurs by interaction between the photon and an inner-shell bound electron in the absorbing material. It is characterised by a photon giving all of its energy to an electron thus exciting or ionising the atom in a single interaction. The photoelectric absorption process occurs when a photon has energy equal or greater than the binding energy of an electron. Therefore:

$$E_e = E_\gamma - E_b$$

where E_e is the electron energy, E_γ is the incident photon energy, and E_b is the binding energy of the electron in its original atomic shell. The vacancy of the ejected electron is filled by an electron from an outer shell causing the emission of characteristic x-rays (or Auger electrons) that represent the difference in the potential energy of the two shells. The probability of a photoelectric interaction σ_τ increases with increasing atomic number (Z) of the absorber material and decreases with increasing energy of the photons (E_γ). This is the prime reason that the detector material is preferred to have a high effective atomic number. There is no single analytical expression for the probability of photoelectric absorption per atom over all ranges of E_γ and Z but in a manner approximated by the empirical formula [Kno00] the cross section is:

$$\sigma_\tau \propto \frac{Z^n}{E_\gamma^{3.5}}$$

where σ_τ is the photoelectric cross-section, Z is the atomic number of the absorber, and the exponent n varies between 4 and 5 depending on the energy region of interest.

4.4.2 Compton scattering

A collision between an incident photon and a loosely bound electron in which the photon transfers a portion of its energy to the electron is called the Compton effect. After collision, the incident photon and the recoil electron move at certain angles with respect to the original direction of the incident photon (Figure 4.3). All angles of scattering are possible and the energy transferred to the electron can vary from zero to a large fraction of the gamma ray energy. The energy of the scattered photon ($E_\gamma^{'}$) is given by:

$$E\gamma' = \frac{E\gamma}{1 + \frac{E\gamma}{m_0 c^2}(1 - \cos\ \theta)}$$

Where E_γ and $E_\gamma^{'}$ are the energies of the incident and scattered photons, respectively. $m_0 c^2$ is the rest mass energy of the electron (511keV) and θ is the scattering angle of the photon with respect to its original direction.

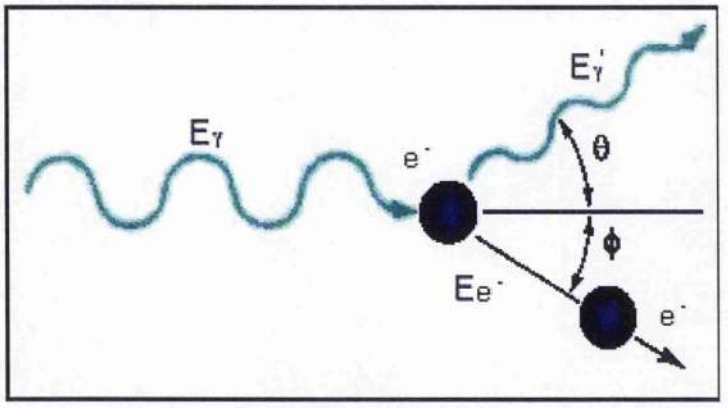

Figure 4.3: The process of Compton scattering [Bra99]

The kinetic energy E_{e^-} of the recoil electron after the collision is given by energy conservation as:

$$E_{e^-} = E_\gamma - E_\gamma'$$

The minimum energy of the incident photon after it has undergone Compton scattering occurs when maximum energy is given to the electron. This occurs for a scattering angle of 180°. By substituting θ=180° into the above equation, the energy $E_\gamma'_{BS}$ of the backscattered gamma-ray becomes:

$$E\gamma'_{BS} = \frac{E_\gamma}{1 + \frac{2E_\gamma}{m_0 c^2}}$$

The energy given to the electron is simply equal to $E_\gamma - E_\gamma'_{BS}$.

The probability of Compton scattering per atom of the absorber depends on the number of electrons available as scattering targets and therefore increases linearly with the atomic number of the scattering material (Z). The angular distribution of scattered gamma rays is predicted by the Klein-Nishina formula for the differential scattering cross section for interaction with a free or very loosely bound electron,

$$\frac{d\sigma}{d\Omega} = Zr_o^2 \left(\frac{1}{1+\alpha(1-\cos\theta)} \right)^2 \left(\frac{1+\cos^2\theta}{2} \right) \left(1 + \frac{\alpha^2(1-\cos\theta)^2}{(1+\cos^2\theta)(1+\alpha\{1-\cos\theta\})} \right)$$

where r_0 is the classical electron radius and $\alpha = \frac{E_\gamma}{m_o c^2}$ which will be equal to 1 for positron annihilation photons.

4.4.3 Rayleigh scattering

In coherent Rayleigh scattering, incident photons are by scattered bound atomic electrons. The atom is neither excited nor ionized and after the interaction the bound electrons revert to their original state. The atom as a whole absorbs the transferred momentum but its recoil energy is very small [Kno00]. The incident photon is scattered with scattering angle and has essentially the same energy as the original photon. The scattering angles are relatively small because the recoil imparted to the atom must not produce atomic excitation or ionization. Coherent scattering is only

significant at low energies below 50keV; however, its practical importance in nuclear medicine is limited as it is not an effective mechanism for transferring photon energy to matter.

4.4.4 Pair production

Pair production occurs when the incident photon energy exceeds twice the rest mass energy of an electron (1.022 MeV). In practice the probability of this interaction remains very low until the photon energy approaches several MeV. This interaction must take place in the Coulomb field of the nucleus. In this process the incident photon disappears and a positron electron pair is created. In the case where the energy of the incident photon is greater than $2\ m_0c^2$, the excess energy is shared as kinetic energy between the electron (E_{e-}) and positron (E_{e+}) produced.

$$E_{e-} + E_{e+} = E_\gamma - 2\ m_0c^2$$

where, m_0 is the rest mass of an electron or positron. The positron will subsequently annihilate after slowing down in the absorbing medium and two annihilation photons are usually produced. The pair production cross-section is proportional to Z^2 per atom and increases rapidly with energy greater than $2m_0c^2$.

4.5 Data acquisition in PET

4.5.1 Coincidence detection

The basic principle of PET relies on the detection of two photons, each with energy of 511keV, in coincidence with each other. These photons are produced when a positron annihilates with an electron. Coincidence detection takes advantage of the fact that the two annihilation photons are emitted in opposite directions and emerge simultaneously from the same event (Figure 4.4).

Therefore if two photons are detected by two opposing detectors simultaneously (i.e. within a narrow time interval), their originating position annihilation event is placed along a line connecting the two detectors which is referred to as a line of response (LOR). It can be regarded as an electronic collimation technique unlike other nuclear imaging techniques where physical collimation is used to provide positional information. To reconstruct a complete cross-sectional image of the object, data from a large number of these LORs are collected at different angles that cover the field of view of the system [Phe06].

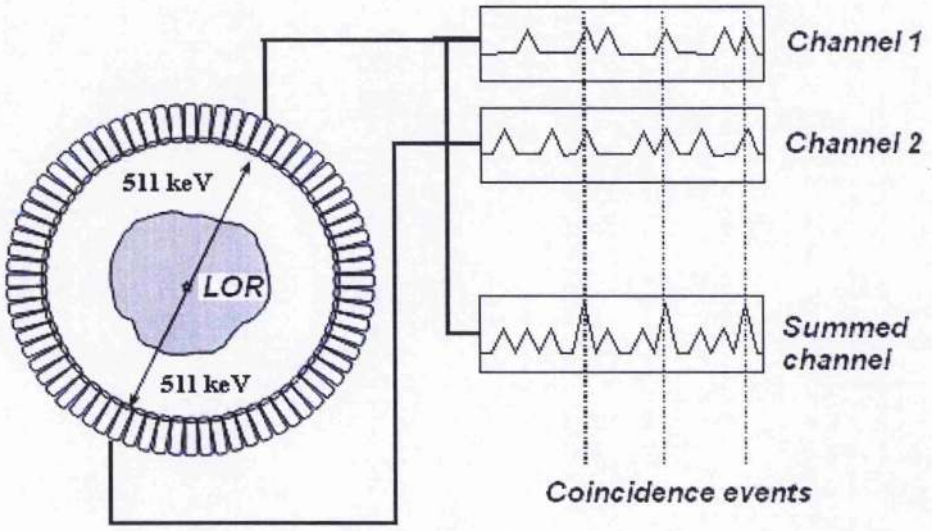

Figure 4.4: Schematic diagram of coincident detection in PET system [Bad06]

During the PET scan, the two annihilation photons can be emitted from anywhere within the scanner's field of view. In most cases, the distance travelled by each of the photons, from the point of annihilation to the detectors will be different. If τ is the width of a pulse in one detector and the second pulse arrives within a predefined time of width 2τ, a coincidence will be registered by the detector system (i.e. the coincidence timing window) [Val03]. For detectors with poor timing resolution (slow scintillator materials) the value of 2τ may be large in order to detect as many valid coincidence events as possible. Typical timing resolution for a BGO or NaI(Tl) based PET detector is approximately 5 to 6 nanoseconds, while for LSO it is approximately 2 to 3 nanoseconds [Phe06].

4.5.2 Types of coincidence events

The detection of events in PET relies on the two photons being detected within the coincidence timing window and subsequently being both within a defined energy window and forming a LOR within an acceptable geometry. Those events that satisfy the above criteria are usually referred to as prompt events. However, not all prompt events are true coincidence events. They can be contaminated with undesirable events.

The coincidence events that are most relevant in PET can be put into three categories: true, scattered and random events. These events are illustrated in Figure 4.5. Each of the shown coincidence events are described below:

4.5.2.1 True coincidence event

Under ideal circumstances, the annihilation photons, originate from the same radioactive decay and reach the detectors on opposing sides without interacting with surrounding atoms (i.e. they are not scattered or absorbed) and will reach the detectors within the coincidence timing window (Figure 4.5).

4.5.2.2 Scattered coincidence event

A scattered event will arise when either one or both of the annihilation photons undergo a Compton scattering interaction that may occur within the object, the detectors, or the surrounding material. The implication of this is that the LOR for this event will not correlate to the origin of the annihilation event (Figure 4.5). These inaccuracies lead to a contribution of low frequency background to the final image, resulting in reduced contrast and compromised quantification [Val03]. Some of the scattered events below certain energies can be discriminated; however the amount of scattered events that this is relevant to, depends on the energy resolution of the detectors. Due to the relatively poor energy resolution of most detectors used in PET, only a certain fraction of the scattered events are rejected. The fraction of scattered events detected can range from 15% to well over 50% in typical PET studies, depending on the size of the object and the geometry as well as the energy resolution of the PET scanners [Phe06].

4.5.2.3 Random coincidence event

A random coincidence event occurs when two separate, independent annihilation photons strike opposing detectors within the coincidence timing window. For this event the system will produce a false coincidence event due to the random nature, is known as a random or accidental event [Val03]. The result of this situation is that the LOR is spatially uncorrelated with respect to the activity distribution within the object. If the number of photon events N_1 and N_2 are detected in a pair of detectors in coincidence within the coincidence timing window '2τ', then the rate of random coincidences N_R is given by:

$$N_R = 2\tau \times N_1 \times N_2$$

where τ is the width logic pulses produced when a photon is absorbed in the detector. The rate of random coincidences is proportional to the square of the activity in the field of view because the count rates N_1 and N_2 are directly proportional to the activity in the field of view of the scanner [Phe06]. In addition the random rate is proportional to the width of the coincidence timing window.

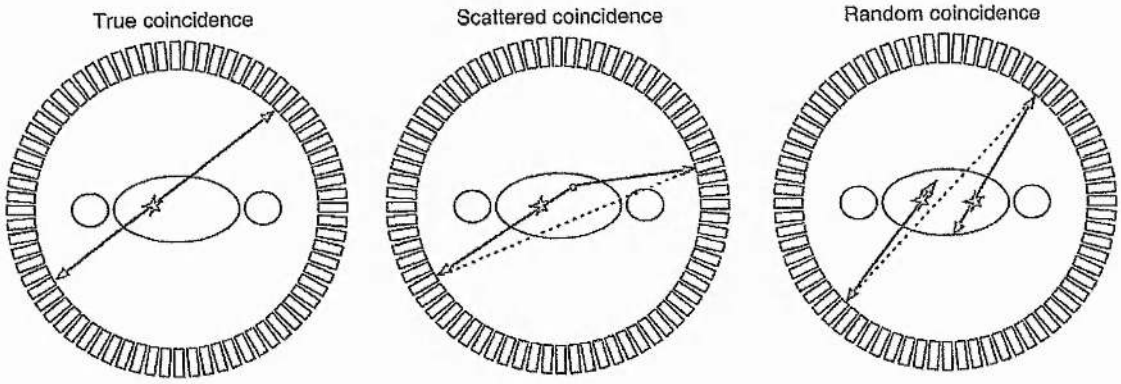

Figure 4.5: Type of coincidence events [Bad06]

Multiple coincidences are also possible to be involved in conventional PET. Multiple coincidences occur when three photons from different annihilation events are detected within the coincidence timing window. Due to the ambiguity in assigning a LOR, multiple coincidences are simply discarded from the prompt events [Val03].

4.6 Detection systems

Radiation detectors are developed upon the basis of the interaction of ionising radiation with matter. The probability of interaction within the detector, by 511 keV photons, is a function mainly of the photoelectric and Compton interaction. The inherent idea in these detectors is to measure the total energy lost or deposited by radiation upon passage through the detector. The radiation detectors convert the deposited energy into a measurable electrical signal or charge. The integral of this signal is then proportional to the total energy deposited in the detector by the radiation. There are two main types of material used in gamma-ray detection; scintillation and semiconductor materials. Scintillation materials are widely used

gamma-ray detectors that form the basis for almost all PET scanners in use today. Scintillation detectors are able to convert energy lost by ionising radiation into pulses of light. The light output is essentially proportional to the energy deposited within a crystal e.g. NaI(Tl). Other technologies for gamma-ray detection using semiconductor materials have been relatively neglected in PET but are likely to gain increasing attention to be practical detector materials for PET such as cadmium zinc telluride (CZT) that has a stopping power similar to NaI(Tl) at 511 keV [Phe06]. The choice of detector largely depends on the type of the study being undertaken whether high resolution or efficiency is required. Generally, scintillation detectors have high efficiency while semiconductor detectors have high energy resolution.

4.6.1 Scintillation detectors

Scintillation detection has been used since the earliest days of radioactivity and is still today employed to measure the whole range of radioactive emission. A scintillation crystal is a material able to convert energy lost by ionizing radiation into pulses of light [Gil95]. In any scintillation detector the collection of the largest possible fraction of the light is desirable to avoid losses in time and energy resolution. Since the scintillation light is emitted isotropically, only a limited fraction travels towards the surface at which the light-detecting device is mounted. The amount of light emitted is proportional to the amount of energy that is deposited in the crystal material. In order to increase the light collection, other faces of the scintillator are normally covered with reflective materials such as Al foil or paint. The scintillation light, which is being collected, is guided through the use of these reflectors to a photon detector usually a photomultiplier tube (PMT). The vast majority of commercial available PET scanners use PMTs due to their high gain (amplification), which leads to high signal-to-noise pulses, good timing properties, and convert the light photons into an electric pulse proportional to the intensity of the incident light and therefore the energy of the detected photon [Phe06]. The energy resolution and stability of a scintillation detector depends mainly on PMTs [Cru03].

A simplified structure of a typical photomultiplier tube (PMT) is illustrated in Figure 4.6. The PMT is attached behind the crystal which consists of an evacuated glass envelop. The three major components inside the tube are a photocathode, an anode and around 10-12 dynodes (electrodes). The main task of the photocathode is to detect

the scintillation light emitted from the crystal and convert it into electrons. The photocathode is made from a thin layer of material that can easily liberate electrons as energy is deposited in it. Each light photon from the scintillator has roughly 20-30% chance to liberate an electron [Kno00]. This probability is called the quantum efficiency of the PMT which is simply defined as the number of photoelectrons emitted over the number of incident photons. A high potential difference accelerates the electrons from the photocathode toward a positively charged electrode called the first dynode (coupled to an electron multiplier structure). The electrons are focused on a dynode which absorbs each electron and re-emits secondary electrons (normally 3 to 4) [Phe06]. These will then be focused on the next dynode. This process is repeated over and over until is reached the final dynode. After amplification through the multiplier structure, a typical scintillation pulse will give rise to $10^7 - 10^{10}$ electrons, sufficient to serve as the charge signal for the original event [Kno00]. Finally, the anode attracts the cascade of electrons producing an electrical pulse corresponding to each photon interaction in the scintillation crystal. Those pulses then pass through a circuit containing preamplifier to amplify and shape the signal for further processing.

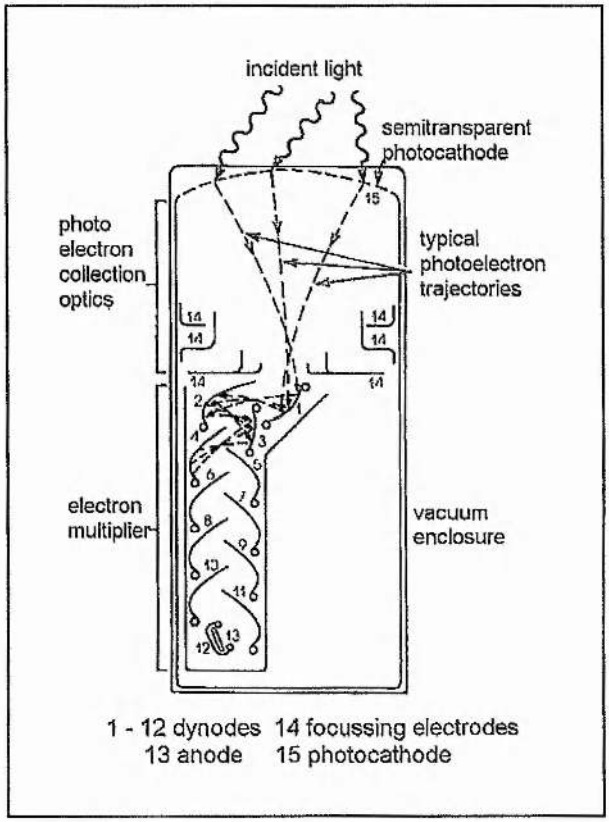

Figure 4.6: Schematic cross section through PMT showing its basic components [Kno00].

An alternative to the PMTs are photon detectors based on silicon photodiodes. There are two general designs of photodiodes, as possible substitutes for PMTs, conventional and avalanche photodiodes. Conventional photodiodes have no internal gain and operate by producing only one detected electron-hole pair per scintillation photon. This leads to reduce the signal-to-noise of the pulses which is roughly 10^6 times weaker than a PMT signal. This is generally not suitable for use in PET. A modification of the photodiodes leads to avalanche photodiodes which incorporate internal gain through the use of higher electric fields that increase the number of charge carriers that are collected. Here additional electron-hole pairs are created, therefore increasing the measured signal. Gain factors of a few hundred are typical yielding improved signal-to-noise over the conventional photodiodes. The quantum efficiency of the avalanche photodiodes is approximately 60% to 80%, providing a much more efficient conversion of photons to electrons than is possible with PMTs [Kno00, Ler01]. The avalanche photodiodes allow for a more compact PET scanner design and may in the future replace PMTs as the photon detector of choice [Phe06].

Scintillation detectors have found great use in PET not only due to their being fast but also because of their high detection efficiency. There are two main types of scintillators; organic-based liquids or plastics and inorganic scintillators which are ionic crystalline substances in the solid state. For the purpose of PET imaging, the scintillator crystal must be a dense material that can stop a large fraction of the incident 511 keV photons. For this reason, dense, inorganic, solid scintillators are the most commonly used detectors for PET. The efficiency of the scintillation process is negligible for inorganic scintillators without adding impurities called activators. There are two types of inorganic scintillators; activated scintillators such as sodium iodide (NaI(Tl)), which is the most commonly used inorganic scintillator activated with 0.5% thallium iodide. Lutetium oxyorthosilicate (LSO:Ce) scintillator becomes fluorescent through the introduction of a small amount of impurity dopant, cerium, into the pure single host crystal. The light output and the decay time for cerium doped scintillators can vary depending on cerium concentration, impurities and growing conditions. The second type is self-activated scintillators such as bismuth germanate (BGO), where the activator atoms are a major constituent of the crystal. The role of the activator is to

produce quantum energy levels, ground and excited states, within the forbidden gap. The electron and hole are transferred non-radiatively to the ionised dopant (activator) during migration in the crystal, creating their own activator-excited states. Relaxation of an electron trapped from an excitation level of the activation centre to the ground state results in the emission of a light quantum or scintillation photon.

The performance characteristics of a PET system will ultimately be defined by its geometry and physical properties of the detectors. The characteristics of an ideal scintillator include [Mel00, Kno00]: a) high detection efficiency, which requires high effective atomic number and high density for large cross-section of interaction; b) short decay constant, for good coincidence timing accuracy, low dead-time and high count-rate capabilities; c) high light output, for high spatial resolution and packing ratio of the detector elements with photomultiplier tubes (PMTs) or other photodiodes; d) good energy resolution, for the discrimination of scattered events; e) refraction index similar to that of the optical coupling of the photodetector (usually near 1.5) for optimal transmission of the scintillation light; f) good mechanical and physical properties e.g. non hygroscopic properties and ruggedness to allow fabrication of small crystals. The physical properties of some of the scintillator materials used or considered for use in PET are listed in Table 4.2. There is considerable variability in published values for a given material, most likely because of differences in impurity levels or variations in the optical quality of the samples.

Sodium iodide Na(Tl) has come to be accepted as the standard scintillation material for routine gamma-ray spectroscopy and imaging. It can be machined into a wide range of sizes and shapes. The detection efficiency of NaI(Tl) detectors generally improves with increasing crystal volume, whereas the energy resolution is largely dependent on the crystal growth conditions [Bra99]. It has an excellent light yield (38 photons per keV) apart from the new cerium-doped lanthanum crystals. The long decay time of NaI(Tl), 240ns is uncomfortably used for some fast timing or high counting rate applications [Kno00]. The crystal is to some extent fragile and can easily be damaged by mechanical or thermal shock. It is hydroscopic and will deteriorate as a result of water absorption if exposed to the atmosphere. Consequently, the crystal must be canned in an air-tight container for normal use, which reduces the geometric efficiency of the PET system. In addition, NaI(Tl) is sensitive to temperature,

therefore room temperature changes should be sought to minimize this [Gil95]. Increasing temperature leads to a drop in the scintillation yield, poor energy resolution and faster response (lower decay time) [Kno00].

Table 4.2: Summary of comparative properties of some conventional and new scintillator materials useful for PET (511keV) [Kno00, Val03, Mos05, Sal07].

Properties of Scintillator Materials	Sodium Iodide (NaI(Tl))	Bismuth Germanate (BGO)	Cerium-doped Gadolinium Oxyortho-silicate (GSO:Ce)	Cerium-doped Lutetium Oxyortho-silicate (LSO:Ce)	Cerium-doped Lanthanum Bromide ($LaBr_3$:Ce)	Cerium-doped Lanthanum Chloride ($LaCl_3$:Ce)
Density (g/cm^3)	3.67	7.13	6.71	7.41	5.29	3.79
Decay time (ns)	240	300	60	40	26	28
Light output (photons/511keV)	19400	4200	4600	13000	32200	25000
Effective atomic number (Z_{eff})	50	74	59	66	47	46
Refraction index	1.85	2.15	1.90	1.82	1.9	1.9
Wavelength (nm)	415	480	440	420	380	350
Hygroscopic	Yes	No	No	No	Yes	Yes

Bismuth germanate (BGO) has the best total absorption efficiency in comparison with other crystals used due to its high density and high effective atomic number. It is commercially available as crystals of reasonable size. It was a widely used detector material in PET systems. It is non-hygroscopic and hence the crystals can be mechanically subdivided, whilst remaining robust. The main problems associated with BGO crystals are relatively long scintillation decay time (300ns) and low light output reported at 10-20% lower than NaI(Tl), which result in relatively poor timing resolution and therefore limits its application at very high counting rates [Kno00].

Furthermore, its high refractive index (2.15) makes efficient collection of the light more difficult than for scintillators with lower index values. BGO remains two to three times more expensive than NaI(Tl). The light output from BGO decreases with increasing temperature as it is common with many other scintillators. Since the light output is already low at room temperature, its rapid dropoff severely limits the usefulness of BGO in high temperature applications.

It was realized, in the late 1980s, that the cerium activator could be incorporated into new categories of crystals, resulting in scintillators with reasonably good light yield. The principal decay time of cerium luminescence ranges from about 20 to 80 ns, depending on the host crystal [Kno00]. Cerium-doped gadolinium oxyorthosilicate (GSO:Ce) can be grown in reasonably large sizes as single crystals and the atomic number of 64 for gadolinium offers attractive properties in gamma-ray spectroscopy. GSO:Ce has lower density compared to BGO and higher light output, therefore producing better timing and energy resolution than BGO. The total light output is about 20% of that of NaI(Tl).

Cerium-doped lutetium oxyorthosilicate (LSO:Ce) was first described as a scintillator in 1991. It has a light output 75% that of Na(TI) and a fast scintillation time of 40 ns. The rapid light decay provides significantly reduced detector dead time and thus higher counts rate capabilities. High count rate performance is essential in clinical PET imaging to use the injected activity most efficiently, and to make the emission scan time as short as possible at an acceptable image quality. The improved time resolution of the LSO detector also allows a narrower coincidence time window and therefore a reduction in random coincidences and scatter. Together with the excellent light output relative to other high-density scintillators this makes LSO the fastest detector available for PET tomographs today. There are two significant disadvantages of LSO that decrease its usefulness for low energy SPECT imaging and also for low background applications due to the naturally occurring unstable lutetium isotope (Lu-176). The second disadvantage of LSO is that it does not have the energy resolution that is expected for such high light output. The resolution at 511keV is a significant improvement over BGO but is not as good as NaI(Tl).

The recent improvement in the growth and packaging of cerium-doped lanthanum halide scintillators, lanthanum bromide ($LaBr_3$:Ce) and lanthanum chloride ($LaCl_3$:Ce), in addition to their superb intrinsic properties of high light output, excellent energy resolution, and fast decay time, make them a viable detection material for PET [Sur03, Kuh04, Lee05]. The most important characteristic of these crystals is represented by the scintillation light yield proportionality as a function of incident gamma ray energy. This involves an absolute innovationa in gamma- ray imaging with the possibility of energy resolution values nearly halved with respect to the past (3-4% at 511keV) [Sha04, Pan07]. Furthermore, it has been reported that the energy resolution of $LaBr_3$:Ce at 662keV approaches that of room temperature semiconductor detectors such as CdTe and CdZnTe [Sha04]. However, the cerium-doped lanthanum halide scintillators have a few drawbacks of their own; internal radioactivity, hygroscopic nature, and a low-energy response that results in the resolution being inferior to that of NaI(Tl) below approximately 100 keV. The internal radioactivity is due to naturally occurring radioisotopes La-138.

4.6.2 Semiconductor detectors

A semiconductor material is packed into separate energy bands and an electron must be confined to one of these bands [Tso83]. The lowest energy band is called the valence band which, in an idealized semiconductor is full of electrons that are bound to the lattice sites within the crystal. The next highest energy band is called the conduction band and in an idealized semiconductor represents an empty band (at temperature equal to zero Kelvin) where the electrons are free to migrate through the crystal. These two energy bands are separated by an energy gap, called the bandgap. The size of this gap is the main factor is classifying the material as a semiconductor or as an insulator; it is about 1 eV in a semiconductor and 5 eV in an insulator [Kno00].

If a gamma-ray photon enters the detector and is photoelectrically absorbed by the semiconductor detector crystal, this will produce a photoelectron that jumps from the valence band (leaving a vacancy or hole) to the conduction band of the crystal. This means that an extra electron is still in the conduction band and an extra hole in the valence band. Applying an electric field across the region causes the negatively

charged electrons to move in the opposite direction to the effective movement of the positively charged holes. Then the charge released by the ionization can be collected and the presence of gamma rays recorded [Kno00].

The value of the energy gap is not constant and changes with temperature [Kno00]. As a general rule for semiconductor materials, the energy gap initially increases linearly as the temperature decreases. However, at very low temperatures, the energy gap reaches a constant value. Therefore, when the temperature is greater than absolute zero, the electrons in the crystal lattice will share thermal energy, giving a probability that an electron can be thermally excited across the band gap into the conduction band. In the case of semiconductor materials, the energy gap is small, Ge (0.7eV) and Si (1.1eV), and gives a large probability of thermal excitation, creating unwanted noise at room temperature (300 K). This thermal noise can be significantly reduced by cooling the semiconductor crystal to liquid nitrogen temperature (77 K) [Del92].

Germanium (Ge) is the most common semiconductor detector material. It has high atomic number (Z=32) higher than silicon (Z=14), which makes Ge practicable for use in the detection of higher energy gamma radiation. However, it is difficult to prepare any material completely free of impurities as in semiconductors; these impurities can have a great effect upon the conductivity. To control the electrical conduction in semiconductors, a small amount of impurities is added to the lattice in a process called doping. The idea of this process is to increase the number of charge carriers (electrons or holes) by adding a material with free charge carriers. In the 1960s, the lithium drifted technique started to be used. The main disadvantage of that type of detector was that it had to be kept cold at all times otherwise the lithium migrated outside the crystal lattice. By decreasing the impurity in the germanium crystal, an active volume can be obtained that was comparable and even larger to those available in Ge(Li) detectors. These detectors are called intrinsic germanium or high purity germanium detectors (HPGe). The major advantage of this type of detector is that room-temperature storage is acceptable because of the absence of lithium drifting [Del92, Kno00]. The energy required to create an electron-hole pair in HPGe detectors is about 3eV. This means that a large number of electron-hole pairs can be formed, and so many charge carriers are released for each gamma-ray interaction. This has two

consequences. Firstly there is a small statistical fluctuation in the number of charge carriers per pulse, and secondly, as a result of the large number there is an excellent signal to noise ratio, and therefore a good energy resolution [Kno00].

Cadmium Telluride (CdTe) and Cadmium Zinc Telluride (CdZnTe) have been regarded as promising semiconductor materials for hard x-ray and γ-ray detection (Eisen et al 1999) and (Scheiber 2000). The high atomic number of the materials (Z_{Cd}=48, Z_{Te}=52) gives high quantum efficiency suitable for a detector operating typically in the 10 - 500 keV range. However, due to incomplete charge collection caused by the low mobility and short lifetime of holes, the energy resolution does not reach the theoretical limit expected from statistical fluctuations in the number of electron-hole pairs. These detectors have high resistivity because of the wide bandgap and also have high photon absorption efficiency because of the large effective atomic number. The electron-hole pairs generated in CdTe and CdZnTe detectors by irradiating with γ-rays cannot be fully collected because of the low transport properties of carriers. This leads to a significant distortion of the spectrum. CdZnTe has become a material of considerable interest in the field of x-ray and γ-ray imaging, and shows great promise as a highly efficient, room-temperature operation detector. The feasibility of using these materials for detection efficiency and scatter rejection capabilities at diagnostic energies has been investigated (Heanue et al, 1996). The timing properties of CdZnTe detectors for positron emission tomography have been investigated (Bertolucci et al, 1997 and Amrmami et al, 2001). The wide band gap allows their use at room temperature and the energy per electron-hole pair offers much better resolution compared to other gamma rays detectors which can be operated at room temperatures, such as the widely used NaI(Tl) detectors. The main properties of CdZnTe detectors are compared with other semiconductor detectors are shown in Table 4.3.

Table 4.3: Summary of comparative properties of some semiconductor detectors [Kno00, Del92].

Properties	Bandgap (eV) 300k	Energy e-h (eV)	Mobility lifetime (e)	Mobility lifetime (h)	Atomic Number	Density g/cm^3
Ge	0.67	2.96	High	High	32	5.35
Si	1.12	3.61	High	High	14	2.33
CdTe	1.5	4.43	Medium	Low	50	6.2
CdZnTe	1.57	4.64	Medium	Low	49.1	5.78

4.7 The positron and positronium fundamental theory

Positron decay occurs in unstable proton rich nuclei which reduce the excess positive charge in the nucleus thereby undergoing beta positive β+ decay [Hil04]. When the positron loses almost all of its momentum energy, it eventually either annihilates with a free electron or combines with an electron to form positronium (Ps). Figure 4.7 shows a flow diagram for the positron annihilation and the ratios are for pure water and depend on the medium [Spy04]. Free positron and positronium annihilations can be distinguished by the differences in their annihilation lifetimes. The most probable of these annihilation processes, when the positron and electron are in a singlet spin state, is the two photon process. In the case of a free positron, the ratio of the cross section for the three-photon to two-photon events is ≈1/372 [Gre64].

4.7.1 Positronium formation and annihilation mechanisms

The positronium atom (Ps), the bound state of a positron and an electron, can be formed, whenever a positron interacts with matter, in the two spin states, S = 0, 1. The singlet states (S = 0), in which the electron and positron spins are anti-parallel, is called para-positronium (p-Ps), whereas the triplet states (S = 1) are called ortho-positronium (o-Ps). The spin state has a significant influence on the energy level structure of the positronium, and also on its lifetime against self-annihilation. The probability of annihilation decreases very rapidly with the number of photons emitted.

For practical purposes the singlet spin states decay into two photons, four photons etc. (even numbers of photon) and triplet states into three, five etc. (odd numbers of photons) [Gre64, Cha01].

Due to spin statistics, about 25% of all positronium (Ps) is formed in the singlet state while the remaining 75% form in the triplet state. The singlet state, para-positronium (p-Ps) decays primarily into two 511 keV gamma rays with a lifetime of 0.125ns in vacuum, while the triplet state ortho-positronium (o-Ps) decays into three gamma rays of different energies adding up to 1022keV in the same plane, with a lifetime of 142ns in vacuum. However, depending on the medium, the lifetime of the Ps, particularly o-Ps, will be changed. This is due to 'quenching' collisions with the surrounding medium [Cha01, Kac04].

In matter, interactions with the surrounding electrons (quenching) typically prevail leading to a direct annihilation of the positron with one of the electrons (pick-off process), the conversion of o-Ps into p-Ps which then decays rapidly to two gamma or to chemical reactions producing short-lived Ps compounds. As a result of the above factors, the effective yield of three gamma annihilation in matter depends on the rates of Ps formation and quenching that, in turn, depends on the fast timescale Ps chemistry in the terminal spur of the positron track. In non-metallic materials, like water, the three gamma yield is usually of the order of 0.5% although in some cases, for example fine powders of alkaline oxides, it can reach 20% or more [Bus64, Hus89, Kac04]. Ps formation in water might be suppressed from the polar molecule as the electron density around the positron may increase [Kan65]. Preliminary results showed by Murtagh et al [Mur06] that Ps formation in water collisions is non-negligible and it has been found to be 6 times larger than a previous estimate [Sue00].

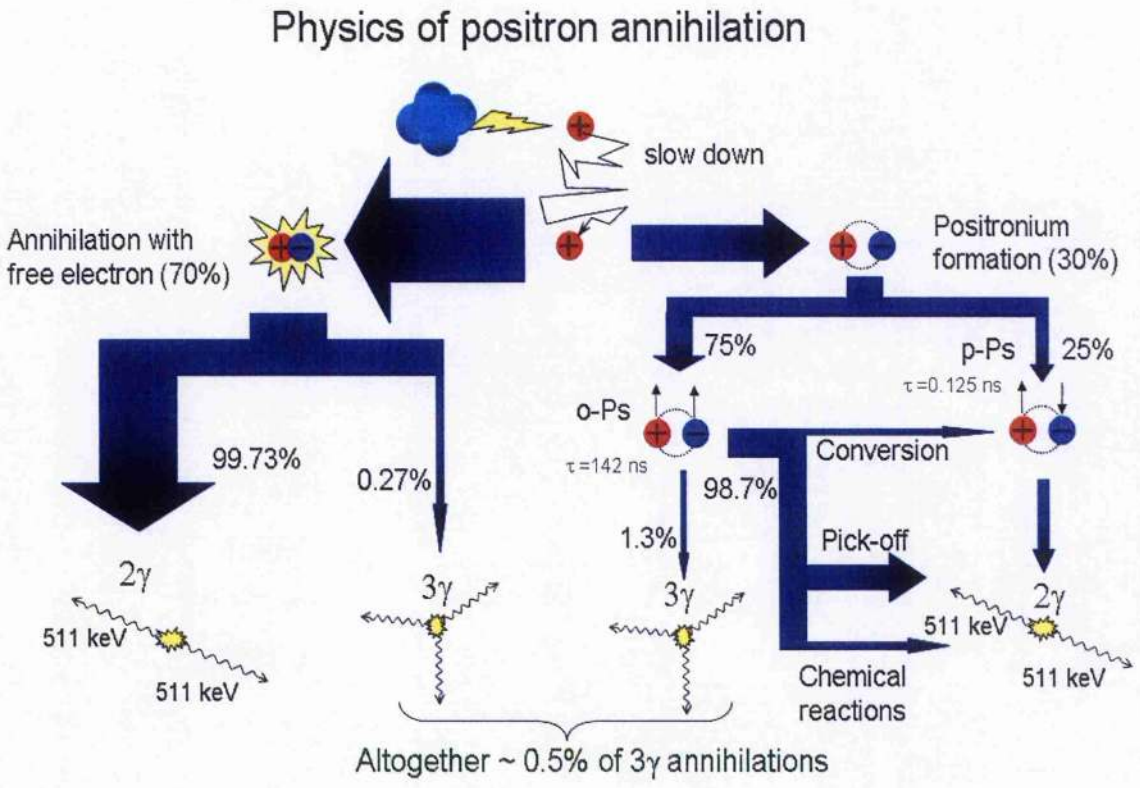

Fig 4.7 Flow diagram for positron annihilation in pure water [Spy04].

It is expected from the spin statistics that positronium will in general be formed with a ratio of o-Ps to p-Ps equal to 3:1, and in the absence of any significant quenching (e.g. via the conversion of o-Ps to p-Ps), most of the o-Ps which are formed will eventually annihilate in this state. Thus, the three gamma-ray annihilation mode will be much more abundant for positronium than it is for free positron annihilation. The three gamma-rays are emitted in a coplanar fashion, with predicted energy distributions by Ore and Powell, 1949; and Adkins, 1983; shown in Figure 4.8 (a) along with an experimental observation by Chang et al 1985 [Ore49, Cha85]. The difference between the near-monochromatic 511keV radiation of free positrons and that of the three gamma-rays annihilation mode allow one way in which to distinguish between these two annihilation modes. This is shown in figure 4.8 (b), which shows gamma-ray energy spectra obtained using a high resolution detector under conditions of 0% and 100% positronium formation by Lahtinen et al 1986 [Cha01].

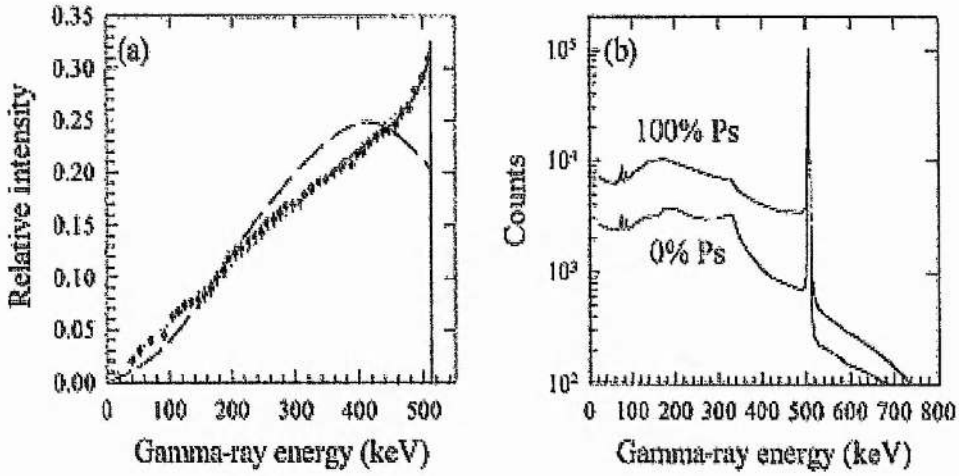

Figure 4.8: (a) The gamma-ray energy spectrum for the three photon decay of ortho-positronium (dashed curve: theoretical). (b) Schematic gamma-ray energy spectra taken using a high resolution detector under conditions where the fraction of positrons forming positronium is 0% and 100% [Cha01].

4.7.2 Positronium quenching

The term quenching expresses the increased probability of annihilation of positronium, with an electron in a relative spin singlet state, leading to the emission of 2γ rays [Cha01]. Experimentally, it means the reduction in the observed three gamma or triplet type positron annihilation events as the reduction of positronium life time [Gre64]. The most noticeable quenching is o–Ps due to the long relative lifetime of p–Ps [Hey61, Hop90]. There are different processes which control quenching depending on the chemical nature of the atoms or molecules. The three predominant mechanisms of ortho-positronium quenching in collisions with an atom or molecule, denoted by X, can be summarized as follows:

4.7.2.1 Pick-off quenching

Pick-off quenching takes place when ortho-positronium (o-Ps) collides with atoms or molecules (X) which have filled outer electronic shells then the positron of the positronium can annihilate with the surrounding electrons in a collision and annihilate in two gamma rays:

$$\text{o-Ps} + \text{X} \rightarrow \text{X}^{+} + \text{e}^{-} + 2\,\gamma\text{-rays}$$

The cross section of this annihilation process is about 10^{-21} cm^2. Pick-off annihilation cross section is smaller than other quenching mechanisms however, when the atom has a closed shell or subshell then it becomes the dominant decay process for o-Ps [Iva02]. The decay rate of o-Ps is proportional to the rate of o-Ps collisions with the atoms or molecules of the material and thus with the electron density [Cha01].

4.7.2.2 Conversion quenching

Conversion or exchange quenching occurs with substances possessing unpaired electrons in their atomic or molecular structure, such as O_2 and NO. It is possible for the electron of the o-Ps to be exchanged with an atomic electron with different spin orientation and to be converted to p-Ps according to

$$\text{o-Ps} + \text{X}(\uparrow) \rightarrow \text{p-Ps} + \text{X}(\downarrow)$$

The conversion cross section is larger than the direct pick-off annihilation cross section. It is of the order 10^{-19} cm^2. The cross section for conversion quenching is decreased as the positronium energy is increased.

4.7.2.3 Chemical quenching

Ortho-positronium (o-Ps) is quenched after forming chemical complexes, which may occur by means of the addition or substitution reactions both of which lead to rapid annihilation of the positron

$$\text{o-Ps} + \text{X} \rightarrow \text{o-PsX} + \text{energy}$$
$$\text{o-Ps} + \text{XY} \rightarrow \text{o-PsX(Y)} + \text{Y(X)}$$

The cross section for the chemical reactions varies depending on the process and the reactive species involved. The cross section for the chemical reactions is much higher than pick-off quenching. It has the most prolific quenching reaction, with a cross section of 10^{-16} cm^2.

In the literature, some basic theoretical problems regarding the values of pick-off, collision and chemical quenching rates of o-Ps with atoms or molecules have still not

been fully solved. However, some progress has been made experimentally. Table 4.4 shows the major quenching reaction for some gases. There are two kinds of gases, inert and active, for the quenching of o-Ps. The inert gases, N_2, Ar, H_2, CH_4, etc., are also inert in an ordinary chemical sense and quench o-Ps mainly by pick-off process. The active gases can be classified into two classes. The gases in the first class quench o-Ps mainly by conversion process, e.g. O_2, NO. The gases in the second class quench o-Ps predominantly by chemical reaction, e.g. NO_2 and halogens. These are also very active chemicals at room temperature [Tao73, Cha01].

Table 4.4 : Major quenching reaction for some gases [Tao73, Cha01]

Gas	Major quenching reaction
Ar	Pick-off
H_2	Pick-off
N_2	Pick-off
CO_2	Pick-off
CH_4	Pick-off
O_2	Conversion
NO	Conversion
NO_2	Chemical
Cl_2	Chemical
Br_2	Chemical

One of the most interesting gases for which low energy positronium interactions have been studied is O_2. This has been the subject of many experimental studies with different methodologies used and has been shown to exhibit both elastic and inelastic exchange quenching [Kak90, Cha01]. Heymann et al [Hey61] found that oxygen and nitric oxide quench too powerfully for the same method to be used. Figure 4.9 shows the observed two spectra of Na^{22} due to the quenching of o-Ps in gases, (Heymann et al 1961). The broken curve is the spectrum when the chamber contained only argon. The solid curve is the spectrum when sufficient nitric oxide (3%) had been added for conversion quenching to remove the three photon annihilation counts from the valley region between 300-440keV and produce a corresponding increase in the photopeak

of 511keV. Celitans et al (1964) used a three-photon coincidence method [Cel64a] and positron lifetime method [Cel64b] to study *o*–Ps formation and quenching in gases. They concluded that the highly quenched *o*–Ps lifetimes were found in oxygen, even at pressures as high as 16.5 atm. Cooper et al (1967) found a reduction in *o*–Ps lifetime by oxygen dissolved in various liquids [Coo67]. Hopkins et al (1990) found the introduction of oxygen into a silica gel sample results in a decrease in the *o*–Ps lifetime [Hop90].

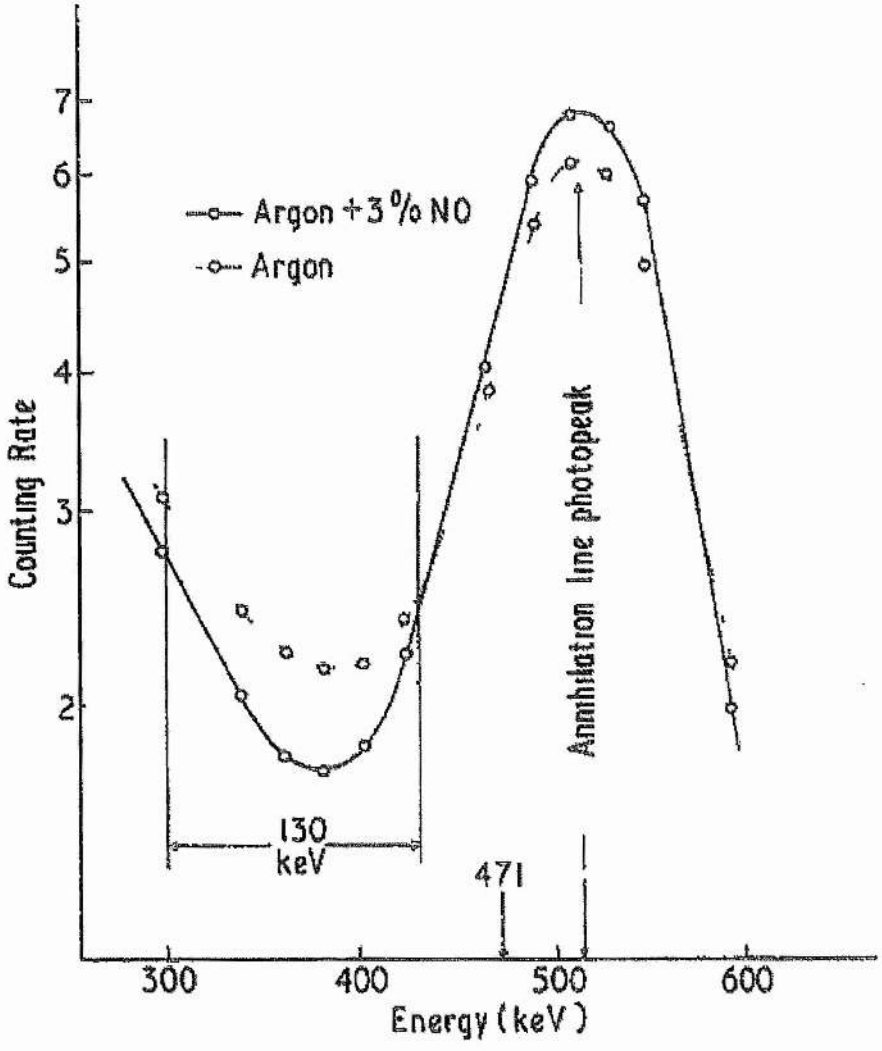

Fig 4.9: Positron annihilation spectra with different nitric oxide concentration [Hey61]

In metals positrons thermalize quickly (<10psec) while their lifetime is ~100psec. This implies that positronium cannot be formed due to the high electron density which screens the Coulomb interaction between positrons and electrons. In a number of insulators the positron lives longer than in metals. It was discovered that in certain materials such as quartz and Teflon, the positron decay curves could not be interpreted in terms of a single life, but resulted from the composite effect of two different lives [Bel53]. Bell and Graham (1953) suggested that positronium is formed in these insulators to explain the presence of these two mean lives. Para-positronium decays promptly and accounts for the short life, ortho-positronium accounts for the longer life, which is a measure of the rate at which it is destroyed in molecular collisions. In agreement with this view, the frequency of three photon annihilation is noticeably greater in the insulators which exhibit the longer positron life [Deb54].

4.8 Two and three photon coincidences

The basic process employed in conventional PET is the annihilation of a positron and an electron that results in two 511 keV gamma ray photons. When these photons are detected in coincidence, a positron annihilation event is recorded along the axis connecting the two detectors. The 2γ decay is, however, not the only available route to positron annihilation. Multiphoton processes are also possible, although their probabilities decrease strongly with the number of decay quanta involved. In the context of PET, one may find the remark that the rates of these events are small and hence do not affect the imaging. In practice, apart from 2γ annihilation, only the decay into three photons is measurable [Deb54, Bas54, Ber65, Man70]. In fact, 4 γ [Ada90, Bus94] and 5 γ [Mat96] decays have also been detected experimentally, but due to a very low probability they cannot be practically used in PET.

Although measurements of the three photons are being used for several years in material science, it has not yet been put into practice for medical applications. The industrial applications of 3γ PET has been used [Van88], in particular in studies of flow and diffusion (especially of gases) in porous media [Kha98], and imaging of their structure. Having a material bereft of water and oxygen and containing microscopically large empty spaces (pores) one can expect much higher 3γ yields making the method more efficient. Kacperski and Spyrou (2004) proposed, for the

first time, to use the 3γ annihilations as an imaging modality, potentially carrying a new kind of clinically valuable information not only about the location, but also the state of oxygenation of tumours.

The double coincidence method of studying two photon positron annihilation is quite simple, not only because of the simple construction of the coincidence apparatus but also because of the high coincidence rate obtained from a relatively week source. However, double coincidence is normally only used in determinations of the angular distribution of the two-photon positron annihilation events. The extension of the coincidence method to three photon positron annihilations, however, introduces more difficulties. In the case of two photon positron annihilations, energy momentum conservation requires that the two gamma rays are emitted in almost opposite directions. In the case of three photon positron annihilations, momentum conservation requires only that the gamma rays are emitted in the same plane and that no more than two in the same half-plane.

Three-photon annihilation coincidence measurements can be made by placing a detection system which consists of three detectors having high energy resolution and efficiency. Three-photon decay occurs when a triplet positron-electron pair annihilates, as when ortho-positronium decays. The three-photon energies can vary between 0-511 keV and their sum is equal to 1022 keV. Energy and momentum conservation does not require a unique directional correlation between the three photons, only that they are emitted in the same plane and no more than two in the same half-plane. Hence the detector and the sample must be placed in coplanarity. A detail of the concept of three-photon positron annihilation imaging is given in Chapter 7.

Chapter 5

Biological oxygen measurement techniques

5.1 Introduction

Positron emission tomography (PET) is a powerful imaging technique for the diagnosis of cancer. A PET scan with additional information about the oxygen levels within tissue would be a useful tool for measuring and imaging oxygenation of tissues in various clinical contexts. Thus the relation between oxygen measurements and the yield of three photon positron annihilation events will open a new field of interest for the diagnosis and treatment of cancer, specifically for tumour hypoxia (radio-resistance). The early diagnosis and determination of tumour hypoxia is very important to novel treatment strategies in planning cancer therapy because hypoxia may be a predictive factor for the occurrence of metastasic disease [Bri95]. There are diverse techniques using biological, chemical or physical methods for the measurement of tumour hypoxia. However, the oxygen level is usually very varied both among patients and within individual tumours [Har 04, Vau01, Pad05].

The studies undertaken examined the experimental procedures to determine oxygen saturation in biological samples as a preliminary study for further sample analysis for a UniS prototype three-gamma PET scanner under development. In addition, to establishing a frame work and documentary information for the PET research group carrying out experimental work which involves imaging the oxygen levels in biological samples. Dissolved oxygen (DO) content (% or mg/L) of defibrinated horse blood and mineral water were investigated by comparison the two main methods of polarography and colorimetery. A compound, AnaeroGen^{TM}, was employed to remove oxygen from the sample environment to allow low oxygen studies [Ana05]. An air pump was used to increase the oxygen content in the samples.

Efforts have been made in this chapter to describe the preparations and the methods employed to measure the oxygen level in biological samples using blood and mineral

water in order to obtain samples with low levels of oxygen in hypoxic regions and normal levels of oxygen for normoxic concentration. Preparation of these samples will help further studies to be conducted in order to investigate the relation between oxygen measurement and three photon positron annihilation using positron emitter e.g. ^{18}F. This will open a new area that helps in the diagnosis and treatment of cancer as well as helping in the development of non-invasive methods for detection of tumour hypoxia by using the dedicated three gamma PET technique.

5.2 Materials and methods

Two instruments were used for sample analysis; a dissolved oxygen meter DO400 and a dissolved oxygen pocket colorimeter. In each case 40mL of samples were treated with AnaeroGen™ substance or a pump aerated system. AnaeroGen™ should induce an anaerobic condition in the samples while the pumping system was applied to increase the dissolved oxygen content in the samples.

The dissolved oxygen meter DO400 employed in the experiments is a portable water-resistant, microprocessor-based and autocalibration dissolved oxygen meter (Figures 5.1 and 5.2). It has applied to measure dissolved oxygen at different temperatures in water and other liquids. The dissolved oxygen amount can be indicated up to hundredths of parts per million (ppm) which can be equated to milligrams per litre (mg/L) or in % of saturation. The temperature range covered was from 0 to 50°C and the estimated accuracy, as quoted by the manufacturer, was ±1.5% [Han05].

The Pocket Colorimeter instrument is a high-quality filter photometer designed for single-parameter colorimetric measurements (Figure 5.3). It is calibrated to measure dissolved oxygen in samples ranging from 0 to 10.0 mg/L. The liquid crystal display provides a direct readout in mg/L oxygen once calibrated. It consists of a light emitting diode (LED) (528 nm wavelength and 15 nm filter bandwidth), silicon cell detector, and is powered by batteries which make it portable. The estimated accuracy, as quoted by the manufacturer, was ±0.2 mg/L. A high range dissolved oxygen (AccuVac Ampul®) reagent was used for the investigation of the sample to develop the colour with sample [Hac05].

1) Battery Compartment
2) Probe Connector
3) Liquid Crystal Display
4) ON/OFF Button
5) CAL Button (to enter or exit calibration mode)
6) FACTOR button (to select altitude F1 and salinity F2)
7) UP and DOWN arrow keys (to select F1 and F2 levels)
8) HOLD key (to freeze displayed value)
9) RANGE button (to select ppm or % of saturation)
10) Power Jack for 12VDC adapter
19) LOW BAT indicator
20) SAMPLE indicator (to indicate the measurement mode)
21) F1 indicator (altitude factor)
22) F2 indicator (salinity factor)
23) % or ppm mode indicator
24) Temperature (and factor) display

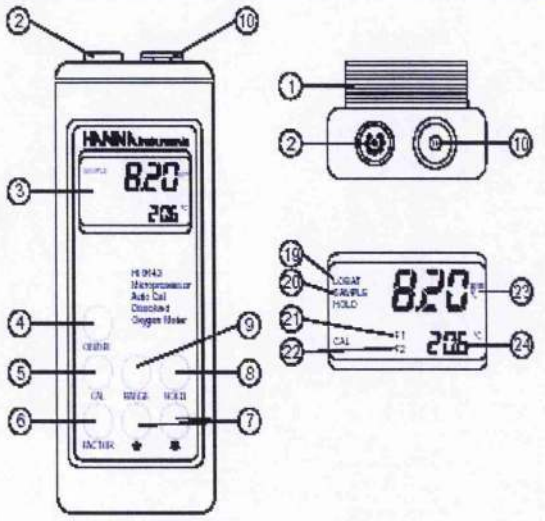

Fig. 5.1 Functional description Dissolved Oxygen Meter [Han05].

1. D.O. Probe
2. Protective Cap
3. Watertight Shielded Cable
4. Polypropylene Probe Body
5. Temperature Sensor
6. O-Ring Seal
7. Silver Chloride Anode (sensor element)
8. Platinum Cathode (sensor element)
9. Oxygen Permeable Teflon Membrane
10. Protective Cap

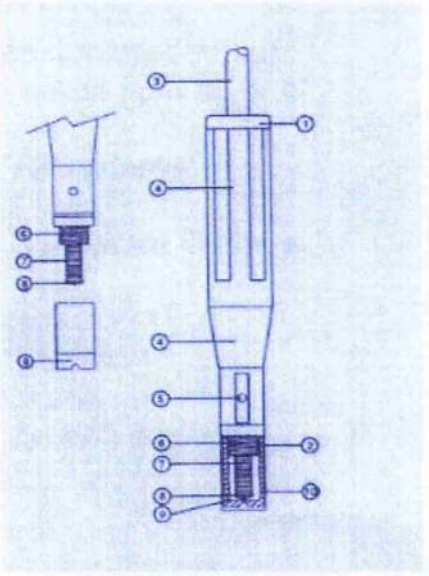

Fig. 5.2 Functional description dissolved oxygen probe [Han05].

1. Pocket Colorimeter, Dissolved Oxygen meter.
2. Dissolved Oxygen High Range AccuVac Ampuls.
3. snapper.
4. Sample Cell, 10 mL.
5. blue ampule cap.
6. the instrument cap
7. Zero button.
8. Read button.
9. Liquid Crystal Display

Fig.5.3 Dissolved Oxygen Pocket Colorimeter

The AnaeroGen™ was used to generate an anaerobic environment. It contains ascorbic acid and activated carbon which reacts on contact with air. When the AnaeroGen™ is placed in a sealed jar, atmospheric oxygen in the jar is rapidly absorbed with the simultaneous generation of carbon dioxide. This technique differs from those commonly used since the reaction occurs with no evolution of hydrogen, and therefore requires no catalyst. Also no addition of water is needed to activate the reaction. The AnaeroGen™ will reduce the oxygen level in a jar to below 1% within 30 minutes and the resulting carbon dioxide level can be between 9% and 13%. This product is for *in-vitro* use only. As soon as the AnaeroGen substance is exposed to the air, the reaction will start. It is therefore essential that the paper is placed in the jar and the jar sealed within one minute. The reaction of the ascorbic acid with oxygen is exothermic. However, the temperature of the AnaeroGen paper will not exceed 65°C. Making sample temperature measurement of further importance.

The defibrinated horse blood was supplied by TCS Biosciences Company. Still natural mineral water (TESCO Ashbeck mountain spring) contained 10 mg/L calcium, 2.2 mg/L magnesium, 10 mg/L sodium, 2.3 mg/L potassium, 13 mg/L bicarbonate, 15 mg/L chloride, 11 mg/L sulphate, 20 mg/L nitrate, <0.1 mg/L fluoride, and <0.01 mg/L iron.

5.3 Results

5.3.1 Polarography Technique

Figure 5.4 shows the percentage of dissolved oxygen content in 40ml mineral water using polarography technique (DO400 probe). The sample was treated for 25 hours in a continuous pumped airflow through it (air-pump treated sample). Dissolved oxygen in mineral water was monitored showing 4.4(±1.5)% rate of increase in DO content over 25 hours of air pumping treatment. This procedure could not be applied for defibrinated horse blood and DO content could not be monitored or detected due to the frothing seen in the blood with loss of the volume of sample under increased air pressure. Figure 5.5 shows the immediate reading of DO content after applying AnaeroGen™ in mineral water was found to be 5.3(±1.5)% and increased to 70.1(±1.5)% after one hour of exposing the sample to atmospheric air. However, results for blood were found to be 14 (±1.5)% increasing to 29.1(±1.5)% after one hour. These results indicate that the rate of DO uptake in blood is slower than that in mineral water.

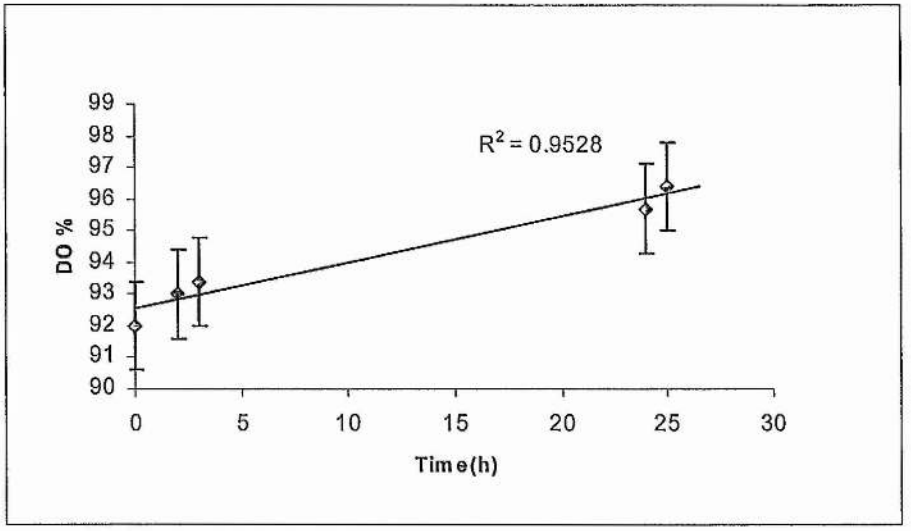

Fig. 5.4 Dissolved oxygen in mineral water using DO-400 probe (air-pump treated sample)

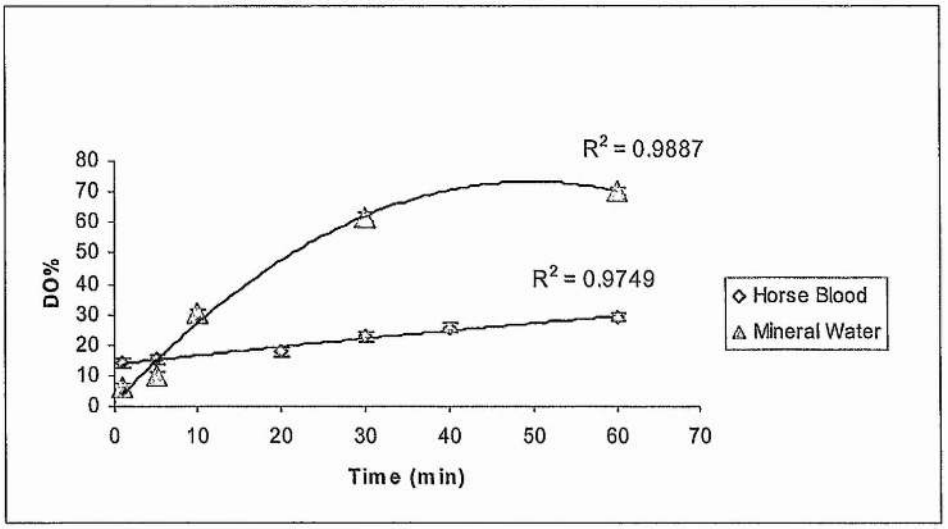

Fig. 5.5 Dissolved oxygen in mineral water and horse blood using DO-400 probe (AnaroGen treatment)

5.3.2 Colorimetery Technique

Figure 5.6 shows dissolved oxygen content (mg/L) of mineral water using the pocket colorimeter. The sample was treated for 3 hours of continuous pumped airflow through the sample. Dissolved oxygen was monitored showing 0.4(±0.2)mg/L rate of decrease in DO content over 3 hours of air pumping treatment. In Figure 5.7 the sample was treated with AnaeroGen™. Dissolved oxygen was monitored showing 5.3(±0.2)mg/L rate of decrease in DO content over 30 minutes of exposing the sample to atmospheric air after treatment with AnaeroGen™. These figures show a decrease in the DO as the time increases. However, this technique is not suitable for the measurement of DO content in blood, due to the high light absorption of the pocket colorimeter in the blood so all measurements of the horse blood sample indicated zero.

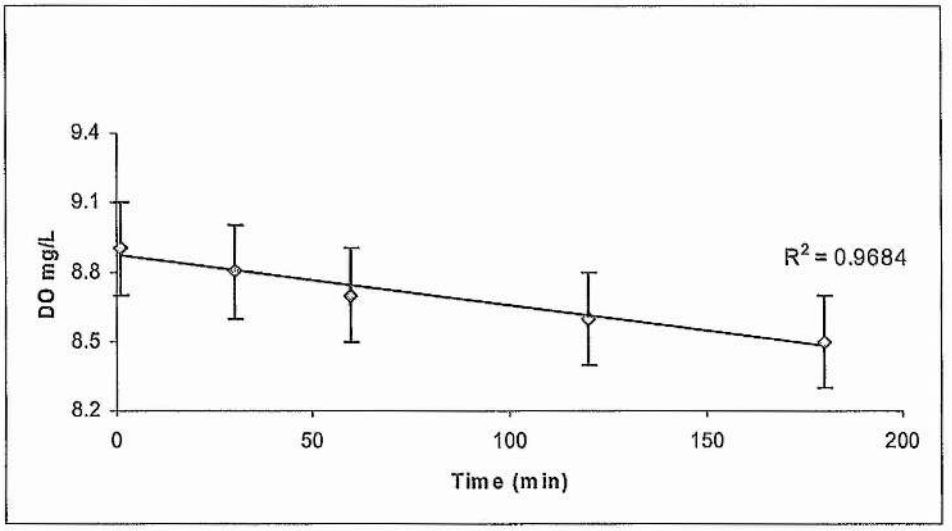

Fig. 5.6 Dissolved oxygen in mineral water using pocket colorimeter (air-pump treated sample)

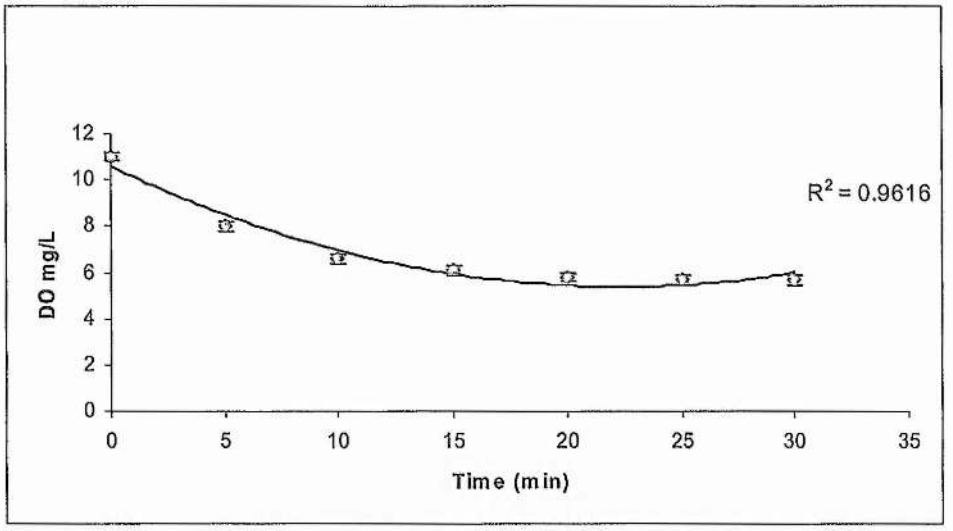

Fig. 5.7 Dissolved oxygen in mineral water using pocket colorimeter (AnaroGen treatment)

5.4 Discussion

In this experiment, a comparison between polarography and colorimetery methods were used in the measurement of dissolved oxygen content in mineral water and defibrinated horse blood samples. The samples were either treated with AnaeroGen™ or increased oxygen content using a pump aerated system. A defibrinated horse blood

sample was chosen here to reduce the hazards and implications of working with human biological sample infection e.g. AIDS or hepatitis.

There are several reports dealing with the properties of horse blood and no comprehensive study has been published on the reactivity of horse blood towards organic phosphate, 2,3-diphosphoglycerate (DPG). The production of DPG increases when the peripheral tissue oxygen's availability decreases, such as in the condition of hypoxia. It has been reported [Gia90] that horse haemoglobin displays a lower oxygen affinity (approximately 60%) in contrast to human haemoglobin. High oxygen affinity has been related to the interaction of the organic phosphate, DPG with red blood cells. Horse's haemoglobin appears to be much less sensitive to organic phosphate and therefore displays a much lower oxygen affinity. The results indicated in figure 5.5 show that the rate of dissolved oxygen uptake in blood is slower than that in mineral water. These results are expected on the basis of the data available in the literature [Tor03] that oxygen does not dissolve easily in plasma and about 97% of oxygen has combined with human haemoglobin due to the fact that the haem group contains a ferrous iron atom, which is capable of carrying oxygen molecules.

It is confirmed through the experiments, that the colorimetric method may not be an efficient method in the measurement of DO concentrations in blood, due to the high absorption characteristics of blood. To overcome this problem, the blood could be diluted and the factor of dilution should be considered in the calculations of the correct concentration of DO in blood. Thus, the colorimetry method is not a suitable method for the measurement of DO concentrations in this research as dilution of the blood may disrupt the proteins and induce rupture of cells in the sample. Moreover, the chemical reagent used in colorimetry can impose a colour change to the solution which may act as interference in % transmittance or absorbance measurements recorded by the instrument.

A gradual increase in DO content as time increased was observed in samples using the polarography probe in both treatments (Figures 5.4 and 5.5) whereas using the pocket colorimeter a decrease in the DO content was shown as time increased (Figures 5.6 and 5.7). This finding was not as expected on the basis of the direct proportionality between DO and pumping airflow time through the sample in Figure 5.3 or after being

treated with AnaeroGen™ Figure 5.4. These results may be due to the presence of magnesium in the mineral water, which can cause a negative interference in the pocket colorimeter.

5.5 Conclusion

In this study, efforts have been made to highlight the advantages of the polarography technique for measuring different levels of dissolved oxygen in blood. Low levels of oxygen in hypoxic blood samples were obtained experimentally here by using AnaeroGen™. Further research is continued, in the next chapter, to study the factors that affect dissolved oxygen e.g. pH, temperature and CO_2 on the influence of blood oxygenation on three gamma annihilation rates after injection of a radioisotope in the sample being monitored by a three gamma detection system. The ultimate aim is to develop a non-invasive method for detection of tumour hypoxia by using three gamma positron annihilation combined with two gamma PET methods.

Chapter 6

Factors which affect dissolved oxygen measurements in biological fluids

6.1 Introduction

The purpose of this chapter is to study the factors that affect dissolved oxygen when preparing biological samples with different levels of oxygen concentration between hypoxia and normoxia. Preparation of these samples will help in further studies to be carried out to investigate the relation between oxygen measurements and three-gamma yield using a positron emitter.

The oxyheamoglobin dissociation curve is an important tool for understanding how blood carries and releases oxygen. The oxyheamoglobin dissociation curve relates oxygen saturation and partial pressure of oxygen in blood (pO_2), and is determined by what is called "haemoglobin's affinity for oxygen", that is, how readily haemoglobin acquires and releases oxygen molecules from its surrounding tissue. Study the factors e.g. pH, temperature and CO_2, that affect the concentration of oxygen in mineral water, defibrinated horse blood and serum samples is measured and highlighted in this chapter.

6.2 Materials and Methods

The dissolved oxygen meter is an instrument employed to gauge the quantity of liquefied oxygen in unit volume of a liquid. There are two dissolved oxygen meters used in these experiments. The DOB-215, Omega brand oxygen meter, is used to measure the level of dissolved oxygen and temperature (Figure 6.1). It consists of three parts: a probe for detection, electronics for signal amplification, and a meter to display the results. The sensor electrode consists of anode, cathode and membrane (permeable to oxygen molecules). It obeys the polarographic technique in determining the quantity of dissolved oxygen where the cathode and anode are immersed into an electrolyte, into which oxygen passes through the membrane. The contents of the

electrolyte solution were 1.5% potassium chloride, 0.05% potassium dihydrogenphosphate, 0.08% sodium hydrogenphosphate, 10% glycerol and 88.36% water. It displays the results in parts per million (ppm), ranging from 0 ppm up to 19.99 ppm of dissolved oxygen with an estimated accuracy, as quoted by the manufacturer, of ± 0.1 ppm, and also measure the temperature from 0 up to 50°C.

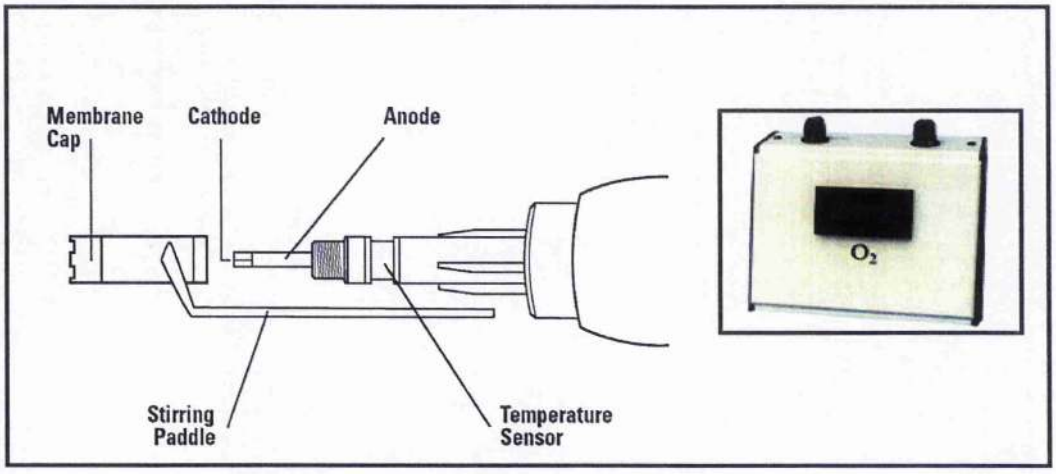

Fig 6.1: The DOB-215, Omega brand oxygen meter.

The DO-400, the second meter, is a portable water resistant dissolved oxygen meter, used in the experiment to measure dissolved oxygen and temperature in all samples. The dissolved oxygen amount can be indicated up to hundredths of parts per million (ppm) which can be equated to milligrams per litre (mg/1) or in % of saturation. The range of temperature that is covered is from 0 to 50°C. The estimated accuracy, as quoted by the manufacturer is ±1.5%.

The Hanna portable pH/Temperature meter, model HI 991301, is an instrument which was used to measure the pH values and temperature in all samples. It has a built-in thermistor for temperature measurement. It measures the pH from 0 to 14 with an accuracy of ±0.01. The pH meter was calibrated using three special buffer solutions. The normal buffer solution options are pH 4, 7 and 10.

The measurement of the dissolved oxygen content, pH and temperature were obtained in three different samples, mineral water, defibrinated horse blood and serum samples. 200mL of mineral water, TESCO Perthshire Mountain Scottish natural water, was used in each experiment. It contains < 60.0 mg/L calcium, < 16.0 mg/L magnesium,

< 13.0 mg/L sodium, <1.5 mg/L potassium, < 11.0 mg/L chloride, < 8.0 mg/L sulphate, and < 3.0 mg/L nitrate. About 60-70% in the adult human body is water. Moreover, the mineral water contains essential elements that are found in the human body.

Horse blood (200mL) was used in each experiment. The blood sample was, as before, defibrinated horse blood, provided by TCS Biosciences Company. 200mL of horse serum was used after separation from the red cells of the sterile defibrinated horse blood. Blood was poured into centrifuge tubes, and placed in the holders of the centrifuge. The blood was spun at half to three quarters speed. After blood has been spun for 8 minutes, the red cells had separated out at the bottom of the tube with a clear liquid floating on top (serum).

Three methods employing bubbling nitrogen gas, carbon dioxide gas and the AnaeroGen compound, were used to prepare in vitro hypoxic samples of mineral water, defibrinated horse blood and serum samples. AnaeroGen is a substance used to generate an anaerobic environment (Chapter 5). Pure nitrogen and carbon dioxide were bubbled through the sample at a constant flow rate of 1 L/minute into 200mL of each sample. Measurements of dissolved oxygen, pH values, and temperature during nitrogen and carbon dioxide bubbling treatment were taken every 5 minute for one hour until low oxygen levels were obtained. Then, measurements were taken every 5 minutes for 3 hours after stopping nitrogen and carbon dioxide bubbling.

6.3 Results and Discussion

Both dissolved oxygen meters, (DOB-215 and DO400) were used in the measurement of the dissolved oxygen content in the mineral water, defibrinated horse blood and serum samples in order to follow the polarographic technique in determining the quantity of dissolved oxygen. In the latter the cathode and anode are immersed into an electrolyte, into which oxygen passes through a membrane. It has been reported that oxygen measurement in tumour hypoxia varies from one study to another using the polarographic technique. This may depend on how technically-skilled the user is or how reproducible the methods for sample preparation used are. As a result there are many interlaboratory variations reported in the literature for oxygen measurements [Hoc93, Nor03]. A comparison of these two dissolved oxygen meters is highlighted in

this chapter, as well as the pH and temperature determination which were measured in different biological samples.

6.3.1 Mineral water

Figure 6.2 shows the reduction of dissolved oxygen content when bubbling nitrogen gas at a constant flow rate of 1 L/minute in 200mL of mineral water for 1 hour. Before bubbling the water sample, the dissolved oxygen was measured and found to be 4.6±0.1 ppm and 5.1±0.1 ppm (68±1.5 %) by the Omega and DO400 meters, respectively. The dissolved oxygen decreased after 1 hour to 0.6±0.1 ppm and 0.41±0.1 ppm (4.9±1.5 %) for Omega and DO400 meters, respectively. Then after nitrogen bubbling was stopped the measurement of dissolved oxygen was carried out and showed an increase of dissolved oxygen in the sample for 3 hours.

Figure 6.3 illustrates the changes in dissolved oxygen content before and after bubbling carbon dioxide at a constant flow rate of 1 L/minute in 200mL of mineral water. The dissolved oxygen dropped from 4.8±0.1 to 0.7±0.1 ppm for the Omega meter whereas it dropped from 5.3±0.1 to 0.35±0.1 ppm (67.2±1.5 to 4.2±1.5 %) for DO400 meter.

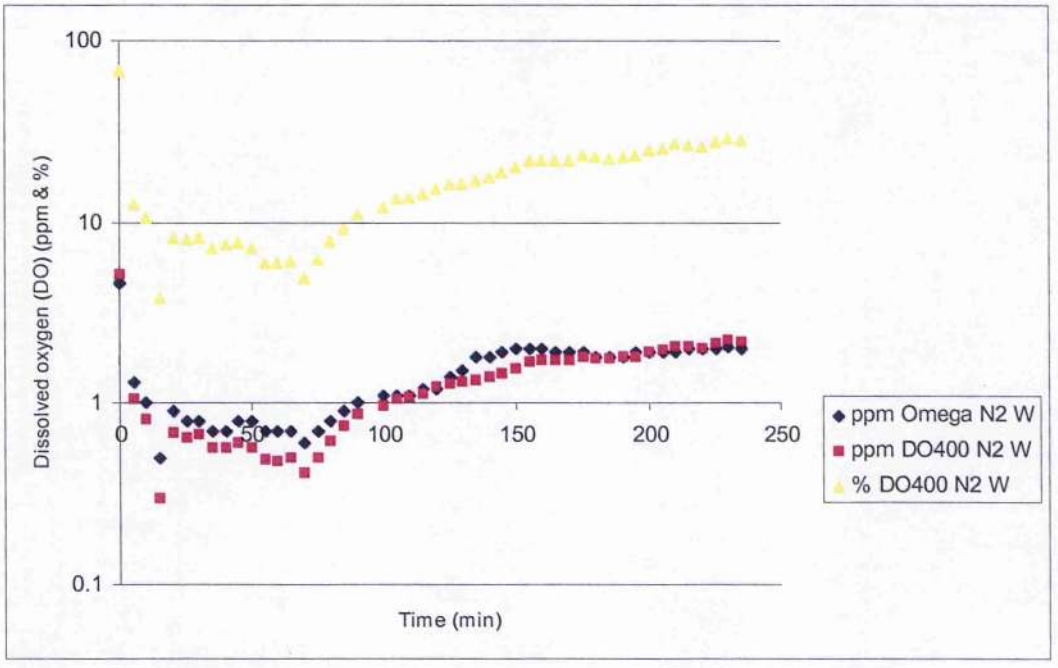

Fig 6.2 Logarithmic scale of dissolved oxygen in (ppm) and (%) for water sample versus time (min) before bubbling (0 time), during bubling (1hr) and after stopping bubbling nitrogen (3hr).

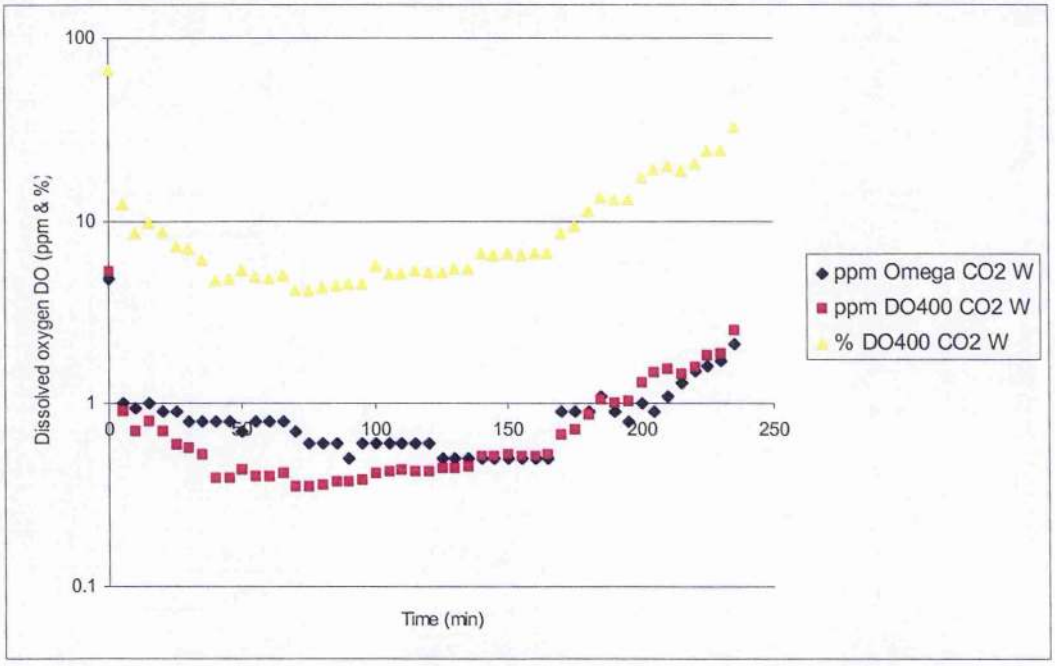

Fig 6.3 Logarithmic scale of dissolved oxygen in (ppm) and (%) for water sample versus time (min) before, during and after bubbling carbon dioxide.

Figure 6.4 is a comparison of dissolved oxygen in water with nitrogen and carbon dioxide bubbling. It shows that a similar reduction of dissolved oxygen within one hour of bubbling both gases in water but the recovery of dissolved oxygen after bubbling carbon dioxide is slower than nitrogen.

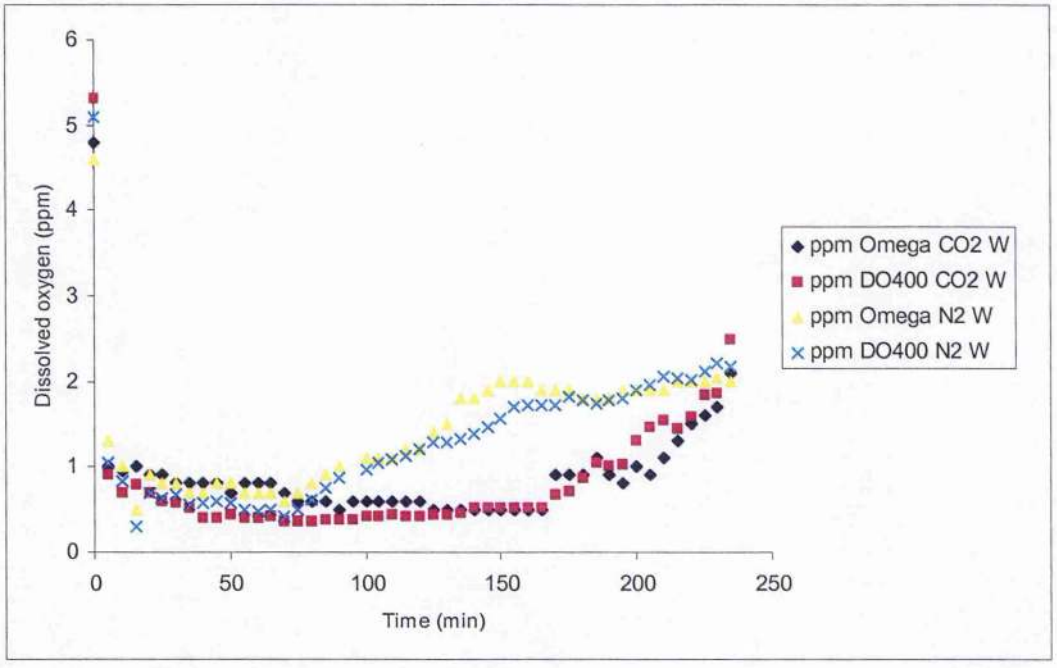

Fig 6.4 Comparison of dissolved oxygen in water between bubbling nitrogen and carbon dioxide.

As temperature is one of the factors that affects the amount of dissolved oxygen, it was important to measure the changes in temperature during the reduction of oxygen by bubbling nitrogen, carbon dioxide and the interaction with AnaeroGen material. The Hanna portable (temperature meter) was used. It measures temperature from 0°C up to 60°C with an accuracy of ± 0.5°C. It can be seen in Figure 6.5 that the temperature in mineral water sample gradually decreased within one hour from 22.3±0.5°C to 19.6±0.5°C and from 20.8±0.5°C to 19.0±0.5°C during nitrogen and carbon dioxide bubbling time, respectively. However, for the sample that was treated with AnaeroGen for an hour, the temperature increased from 23.5±0.5°C to 25.7±0.5°C.

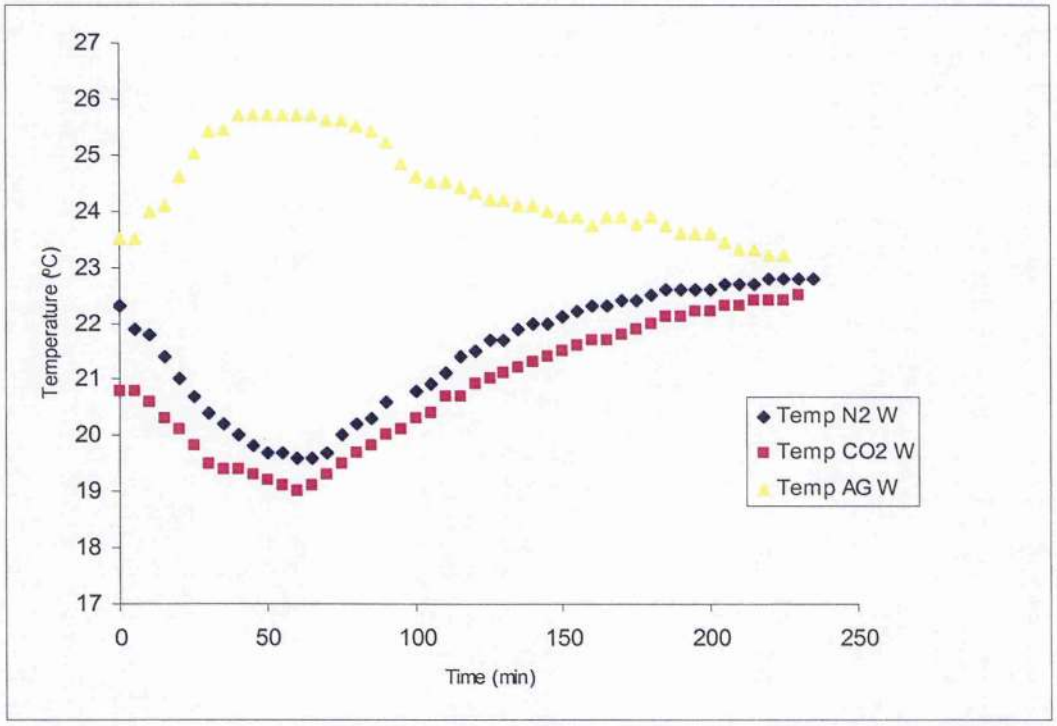

Fig 6.5 Temperature measurement (°C) in water versus nitrogen, carbon dioxide and AnaeroGen treatment time.

The pH changes were measured using Hanna portable pH meter. This measures the pH from 0 to 14 with an accuracy of ± 0.01 pH. Figure 6.6 shows that the pH in the water sample that was treated with AnaeroGen decreased from 7.91±0.01 to 6.9±0.01 after about 30 minutes. But there was a very sharp reduction of pH in the sample treated with carbon dioxide from 7.84±0.01 to 5.1±0.01 in the first 5 mintues, and then the pH remained steady at about 5.04±0.01 after one hour. On the other hand, an

increase of pH was observed during bubbling nitrogen from 7.7±0.01 to 8.93±0.01 after an hour.

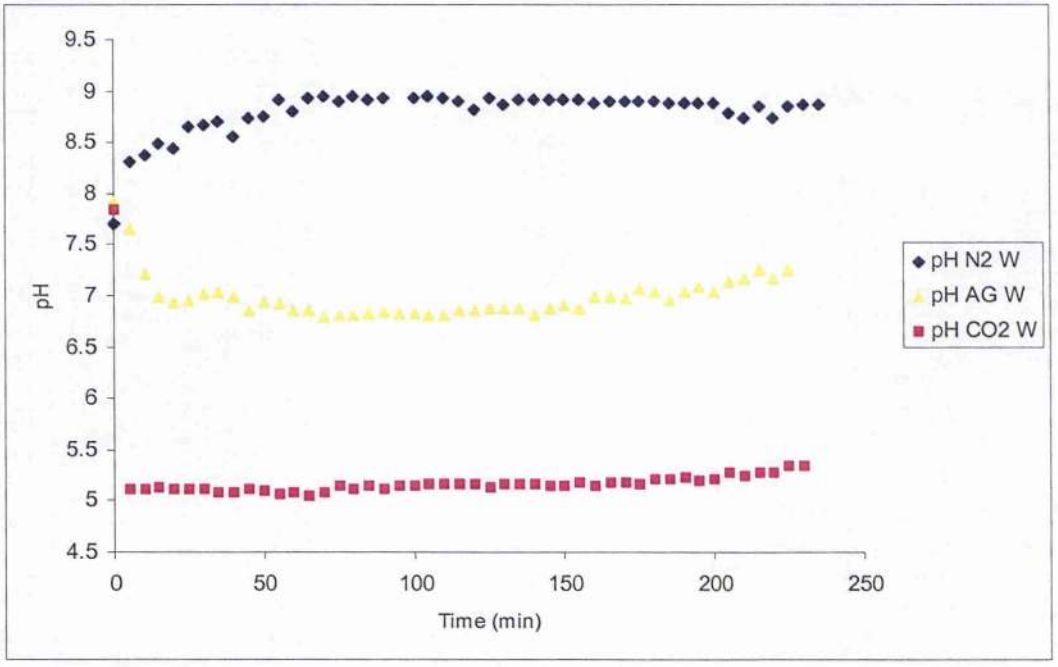

Fig 6.6 pH measurement in water versus nitrogen, carbon dioxide and AnaeroGen treatment time.

6.3.2 Defibrinated horse blood

The defibrinated horse blood was supplied by TCS Biosciences Company. Defibrinated blood consists of blood which has had the fibrin removed from the plasma in order to prevent blood coagulation. The horse blood sample was chosen here to reduce the hazards and implications of working with a human biological sample which may be infected unless carefully screened. The decrease of dissolved oxygen was observed to have the same trend for both meters in Figure 6.7 and Figure 6.8 where the horse blood was treated by bubbling nitrogen and carbon dioxide, respectively.

The initial readings before bubbling nitrogen in blood for dissolved oxygen with both meters were 3.2±0.1 ppm and 3.8±0.1 ppm (47.7±1.5 %) for Omega and DO400 meters, respectively. But the lowest readings were found to be 0.5±0.1 ppm and 0.58±0.1 ppm (7.2±1.5 %) for Omega and DO400 meters, respectively. On the other hand, before using carbon dioxide the initial readings were 3.3±0.1 ppm and 3.65±0.1 ppm (45.2±1.5 %) for Omega and DO400 meters, respectively. Then the dissolved

oxygen dropped to 0.5±0.1 ppm and 0.67±0.1 ppm (7.3±1.5 %) for the Omega and DO400 meters, respectively. These reading show the similarity of dissolved oxygen measurements in both meters for blood samples treated with nitrogen and carbon dioxide.

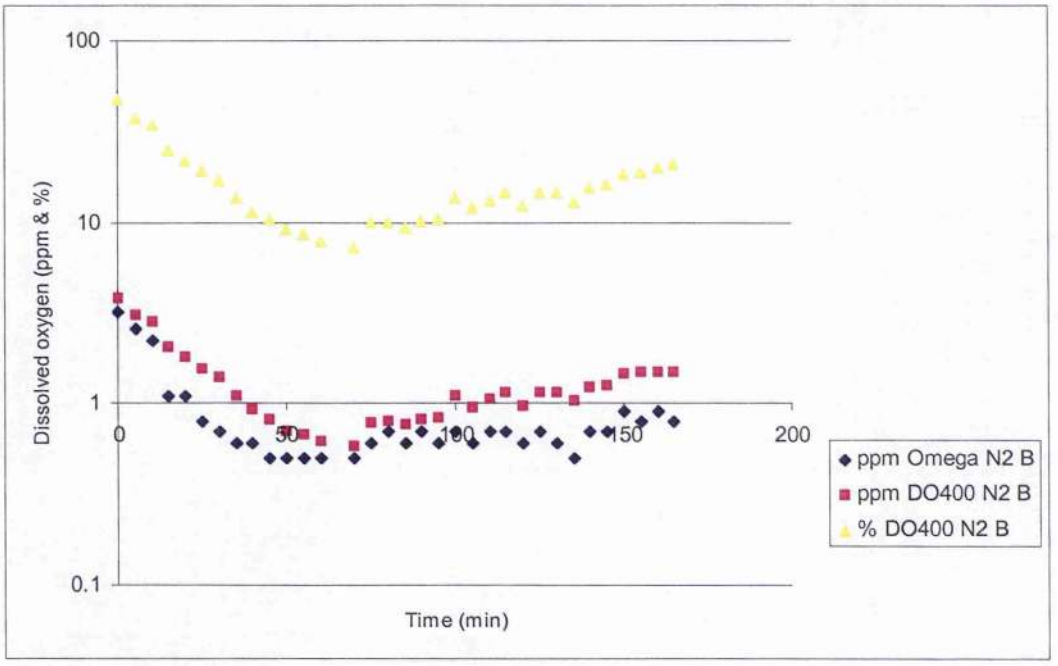

Fig 6.7 Logarithmic scale of dissolved oxygen in (ppm) and (%) for blood sample versus time (min) before, during and after bubbling nitrogen.

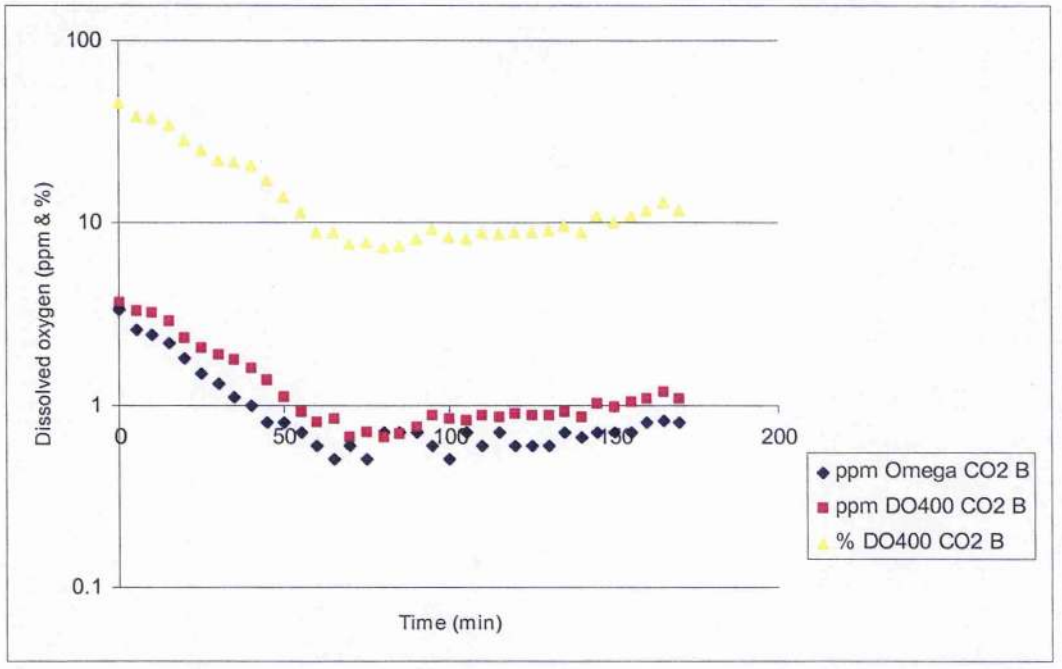

Fig 6.8 Logarithmic scale of dissolved oxygen in (ppm) and (%) for blood sample versus time (min) before, during and after bubbling carbon dioxide.

The comparison of dissolved oxygen in blood samples treated with nitrogen and carbon dioxide is illustrated in figure 6.9 and 6.10. It can be seen that the recovery of dissolved oxygen after one hour of bubbling was slower in the blood sample treated with carbon dioxide than with nitrogen.

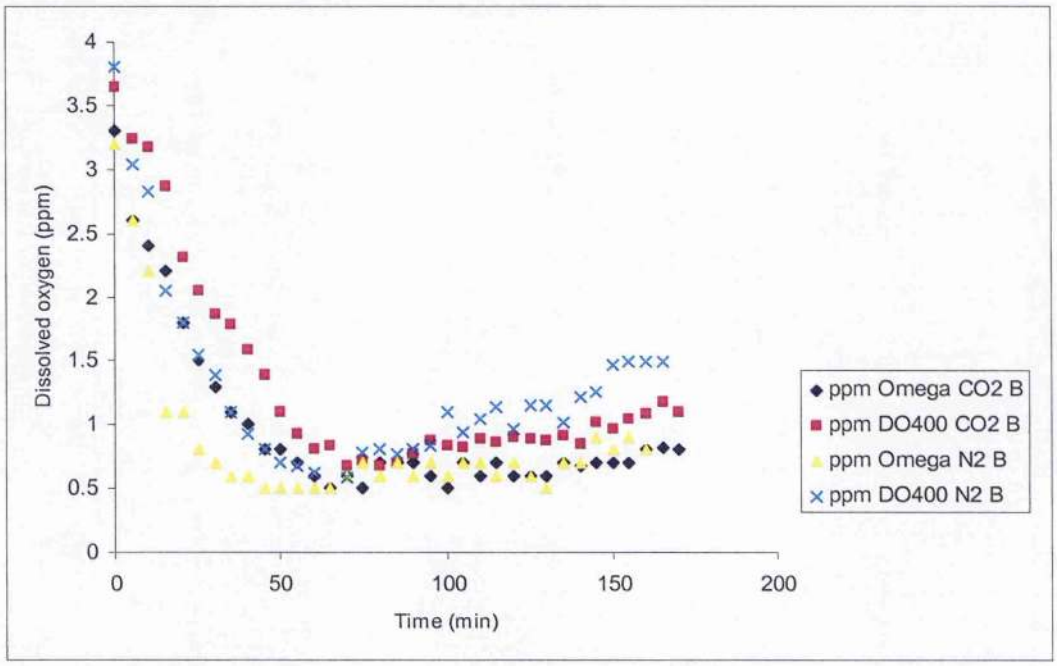

Fig 6.9 Comparison of dissolved oxygen in blood (ppm) between bubbling nitrogen and carbon dioxide.

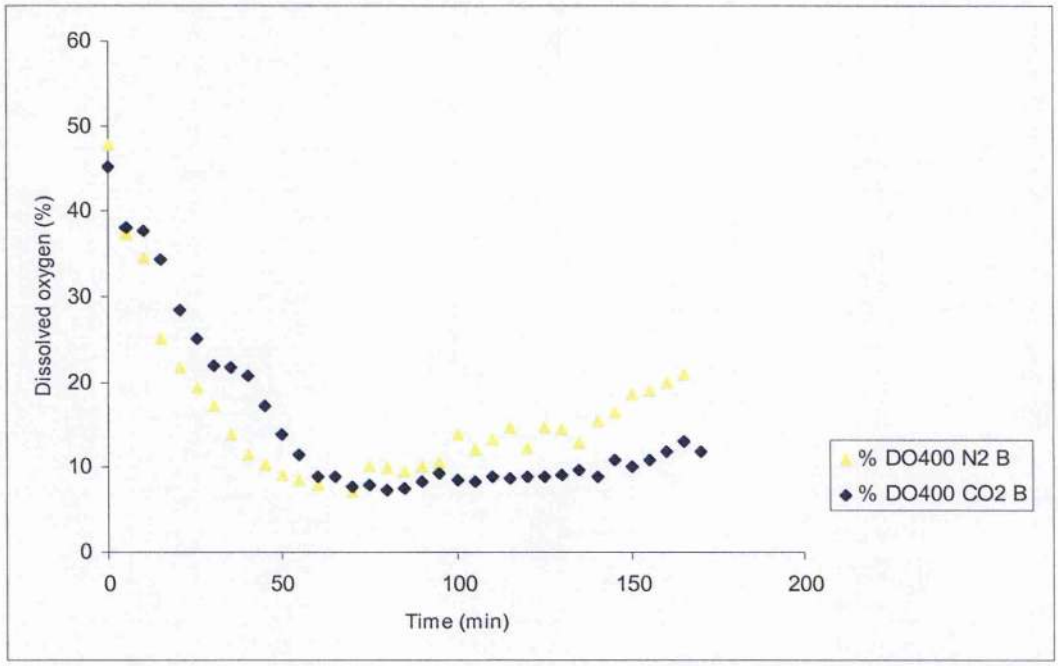

Fig 6.10 Comparison of dissolved oxygen in blood (%) between bubbling nitrogen and carbon dioxide.

It seems from figure 6.11 that the 'cold' horse blood behaves differently from water but this is not the case because the experiment was performed immediately after taking the blood out of the fridge. The increases of the temperature observed in cold horse blood while bubbling nitrogen or carbon dioxide was due to the blood trying to reach the thermal equilibrium with the laboratory temperature. The changes of temperature for cold horse blood during the first hour of bubbling nitrogen, carbon dioxide and interaction with AnaeroGen, respectively; were from 15.9±0.5°C to 19.17±0.5°C, from 15.3±0.5°C to 19.1±0.5°C and from 19.1±0.5°C to 22.4±0.5°C. However, another temperature measurement was obtained for room temperature (warm blood) which showed that the decrease of temperature from 21.9±0.5°C to 21.1±0.5°C during the first hour of bubbling nitrogen.

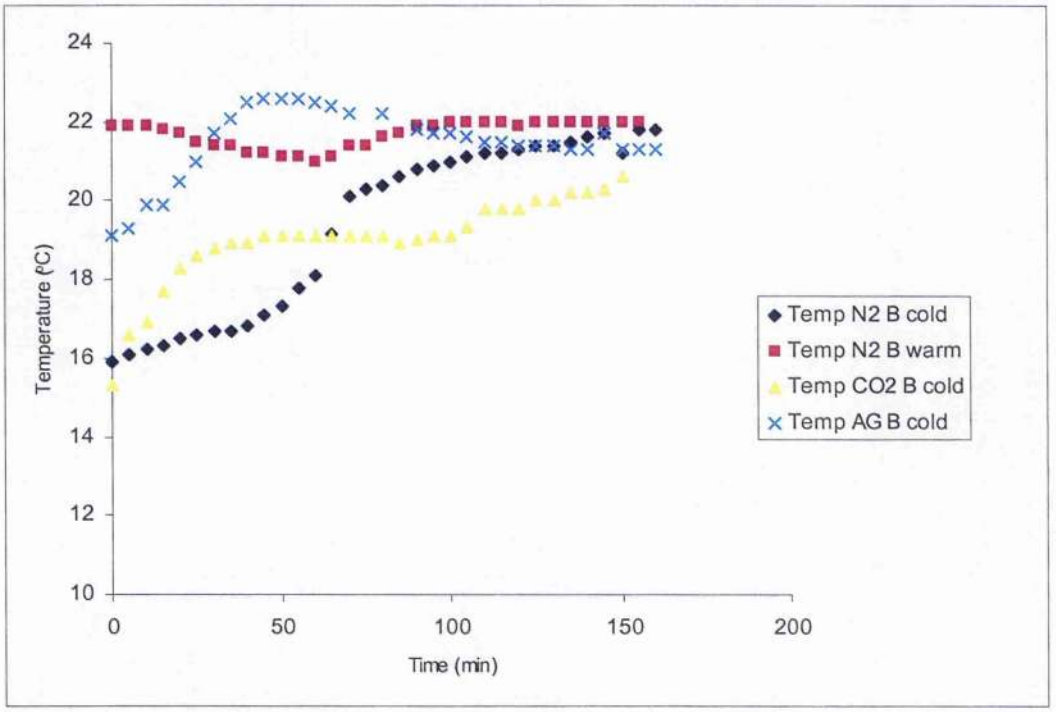

Fig 6.11 Temperature measurement (°C) in horse blood versus bubbling nitrogen, carbon dioxide and AnaeroGen treatment time.

The pH changes of horse blood samples in figure 6.12 were similar to those found in water. The reason for the pH increase when the sample was treated with nitrogen may be due to the formation of ammonia NH_3 and ammonium NH_4^+ (alkaline) with water molecules in the samples. This can be explained by:

$$NH_3 + H_2O \leftrightarrow NH_4^+ + OH^- .$$

On the other hand, the reduction of the pH when the samples were treated with AnearoGen or bubbling carbon dioxide was observed in all samples. This is due to the fact that AnaeroGen consumes oxygen and produces carbon dioxide; therefore carbon dioxide dissolves in the samples and forms carbonic acid which is causing acidosis in all samples.

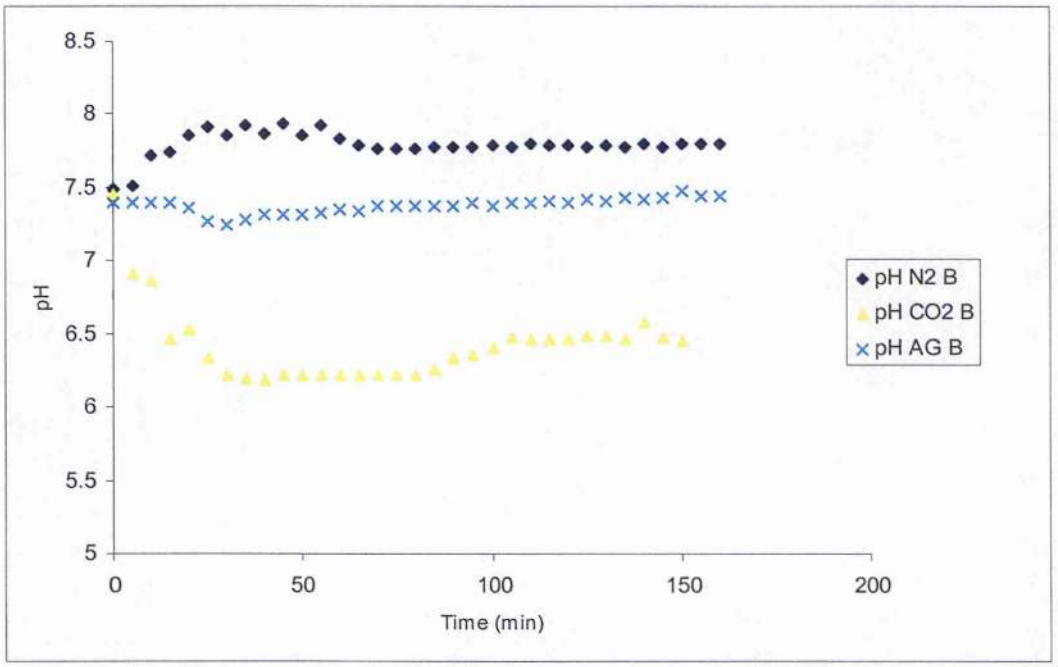

Fig 6.12 pH measurement in horse blood versus bubbling nitrogen and carbon dioxide and AnaeroGen treatment time.

6.3.3 Horse serum

The serum was separated from the defibrinated horse blood that was supplied by TCS Biosciences Company. The reduction of dissolved oxygen content was measured during the bubbling of nitrogen gas (Fig. 6.13) and bubbling of carbon dioxide gas (Fig.6.14) at a constant flow rate of 1 L/minute in 200mL of serum for 1 hour. Before bubbling nitrogen in the serum, the dissolved oxygen was 3.2±0.1 ppm and decreased to 0.2±0.1 ppm for Omega meters whereas on the DO400 meter the dissolved oxygen was 4.84±0.1 ppm (62.2±1.5 %) and decreased to 0.91±0.1 ppm (11.5±1.5 %). The variation of dissolved oxygen measurement was 0.7±0.1 ppm of these dissolved oxygen meters. However there was no variation in the reduction of dissolved oxygen in both meters when bubbling carbon dioxide. The comparison between dissolved oxygen measurements in both meters during bubbling nitrogen and carbon dioxide in serum is shown in figure 6.15.

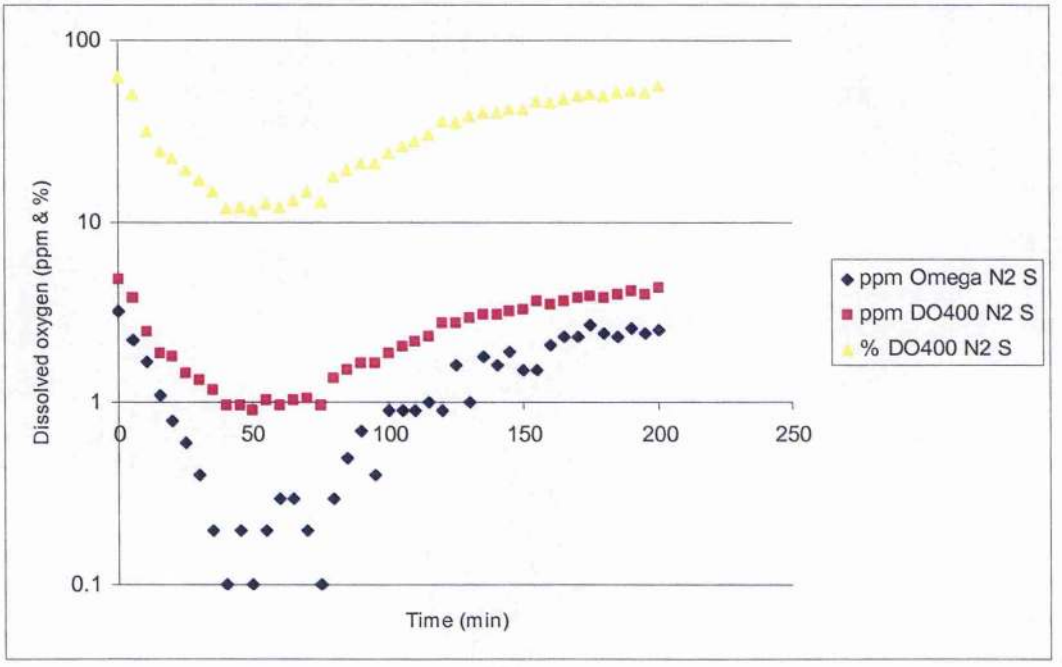

Fig 6.13 Logarithmic scale of dissolved oxygen in (ppm) and (%) for serum sample versus time (min) before, during and after bubbling nitrogen.

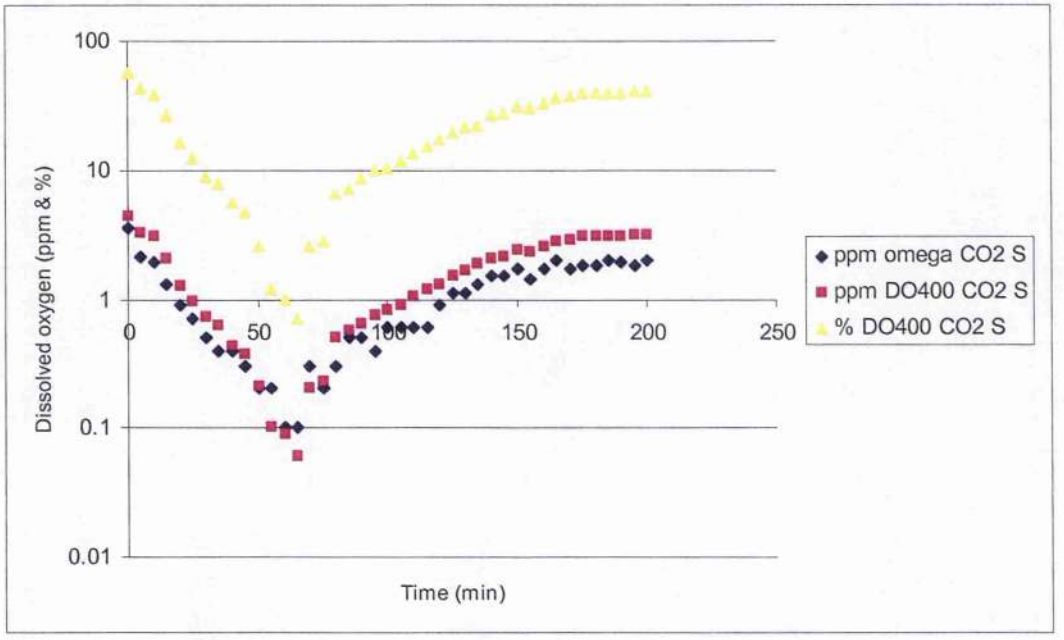

Fig 6.14 Logarithmic scale of dissolved oxygen in (ppm) and (%) for serum sample versus the time (min) before, during and after bubbling carbon dioxide.

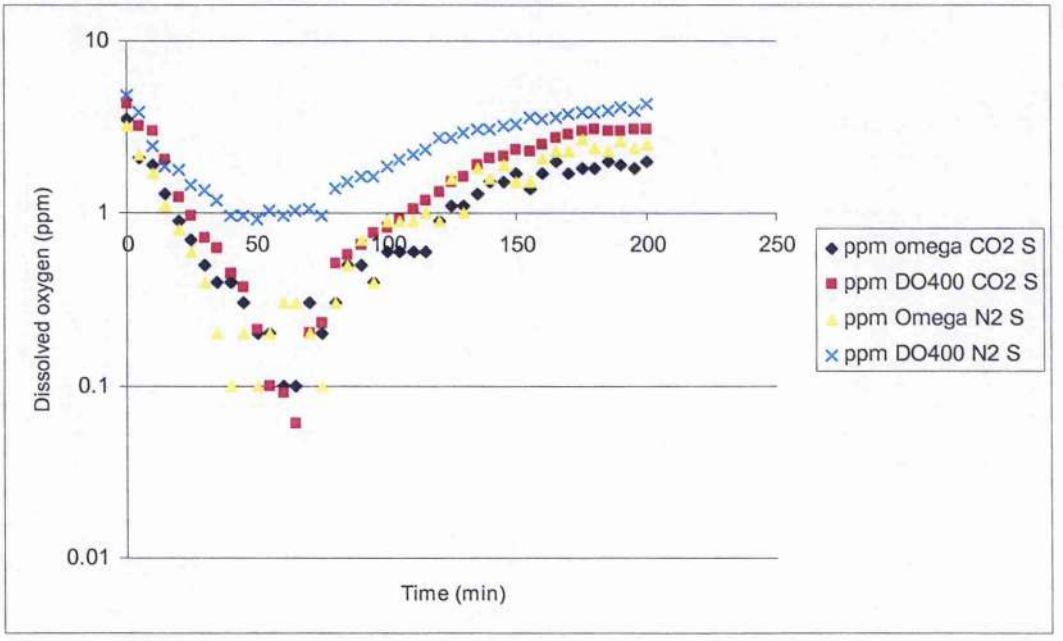

Fig 6.15 Comparison of dissolved oxygen in serum between bubbling nitrogen and carbon dioxide.

Temperature (Fig 6.16) and pH (Fig 6.17) were measured during the treatment of serum with bubbling nitrogen, carbon dioxide and AnaeroGen. Decreases of temperature were observed during bubbling nitrogen and carbon dioxide but increases were observed during AnaeroGen interaction with serum, due to the exothermic reaction of the ascorbic acid in the AnaeroGen sachet. The decrease of pH was also observed during the bubbling of carbon dioxide and when using the AnaeroGen sachet but it increased during bubbling of nitrogen.

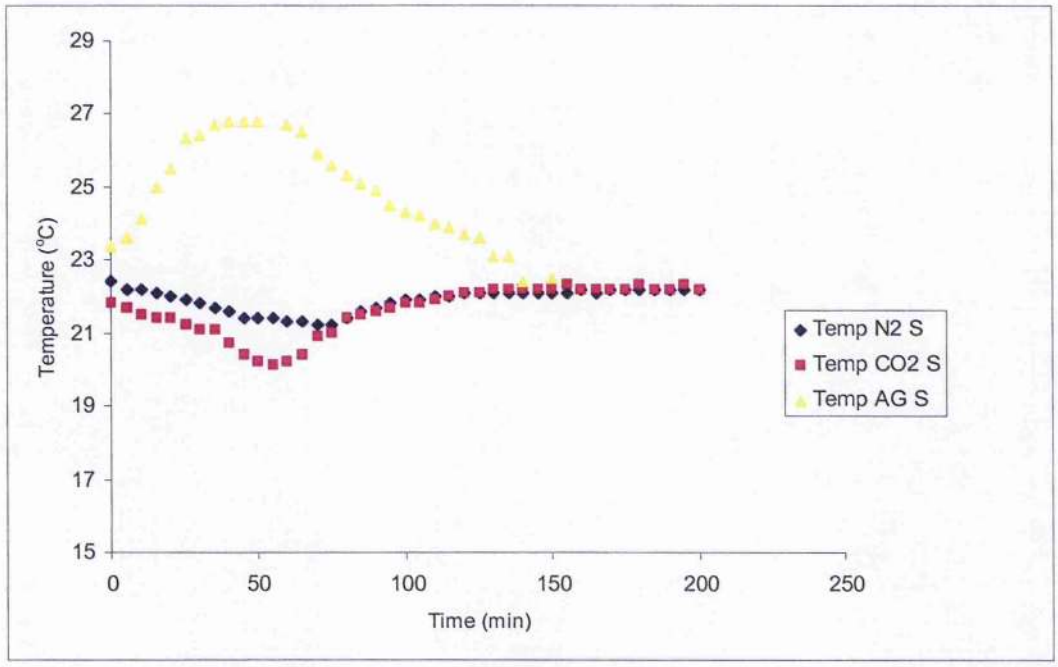

Fig 6.16 Temperature measurement (°C) in serum versus bubbling nitrogen, carbon dioxide and AnaeroGen treatment time.

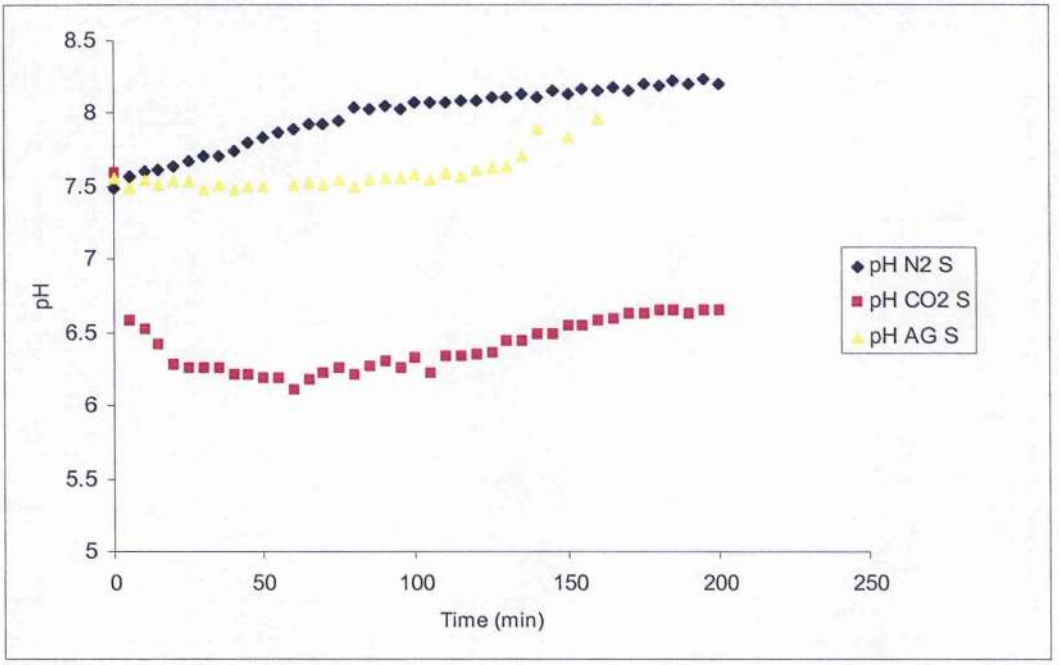

Fig 6.17 pH measurement in serum versus bubbling nitrogen, carbon dioxide and AnaeroGen treatment time.

The comparisons of dissolved oxygen between blood and serum samples treated with carbon dioxide and nitrogen are illustrated in Figures 6.18 and 6.19, respectively. It can be seen in both figures that the recovery of dissolved oxygen, after one hour of bubbling carbon dioxide and nitrogen, was slower in the blood than in serum samples.

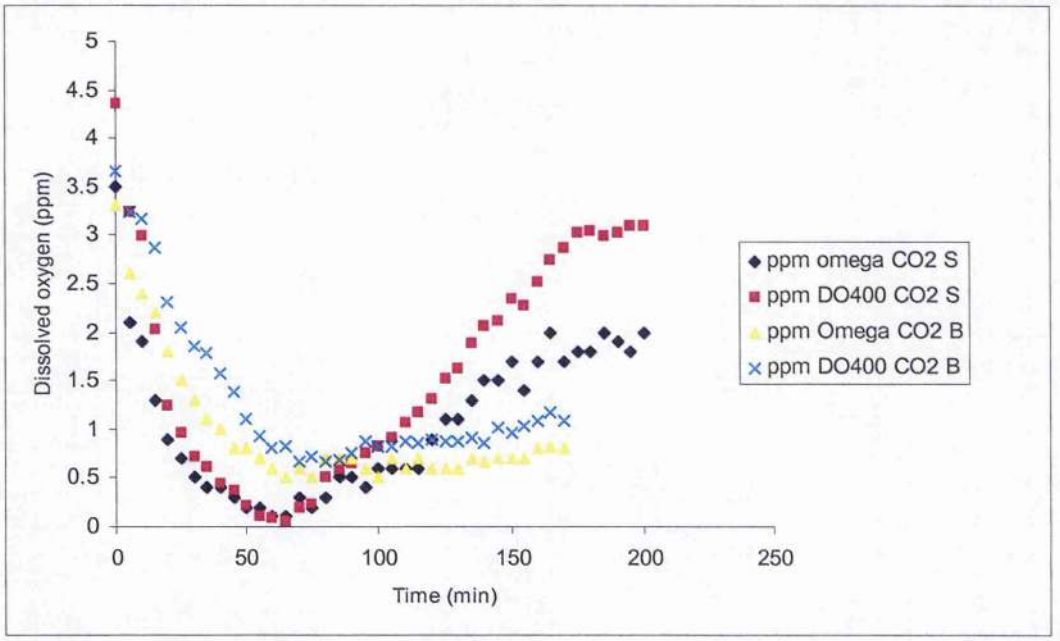

Fig 6.18 Comparison of dissolved oxygen between horse serum and blood during bubbling carbon dioxide.

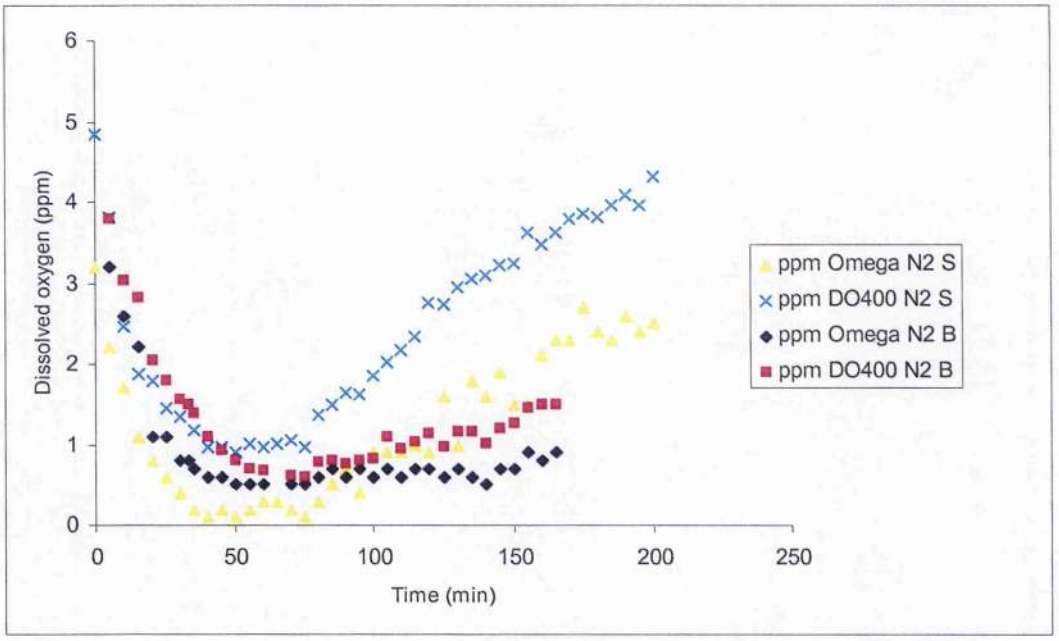

Fig 6.19 Comparison of dissolved oxygen between horse serum and blood during bubbling nitrogen.

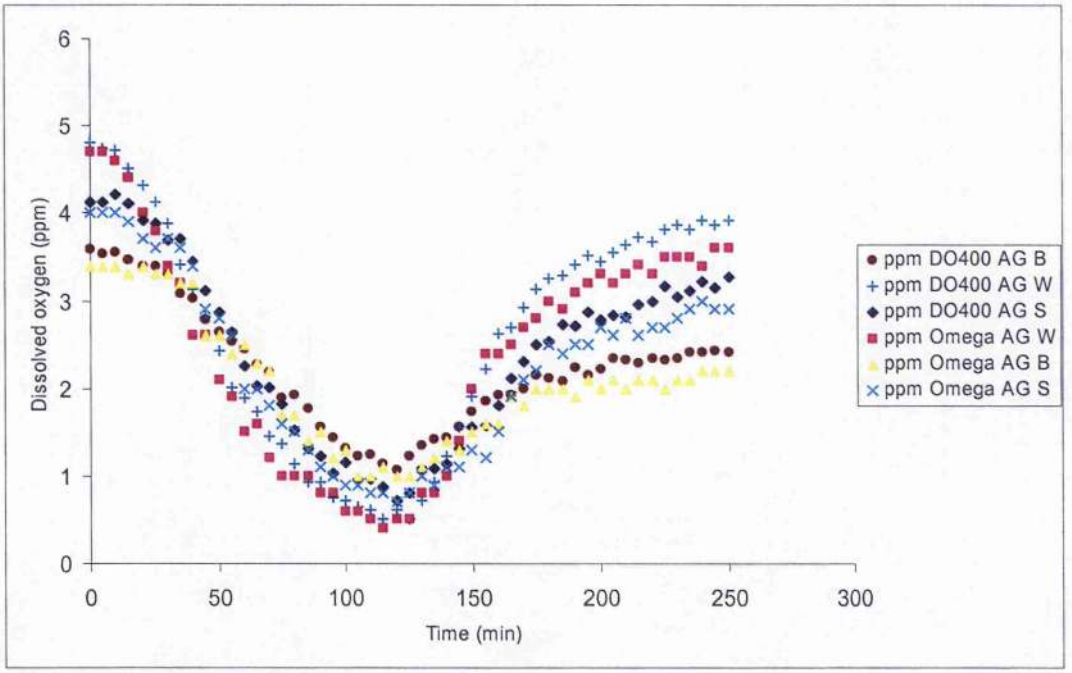

Fig 6.20 Comparison of dissolved oxygen in water, horse blood and serum using AnaeroGen compound.

A comparison of dissolved oxygen measurement in mineral water, horse blood and serum samples treated with AnaeroGen is illustrated in Figure 6.20. The reduction time of dissolved oxygen in samples using AnaeroGen is longer than bubbling carbon dioxide or nitrogen gases as in Figures 6.18 and 6.19, respectively. The recovery of dissolved oxygen, after two hours of AnaroGen treatment, was slower in blood than in water or serum samples.

Most of the figures of trends in dissolved oxygen show that there is a difference between the readings from these meters significantly greater than the estimated accuracy figures quoted by the manufacturer, in particular, Figures 6.9, 6.13, 6.18 and 6.19. There are many factors that may affect the measurement of dissolved oxygen. For example, the probe membrane should be checked and replaced when readings become erratic or the calibration is unstable. If the filling solution (electrolyte) evaporates or a large bubble forms in the reservoir, the probe should be refilled. It is necessary to insure a steady and continuous movement of the probe in order not to deplete the oxygen surrounding the probe. Stirring can be accomplished by circular movement or raising and lowering the probe in the sample. In the lab, a magnetic stirrer was also used to adjust the stirring speed at a constant value however this increases the temperature of the fluid and affects the dissolved oxygen. In some applications (i.e blood and gelatine samples), build-ups of residuals may form on the membrane and reduce permeability. Therefore frequent cleaning or membrane replacement may be required. All these factors may introduce errors in meter reading.

6.4 Conclusion

The factors that affect dissolved oxygen such as partial pressure of carbon dioxide, temperature and pH were studied for mineral water, horse blood and horse serum samples. Three methods; bubbling nitrogen gas, carbon dioxide gas and the AnaeroGen compound, were used to prepare in vitro hypoxic samples. The oxyhaemoglobin dissociation curve is an important tool for understanding the factors that influence haemoglobin attraction to oxygen. A decrease of haemoglobin affinity to oxygen is caused by a decrease in pH, an increase in carbon dioxide concentration and an increase in temperature. From the experimental results obtained, bubbling

nitrogen is not the method of choice for preparing hypoxic samples due to the conflicting effects of decreasing temperature and increasing pH values in all samples during the reduction of oxygen concentration. Bubbling carbon dioxide in all samples causes an increase in their acidity as in the case of hypoxic tumours, due to the formation of carbonic acid, however the temperature is reduced. On the other hand, using AnaeroGen is the choice method for preparing hypoxic samples due to the easy handling of the AnaeroGen sachet as well as the good agreement with the factors that affect oxygen reduction.

Chapter 7

3γ Yield - Triple coincidence measurements

7.1 Introduction

Positron emission tomography (PET) is an advanced method of functional imaging which has rapidly expanded over recent years. It is used to trace metabolic pathways of specific radiolabelled tracers for obtaining in-vivo quantitative information about tissue physiology, biochemistry and pharmacology. The presence of hypoxic tissue has been increasingly recognized to be resistant to chemotherapy and radiotherapy, both in vitro and in vivo, and accelerates tumour progression. The development and validation of an ideal hypoxic marker in nuclear medicine for detection of tumours demands that its oxygen dependency and the products which bind to cells or are retained within them are essential. The use of three-gamma annihilation as a new PET molecular imaging modality which can predict tumour hypoxia was proposed by Kacperski and Spyrou in 2004. The positronium and its annihilation, could then serve as an oxygen-sensitive marker. The mechanism of the three-gamma decay process is determined by the chemical and physical state of the environment.

The human body is composed of biochemicals. The complex physiological mechanisms of the physical and chemical principles of O_2 and CO_2 transport play an important and complex role in blood and other tissues. Generally CO_2 diffuses in the opposite direction to that of O_2. In tumour hypoxia, the deficiency of oxygen occurs with uncontrolled cell division causing unbalanced biochemical composition of the tissue, such as the reduction of O_2, production of CO_2, and the formation of free radicals, species containing one or more unpaired electrons. Several types of reactive oxygen species (ROS) are generated as a by-product of mitochondrial electron transport as probable consequence in rapidly dividing cells [Kin06, Pec05]. Though human beings have strong defence systems, various ROS cannot be scavenged completely even with the use of free radical scavengers like ascorbic acid, and

eventually abnormal happenings occur. Therefore, a non-invasive technique to assess the biochemical environment of hypoxic tumour tissue is the need of the day.

In this chapter the main concept of three-photon positron annihilation imaging and proof-of-principle experiments are explored in order to provide an overview of the technique to be developed as an additional imaging modality to conventional PET. A new analytical technique and methodology for assessing triple coincidence imaging techniques is proposed by using two different conditions in normoxic and hypoxic environments to explore the possibility of exploiting 3γ annihilation in PET imaging for measuring the relative oxygenation of tissues in oncology.

7.2 The concept of three-photon positron annihilation imaging

In spite of the relative rarity of positron annihilation into three photons (Chapter 4), it may still be possible to develop a new imaging modality. It would provide information not only about the distribution and local concentration of a radionuclide, but also, by virtue of the chemical interactions of positronium, the local chemical environment in tissues. In particular, the concentration of oxygen could be determined, which would have significant advantages in oncology applications of PET.

Consider a three-photon decay event that occurs at a point r = (x,y,z) (Fig.7.1). The three annihilation photons can have energies between 0 and 511keV, fulfilling the laws of energy and momentum conservation. Their probability distribution ρ (E_1, E_2, E_3) is roughly uniform over the allowed domain [Ore49]. If the three photons of energies E_1, E_2, E_3 are detected in coincidence by three detectors at points r_1, r_2, r_3, respectively, then from the momentum conservation law we obtain:

$$p_X = \frac{E_1}{c}\frac{x-x_1}{|\mathbf{r}-\mathbf{r}_1|} + \frac{E_2}{c}\frac{x-x_2}{|\mathbf{r}-\mathbf{r}_2|} + \frac{E_3}{c}\frac{x-x_3}{|\mathbf{r}-\mathbf{r}_3|} = 0,$$

$$p_Y = \frac{E_1}{c}\frac{y-y_1}{|\mathbf{r}-\mathbf{r}_1|} + \frac{E_2}{c}\frac{y-y_2}{|\mathbf{r}-\mathbf{r}_2|} + \frac{E_3}{c}\frac{y-y_3}{|\mathbf{r}-\mathbf{r}_3|} = 0, \qquad (7.1)$$

$$p_Z = \frac{E_1}{c}\frac{Z-Z_1}{|\mathbf{r}-\mathbf{r}_1|} + \frac{E_2}{c}\frac{Z-Z_2}{|\mathbf{r}-\mathbf{r}_2|} + \frac{E_3}{c}\frac{Z-Z_3}{|\mathbf{r}-\mathbf{r}_3|} = 0$$

and from the energy conservation law

$$E_1 + E_2 + E_3 = 2m_e c^2 = 1022keV \qquad (7.2)$$

where m_e is the electron rest mass. With known detector positions r_1, r_2, and r_3, the measurement of energies E_1, E_2, and E_3 enables the solution of the non-linear set of equations (7.1) to determine the point r; the position at which the annihilation took place. Since the three photons are co-planar, the set of equations in (7.1) can be transformed into a two dimensional one, due to the finite energy resolution of the detectors [Kac04]. Image reconstruction from the three-photon annihilations is less complex than that of 2γ PET, and only needs to solve numerically the above equations. In contrast to the 2γ decay, in three-photon decay we obtain complete information about the position of annihilation from a single event, rather than requiring set of line of responses (LOR). This can be regarded as perfect electronic collimation.

The density of points in a given region (Figure 7.2) is proportional to the concentration of the radionuclide as well as the 3γ yield in that region. The conventional 2γ PET scan can be performed simultaneously since the 3γ photons have their distinct energy range excluding 511 keV, and fulfil the additional constrain in equation (7.2). One however needs additional triple coincidence circuitry with pulse analysing and registration channels. After the appropriate correction procedures the 3γ image can be compared to the one obtained from the conventional 2γ scan which only contains the information about the radionuclide concentration. Taking a ratio of the two images the spatial distribution of the 3γ yield can be derived. In this way, new kinds of information about the state of a tissue or biochemical processes which are taking place can be gathered.

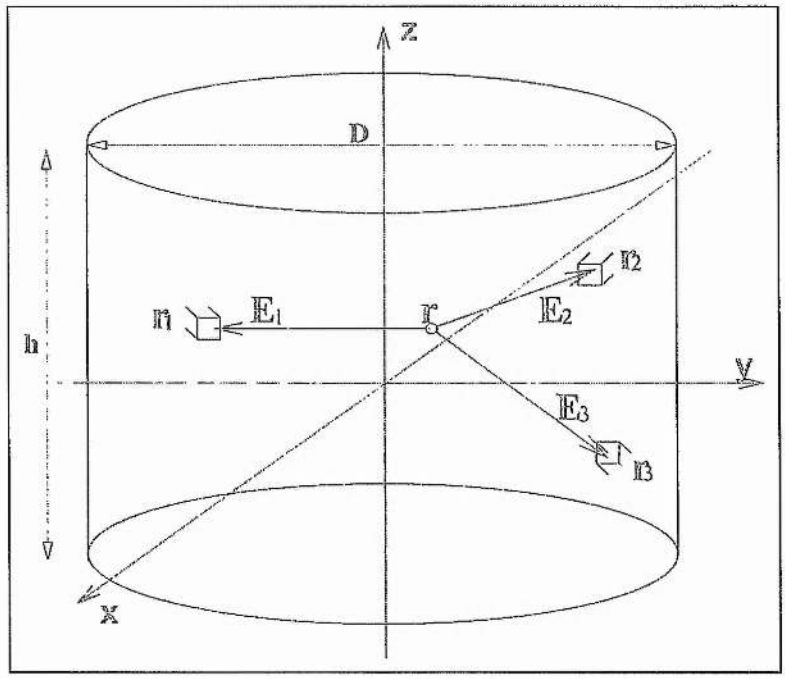

Figure 7.1: Scheme of 3γ imaging [Kac04a]

7.3 Proof-of-principle Experiments

A simple proof-of-principle experiment in which the energies of photons in triple coincidence were measured by one HPGe (55×51 mm) and two NaI(Tl) (76.2× 76.2 mm) detectors were arranged in a plane forming angles of about 120° with respect to each other to form a simple 3γ scanner [Kac04a]. Two thin kapton foil sealed ^{22}Na sources of activities 0.23 MBq (A) and 0.4 MBq (B) were placed in samples of fine silica powder and sealed in glass containers under a nitrogen atmosphere, were used as phantoms (Figure 7.2). After rejecting the energy triplets that do not fulfil condition equation (7.2) the image was reconstructed. The energy window for detection of 3γ was set to 150–480 keV. The resolution is optimal for the symmetric three-photon decay with all energies equal to 340.7keV and deteriorates as we move towards extreme values. In practice, we never detect energies from the entire 3γ spectrum 0–511 keV. At the upper end the 511 keV photopeak resulting from the dominating 2γ decays has to be cut off. On the other hand, there is a detector and noise-related low-

energy detection limit which introduce large errors in position reconstruction. The position of the two sources is well reproduced, although the spatial resolution is rather poor. The dispersion is partly due to the relatively long range of positrons in the fine silica powder (non-point sources), but it is mainly due to the inferior energy resolution of the NaI(Tl) detectors (about 10% FWHM)

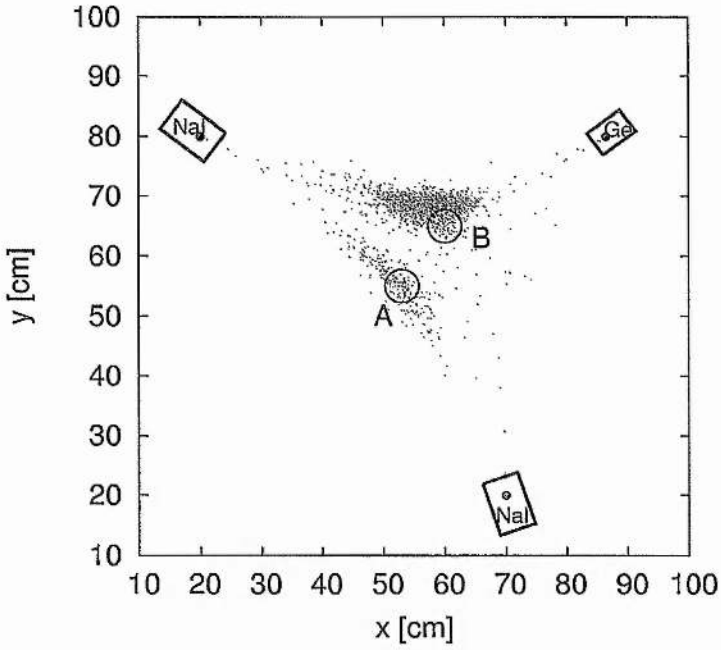

Figure 7.2: Arrangement of 3γ imaging experiment using one HPGe and two NaI(Tl) detectors [Kac04a].

The energy resolution is the crucial factor determining the spatial resolution of 3γ imaging. Figure 7.3 shows the result of another set of experiments using three high energy resolution detectors (two HPGe: 55×51 mm and 42×44 mm respectively, and one Ge(Li) 35×37 mm) which were positioned as indicated in the figure [Spy05]. Two thin kapton foil sealed ^{22}Na sources of activities 0.19 MBq (A) and 0.14 MBq (B) were placed in samples of fine silica powder and sealed in glass containers under nitrogen atmosphere. The image is formed as a set of dots, each corresponding to a single 3γ positron decay as in Figure 7.2 and 7.3. The density of points in a given region is proportional to the concentration of the radionuclide as well as the 3γ yield in that region.

It can be seen from Figure 7.2 that the location of the annihilation site is broadened into a region surrounding the non-point sources. The spread is nonuniform as a consequence of the particular position of the detectors. The shift in the centre of mass of the reconstructed source positions is caused mainly by using poorer energy resolution scintillator detectors compared to HPGe semiconductors. In addition a small drift in one of the electronic channels for NaI(Tl) over the long period of counting, about 50 hours, may have also contributed to a poorer spatial resolution than in Figure 7.3. This may be due to variation in laboratory temperature over this period which is not encountered with the HPGe liquid nitrogen-cooled detector. Moreover, the spatial resolution of the non-point sources in 3γ imaging is affected by various parameters of the system which may have the influence on the system stability, such as the scanner's field of view (FOV), source-detector distance and size of detectors. Poor spatial resolution increases linearly with the linear size of the detectors and the diameter of the scanner. It should be noted that the NaI(Tl) detectors are of different size from the HPGe semiconductor. A few point far from the sources obtained most probably from random triple coincidences.

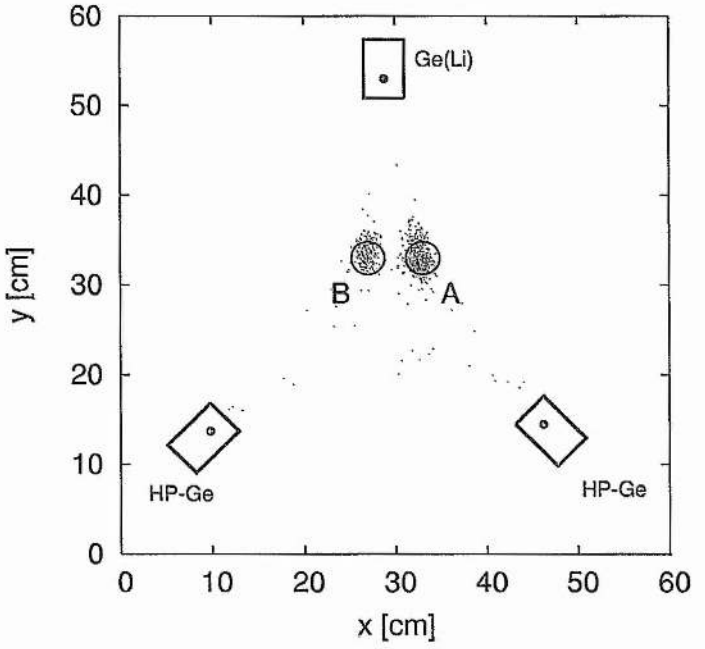

Figure 7.3: Arrangement of 3γ imaging experiment using two HPGe and one Ge(Li) detectors [Spy05].

The detectors most widely used in PET scanners had been based on bismuth germanate (BGO) scintillators but in the last 10 to 15 years were replaced by lutetium oxy-orthosilicate (LSO) scintillation detectors. Their energy resolution of about 12% would give a spatial resolution >8 cm, which is not adequate to obtain a useful image [Kac05]. But if HPGe detectors of energy resolution about 0.2% are employed, the spatial resolution decreases below 1 cm, which is comparable to the influence of the size of detectors used [Kac05]. Scintillator detectors are now chosen for PET scanners mainly because of their good stopping power and relatively low cost. However, recent progress in the physics and technology of broad-band semiconductor materials, in particular cadmium telluride (CdTe) and cadmium zinc telluride (CdZnTe), used as high resolution, room-temperature gamma-ray detectors opens-up the possibility of a wide range of their applications in medical imaging, including PET [Eis99, Amr01]. The achieved energy resolutions of less than 2% FWHM at 356 keV gamma photons would give a reasonable spatial resolution in 3γ imaging. Certainly, a number of various technical problems have to be resolved to obtain an overall good performance scanner based on these types of detectors. Probably the main reason why the 3γ annihilations have not been considered useful for imaging so far is the limitation of the choice of detector.

7.4 Experimental procedure and sample preparation

7.4.1 Experimental set-up

It is important for the three-photon positron annihilation detection system to have a good system of optimising and coupling between the output of the detectors and the rest of the counting system to minimise any sources of noise that may change or affect the signal quality and amplify the signal before it can be recorded. The preamplifier is the first element in a signal-processing chain and its function as an interface between the detectors and the electronics. It is used to amplify the small signals produced by the detectors, shape the signal pulse and match the levels of impedance between detectors and electronics that follow. A spectroscopy amplifier is also used to amplify and reshape the pulse signal from the preamplifier in order to minimise pile up and overload. On the other hand, it is used to maximise the performance at high counting

rates. It also helps to provide better signal-to-noise ratio in the analysis of individual pulse amplitude [Kno00, Che03]. The set-up used in the experiments is shown in figure 7.4.

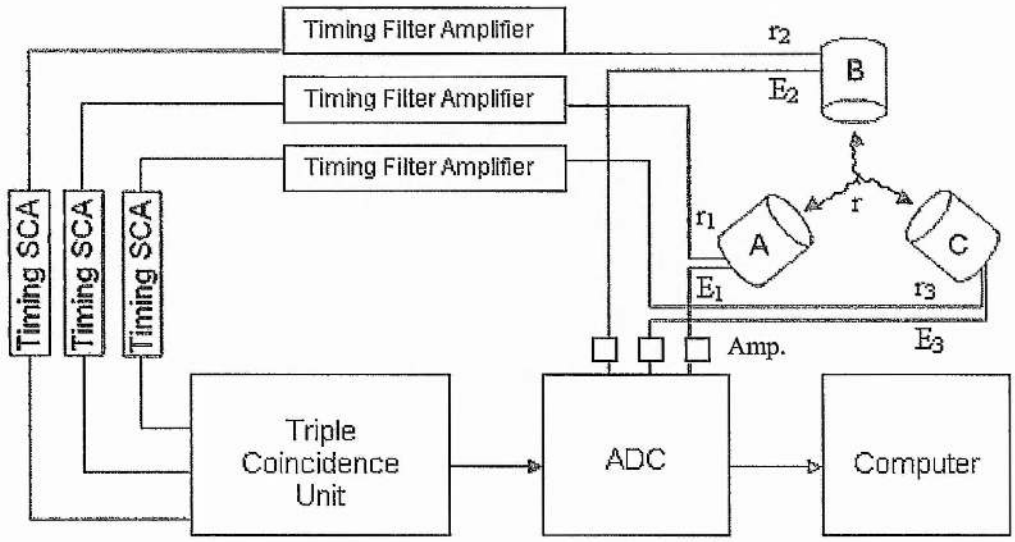

Figure 7.4: Experimental set-up

The coincidence time is the measure of the accuracy in time within which three simultaneous events can be detected by the three detectors. When the annihilated photons are recorded, the three detectors should trigger the pulse height discriminator at the same time. This time spread in response of the three detectors requires that a finite time window setting into the coincidence circuit. The timing signals have to be amplified then fed to the timing single channel analyzers (TSCAs) before the triple coincidence unit. TSCAs are used to generate logic pulses that correspond to the energy range of interest.

The triple coincidence unit is a fast coincident unit, which combines the pulses that arrive from the three TSCAs. This unit can be regarded as an electronic collimator. It generates a logic output pulse when leading edges of all of the enabled logic inputs occur within the selected coincidence window. The analogue-to-digital converter (ADC) unit used in this measurement has the capability of accepting four sampling channels; it has four ports from which three are receiving the energy signals from the detectors while the fourth receives the timing signal from the coincidence unit. All these analogue signals will be converted to digital signals before being directed to the computer. The computer has an analyser supported by Lab View Software under a windows operating system used to record and store pulses in channels which correspond to certain energies.

The output energy signals, collected from the three detectors, are amplified by three spectroscopic amplifiers before these signals are fed into the ADC. The energy calibration of the detection system is important in order to have a uniform response and for the collected spectra to be quantitative. In order to cover the entire energy range of interest from 81keV to 511keV for the three photon positron annihilation energies, ^{133}Ba and ^{22}Na sources were used for the calibration of the HPGe and CZT detectors. The spectrum analysis was performed by the computer program (Wingraph) that selects six photopeaks corresponding to the energies of interest. The channel number that corresponds to the highest count rate of each selected photopeak was recorded. Then after plotting the linear graphs of energy against channel number for each detector, gradient, intercept points and correlation coefficient were calculated. These figures were used for the calibration of the system.

Table 7.1: Energy calibration for the three HPGe detectors.

Source	Energy (keV)	Channel number		
		Detector A	Detector B	Detector C
^{133}Ba	81	311	268	279
	276	1053	919	973
	302	1153	1006	1068
	356	1357	1179	1259
	383	1466	1279	1359
^{22}Na	511	1952	1696	1810
Intercept point (keV)		-0.17	-0.13	2.57
Gradient (keV/ch)		0.262	0.301	0.281
Correlation coefficient (R^2)		1.00	0.99	1.00

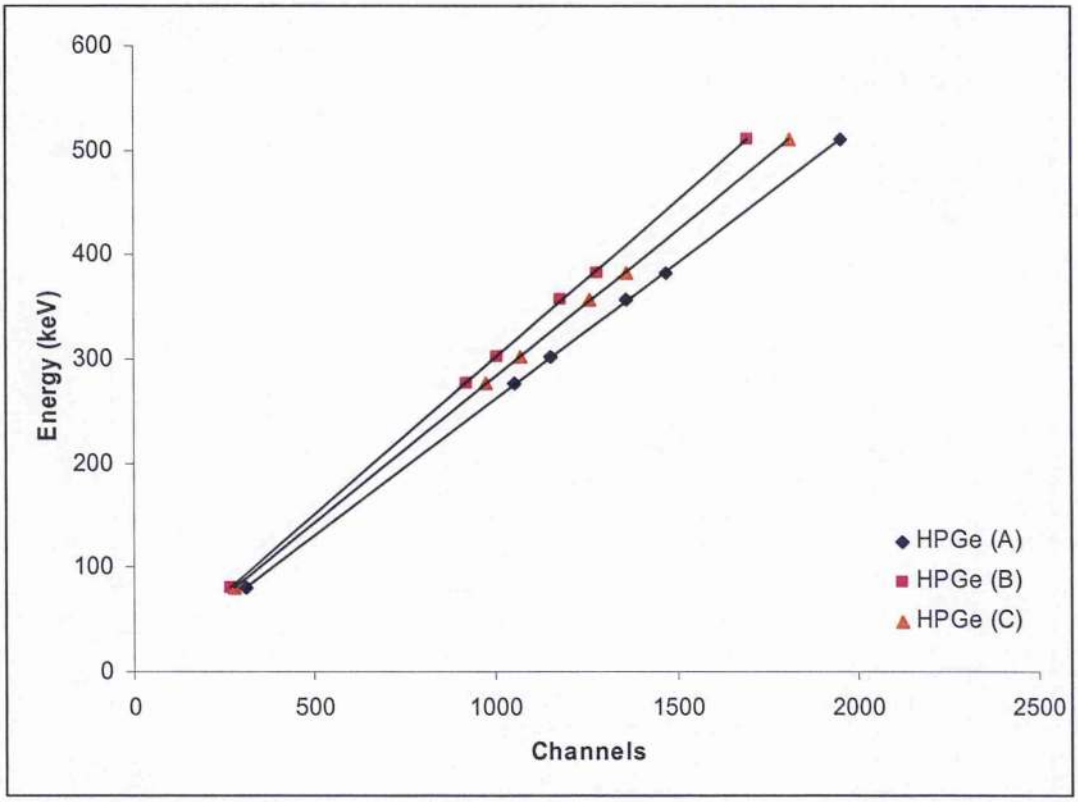

Figure 7.5: Energy calibration for the three HPGe detectors

Table 7.2: Energy calibration for the three CZT detectors.

Source	Energy (keV)	Channel number		
		Detector A	Detector B	Detector C
^{133}Ba	81	222	263	273
	276	803	968	937
	302	868	1054	1020
	356	1020	1237	1198
	383	1107	1336	1310
^{22}Na	511	1484	1801	1718
Intercept point (keV)		4.86	6.92	-0.96
Gradient (keV/ch)		0.342	0.281	0.297
Correlation coefficient (R^2)		0.99	0.99	0.98

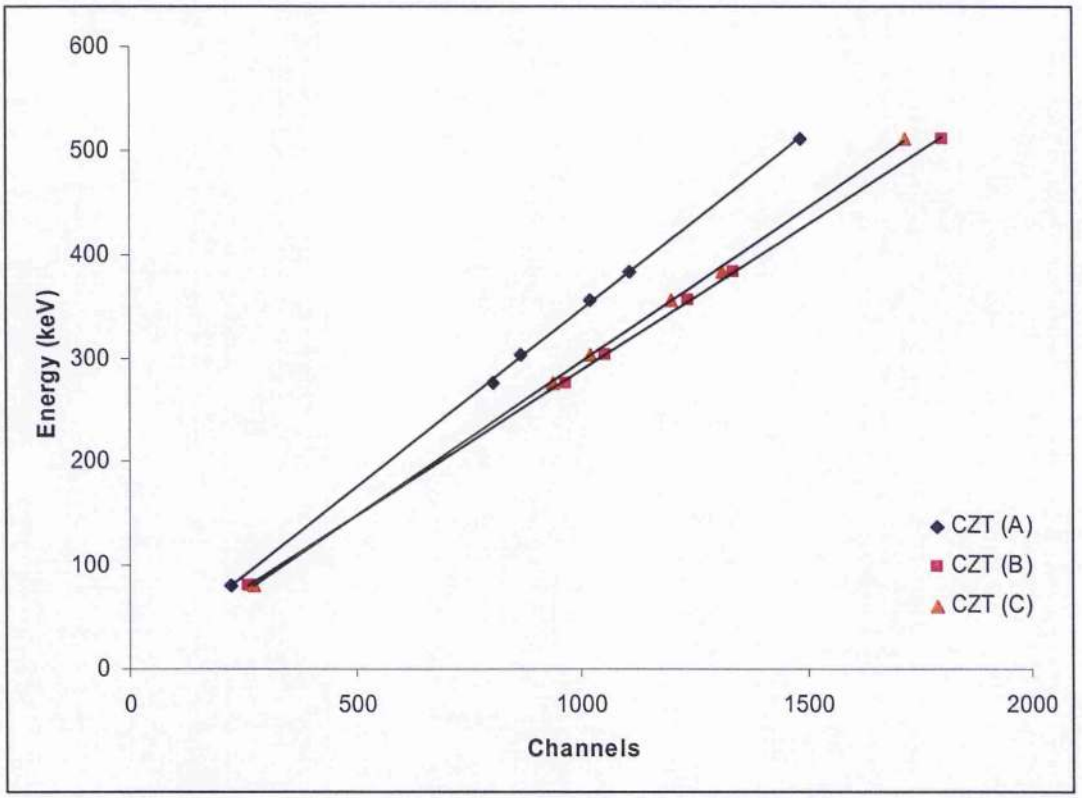

Figure 7.6: Energy calibration for the three CZT detectors.

7.4.2 Procedure of the Measurement and Sample Preparation

Three high-purity germanium (HPGe) detectors (EG&G Ortec) were connected in coincidence and arranged in a plane with angles of about 120° to each other to form a simple three photon positron annihilation scanner (Fig. 7.4). The size and operating voltages for the three HPGe detectors respectively were as follows: Ø 55.0 × 51.0 mm, -2500 V; Ø 42.4 × 44.1 mm, +3000 V and Ø 66.5 × 66.5 mm, +2200 V. A ^{22}Na source of activity 0.094 MBq was used which has the decay characteristics shown in Figure 7.7. It decays by positron emission (90.4%) and electron capture (9.5%), followed by a gamma energy of 1274 keV (99.9%) almost simultaneously. For coincidence studies it should be noted that 1274keV can increase the probability of random coincidences occuring. The source was embedded in fine silica powder to form orthopositronium into the free volume between the powder grains in a jar [Bra68]. The upper and lower energy discrimination windows of the timing single channel analysers (TSCA) were adjusted to form an adequate time window for selecting the events of interest and the output presented to the triple coincidence unit. The triple coincidence events were identified with a timing resolution window about 40ns and the energies in the three channels were registered by simultaneous sampling through an analogue-digital converter (ADC).

The 3γ yield was studied in two different environments, ambient air (normoxic environment) and in a hypoxic environment where AnaeroGen™ material (AN0025A, from OXOID Ltd., Hampshire, England) was used [Ana05]. The AnaeroGen™ contains ascorbic acid and activated carbon which reacts on contact with air. Atmospheric oxygen is consumed by the AnaeroGen™ and produced about 9% of carbon dioxide in a sealed jar. This technique significantly differs from those commonly used as hypoxic conditions occur with no evolution of hydrogen. Also no addition of water is needed to activate the reaction.

The experimental study was designed to measure the 3γ yield by using 3γ coincidence events having an energy sum of 1022keV under two different conditions in normoxic and hypoxic environments to explore the possibility of exploiting 3γ annihilation in PET imaging for measuring the relative oxygenation of tissues in oncology.

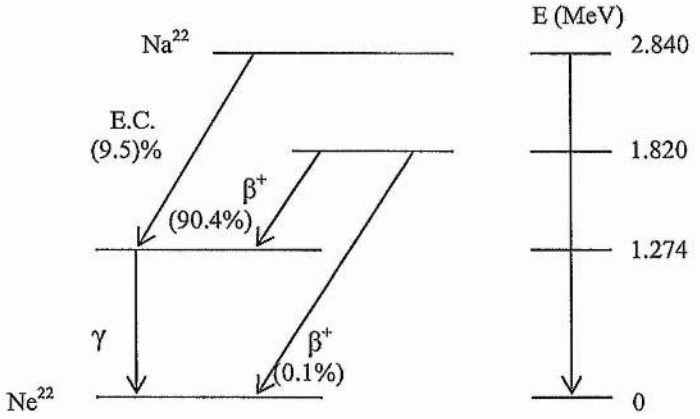

Figure 7.7: Decay scheme of Na^{22}.

7.5 Results and Discussion

Measurement of the 3γ yield in the two different samples was recorded under identical operating conditions, each started with equal positron activity and counted for the same time of 48 hours. In figure 7.8 the green dashed curve in each spectrum represents the data fitting of true triple coincidence photon events in which the three detected photons have deposited their total energy of 1022keV in three detectors combined. In order to extract the events corresponding to the full-peak energy photopeak (1022keV) detected 3γ annihilations, filtering has to be performed, in which only events with all three energies are less than or equal to 511keV and fulfil equation (7.2). The background underneath the full-peak was considered as a decaying exponential shape. The results show that the total registered events for the

sample in the normoxic environment and the hypoxic environment were 19722±140.4 counts and 19741±140.5 counts, respectively. However, the true 3γ events found after fitting the sum peak of 1022keV were 1374±37 counts in the normoxic environment and 1738±42 counts in the hypoxic environment. Therefore, the percentage of the events qualified as 3γ is about 26.5% higher in the hypoxic environment. It should be noted that the error in the peak yield 1022keV due to fitting was found smaller than the statistical error.

It has been reported that ortho-positronium is highly quenched by oxygen [Hey61, Coo67, Cha01]. In this experiment the 3γ yield in these two environments was different due to a variety of quenching processes including conversion of ortho-positronium to para-positronium. The spin conversion operates rapidly in paramagnetic media, such as O_2, to allow an equilibrium statistical distribution of the positronium spin state, exactly as in free annihilation. Therefore, the number of ortho-positronium (3γ) to para-positronium (2γ) is quenched rapidly in the normoxic environment. The variation of quenching rate can be determined both, in a high quenching rate medium as in O_2 or in a low quenching rate medium as in CO_2, thus providing valuable information about hypoxic conditions. This allows the development of a non invasive method which can be tested against existing oxygen measurement devices for determining and imaging the relative oxygenation of tissues in oncology.

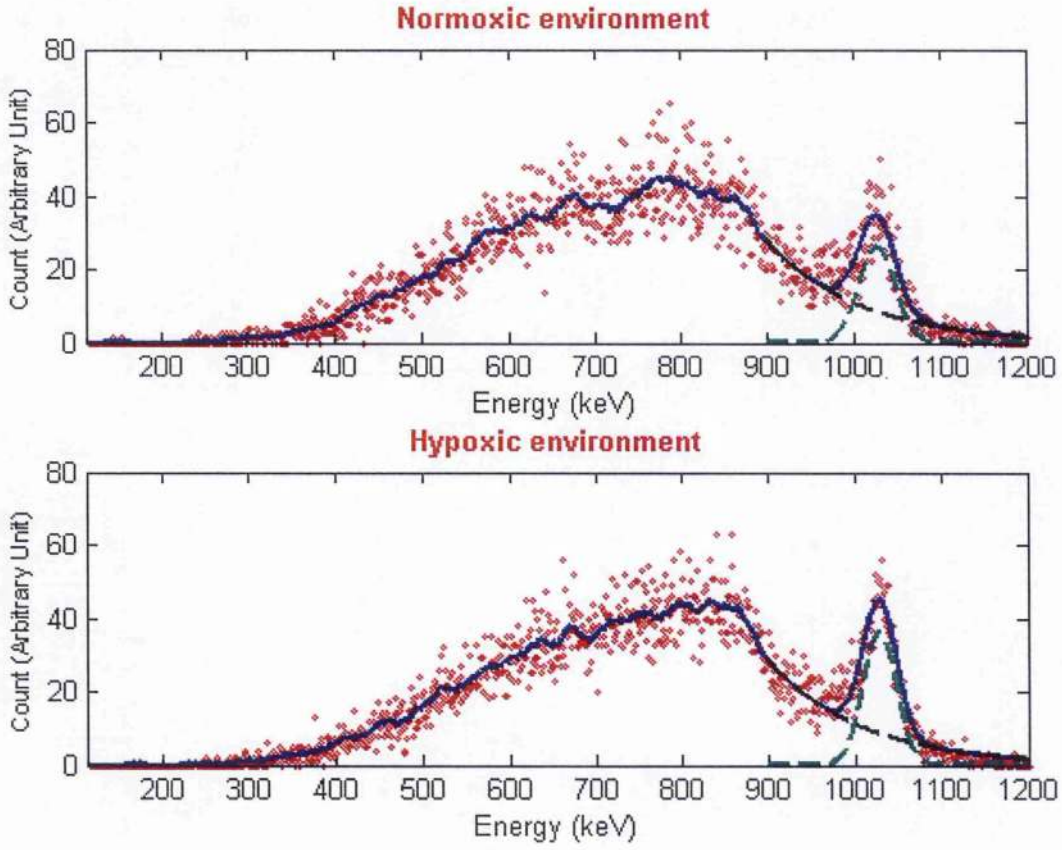

Figure 7.8: Summed energy spectrum of three gamma coincidence events in the normoxic and hypoxic environments for the same time of counting.

Image reconstruction with three photon positron annihilation is unlike the complex methods required for conventional 2γ PET. One only needs to solve numerically the non-linear equation (7.1) to retrieve r from 3γ event. A simple method of image reconstruction was developed by Kacperski and Spyrou (2004). By making use of the energy dependence of the positioning a 'set of points' image was produced. Figures 7.9 and 7.10 show the 3γ images in hypoxic environment and normoxic environment, respectively. Maple software was used to reconstruct three photon images. Attenuation correction for 3γ events is in general difficult [Kac05, Spy05]. It does not have the advantage of relatively easy attenuation correction as in conventional 2γ PET, where the attenuation along any line of response is constant, independent of the

site of annihilation and can be measured directly by a transmission scan. For each point in an object and each particular combination of energies and emission directions of the three photons, the attenuation factor will be different. In general attenuation for 3γ photons is higher than for 2γ because of lower energies.

If there are nuclear decay gamma-ray photons accompanying positron emission, e.g. Na^{22}, the rate of triple coincidences and false 3γ events may increase significantly, although still most of them could be rejected due to the energy conservation condition equation (7.2). The main source of spurious counts is the 2γ random coincidences where two 511 keV photons pass through two of the detectors, while the third one is hit by one of the 1274 keV photons, which are partially detected, so that they fall within the energy range of the 3γ spectrum. The sum energy can then be larger or smaller than 1022 keV depending on the energies deposited in the detectors. The few points that are far from the source in the reconstructed image probably arise from the random triple coincidences. The level of background would be much lower for a pure positron emitter like ^{18}F, which is most commonly used isotope in clinical PET scan.

The set up of many 3γ experiments was carried out using three CZT detectors. They were connected in coincidence and arranged in a plane with angles of about 120° to each other to form a simple three photon positron annihilation scanner. The size of the three CZT detectors was 10mm × 10mm × 7.5mm for each one. A thin kapton foil sealed ^{22}Na source of activities 0.107 MBq were placed in samples of fine silica powder and sealed in glass containers under nitrogen atmosphere. The total registered events were 99392±315 counts and only 800±28 events qualified as true 3γ registered during a period of 9 days. Unfortunately the small crystal sizes of CZT detectors, are showing that these particular detectors are not appropriate for coincidence circuit measurements. Thus there are no valid conclusions for the suitability of CZT detectors in 3γ PET imaging can be extrapolated from the specific dimensions and experimental set-up.

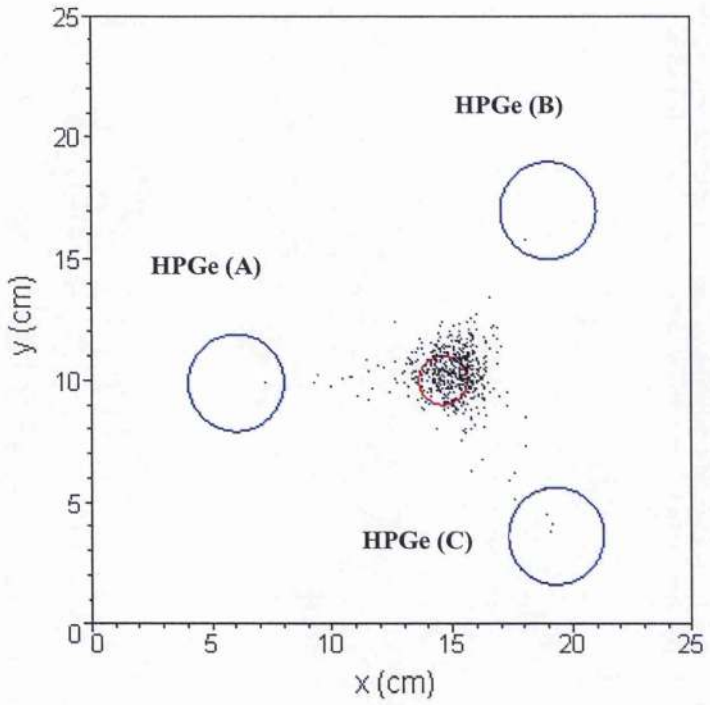

Figure 7.9: 3γ imaging in hypoxic environment.

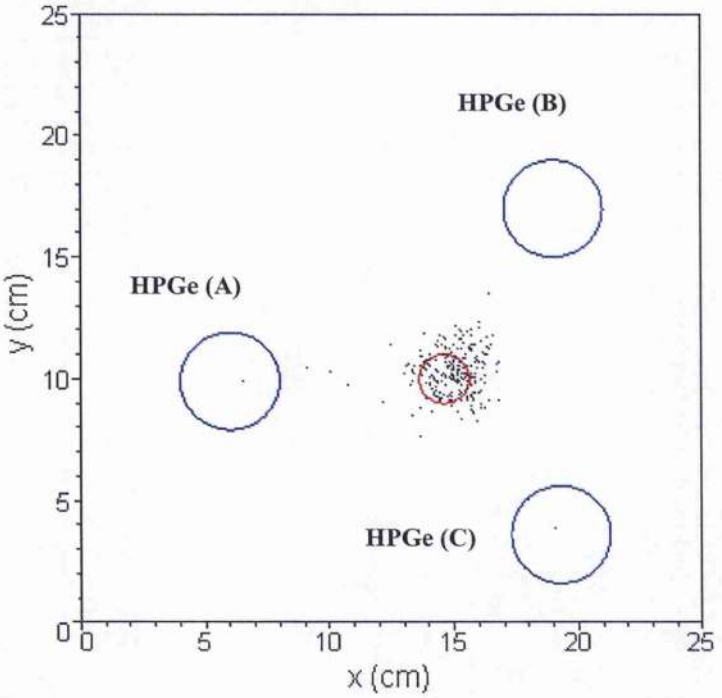

Figure 7.10: 3γ imaging in normoxic environment.

7.6 Conclusion

The 3γ yield was measured in normoxic and hypoxic environments using the triple coincidence measurement of three high-energy resolution detectors (HPGe). The AnaeroGen™ was used to generate a hypoxic environment. The percentage of the coincidence events qualified as 3γ was 26.5% higher in the hypoxic environment. This is due to the variation of quenching processes of triplet positronium into its singlet state when o-P_s collides with atoms or molecules in a media. The exploitation of 3γ imaging may open up a new area of interest in medical positron emission tomography (PET) as a new analytical method to evaluate hypoxic tumour in oncology. Oxygen is known to be a strong o-P_s quencher where 2γ annihilation replaces the 3γ process. Therefore, it is possible for hypoxic cells to be characterised by higher 3γ rates than those cells which are well oxygenated. 3γ imaging could be used as a monitoring tool to determine oxygen contents in different physiological and oncological conditions. It is predicted that the 3γ imaging of hypoxic tumour cells with a PET scanner will yield 'hot spots'.

The limitations of 3γ imaging seem to be in the first place the low number of counts, especially with high attenuation and the spatial resolution limited mainly by the energy resolution of detectors. High energy resolution would be able to resolve events arising from Compton scattering which do not correspond to 3γ events that fall within the energy range of the 3γ spectrum. It has been demonstrated that the simple system of three high-energy resolution detectors (HPGe) is able to produce images of three photon positron annihilations using the simplest possible procedure by solving equation (7.1) for each registered 3γ event and producing a set of point images. HPGe detectors offer superior energy resolution however the need for cryogenic cooling and cost make the choice rather impractical at least for clinical PET. The most likely appropriate semiconductor detectors to be used for a PET scanner incorporating three photon annihilations are the room temperature semiconductors like CZT. Although their energy resolution is not as good as that of HPGe, they have a significantly better stopping power and are much more convenient to handle without the need of cryogenic cooling.

High resolution spectroscopy and sufficient number of counts obviously needs to be addressed for 3γ imaging. It is therefore important to find out whether the new scintillator detector materials which are gradually making their way into PET and SPECT imaging technology can be used, instead of semiconductors, for this application. A series of experiments was carried out with different samples in order to study the effect of ortho-positronium formation as explained in the next chapter. Two methods, apart from triple coincidence, were compared in the measurement of the relative 3γ to 2γ yield.

Chapter 8

The relative yield of 3γ/2γ positron annihilation using semiconductor and scintillation detectors

8.1 Introduction

The mechanism of the 3γ decay process is determined by the chemical and physical state of the environment in which the interaction between the positron and medium can be investigated on the basis of two fundamental phenomena; inhibition of positronium formation which leads to 2γ annihilation or formation of the positronium which leads to 3γ annihilation (Chapter 4). If positronium is formed, the ratio of 3γ to 2γ will approach the limit three to one for 100% positronium formations because of the three to two distribution of triplet to singlet positronium. Quenching of the ortho-positronium (3γ state) into para-positronium (2γ state) takes place when ortho-positronium interacts with the atoms or molecules in the medium. This will reduce the ratio of three-photon to two-photon events and also the lifetime of ortho-positronium.

In condensed materials such as metals, positronium cannot be formed because of the presence of free electrons [Dau81]. The 3γ yield to be expected in the complete absence of positronium formation is given by the calculation for a positron in a free annihilation and is equal to 1/372, i.e. 0.27% [Ore49]. In most polymers, molecular liquids, fine powders and gases the positronium is formed but the quenching effect of ortho-positronium state varies [Hei57, Bel65, Lee65]. Strong quenching of the ortho-positronium state is found in oxygen, which is known to catalyse the conversion of triplet positronium to singlet state [Deb54, Hei57, Hey61]. Kacperski and Spyrou [Kac04a] proposed that useful information can be extracted from the ortho-positronium 3γ decay in positron emission tomography (PET) imaging as a measure of the oxygen content in biological tissues and particularly in hypoxia by determination of this relative yield. However, high resolution spectroscopy is required and it is therefore important to find out whether the new generation of scintillator detectors can be used, instead of semiconductors, for this application.

Progress in the physics and technology of broad-band semiconductor materials and scintillation detectors has made possible a wider range of their application in medical imaging. In this experimental study, a comparison between high-purity germanium (HPGe), sodium iodide (NaI(Tl)), lanthanum chloride ($LaCl_3$:10%Ce) and lanthanum bromide ($LaBr_3$:5%Ce) was carried out in terms of the relative 3γ/2γ yield obtained. Ideally, scintillation crystals or semiconductor materials used in medical imaging applications should have high detection and scintillation efficiency, good energy, time and spatial resolution, short dead time, fast scintillation response and mechanical and chemical stability. Unfortunately not all these requirements can be met by any of the commercially available detectors. Thus there has been considerable research and development of new inorganic scintillators with enhanced performance [Dam06, Kuh04]. Table 8.1 summarises the comparative properties of $LaBr_3$:Ce, $LaCl_3$:Ce, NaI(Tl) and HPGe detectors used in this study [Kno00, Mos05].

The aim of this study is to evaluate and characterise $LaBr_3$:Ce, $LaCl_3$:Ce, NaI(Tl) and HPGe detectors for the determination of the 3γ yield with different quenching materials. In addition, this work is aimed to compare detection properties of these detectors in order to investigate the potential use of the relative new scintillator materials for three photon positron annihilation imaging where high energy resolution and good efficiency are required. A series of experiments was carried out with different samples in order to study the effect of orthopositronium formation. The peak-to-peak and the peak-to-valley methods were compared in the measurement of the relative 3γ to 2γ yield.

Table 8.1: Summary of comparative properties for $LaBr_3$:Ce(5%), $LaCl_3$:Ce(10%), NaI(Tl) scintillators and HPGe semiconductor detectors [Kno00, Mos05, Sal07].

	$LaBr_3$:Ce	$LaCl_3$:Ce	NaI(Tl)	HPGe
Density (g/cm^3)	5.29	3.79	3.67	5.35
Decay time (ns)	26	28	240	-
Light output (photons/511keV)	32200	25000	19400	-
Effective atomic number (Z_{eff})	47	46	50	32
Energy resolution (at 511 keV)	3%	4%	7%	<1%
Wavelength (nm)	380	350	415	-

8.2 Methods for calculating the relative yields of 3γ/2γ annihilation

The measurement of the relative yields of the three photon positron annihilation to two photon positron annihilation is one of the methods for investigating the formation and quenching processes of positronium that affect the yield rate of the three photon positron annihilation. Besides the application of the simple triple coincidence technique (Chapter7), two methods have been used and evaluated to measure three photon positron annihilation using a single detector. These are the peak-to-peak and the peak-to-valley methods. None of the positron annihilation processes measured by these methods is currently captured and utilized by conventional PET. The yields were used to obtain three photon estimates from the reduced counts in the full-energy photopeak at 511 keV as was done by previous workers [Hey61, Bus64, Gai64, Ber65, Rao72, Tan82]. They were used to measure the relative yields of 3γ/2γ positron annihilation in magnesium oxide, Teflon, silica and different metals. Recently these two methods were investigated using biological samples [Chi09] and assessed by employing a single detector of HPGe, NaI(Tl), $LaCl_3$:Ce and $LaBr_3$:Ce in turn [Alk09].

8.2.1 Peak-to-peak method

The peak-to-peak method was applied to estimate the relative yields of three photon positron annihilation, using a single detector. This method measures the full energy photopeak area of the 511 keV gamma peak obtained with the sample and the same for the reference material. This method works under the natural assumption of the equality of positrons emitted in both cases [And01]. The ^{22}Na source used has a positron yield of 90.4% as well as gamma-ray energy at 1274 keV of relative intensity 99.9% which is emitted almost simultaneously. The number of photons detected in the full energy photopeak area of the 1274 keV peak obviously does not depend on the formation of positronium. The spectrum is normalized in order to have the same full energy photopeak area of the 1274 keV peak.

If ε_1 is the intrinsic efficiency of the 511 keV photon peak produced from the annihilation of the positron and ε_2 is the intrinsic efficiency of the 1274 keV photon peak then for the reference material the count rate can be calculated as:

$$R_{511_{ref}} = 2 \times \varepsilon_1 \times A \qquad (8.1)$$

$$R_{1274_{ref}} = \varepsilon_2 \times A \qquad (8.2)$$

where ε_1 and, ε_2 are the intrinsic efficiencies for 511 keV and 1274 keV gamma-ray peaks, respectively. A is the activity of the source and R is the count rate for the two different quanta [And01]. In an analogous way for the sample under examination:

$$R_{511_s} = 2 \times \varepsilon_1 \times A \times (1 - P_{3\gamma}) \qquad (8.3)$$

$$R_{1274\,s} = \varepsilon_2 \times A \qquad (8.4)$$

where s refers to the sample under investigation and $P_{3\gamma}$ is the probability of positronium formation. The count rates of the 1274 keV peak should be equal since the emission of these quanta does not depend on the formation of positronium.

$$R_{1274_{ref}} = R_{1274s} \qquad (8.5)$$

By subtracting the count rates for the 511 keV peaks, the $P_{3\gamma}$ can be measured according to the following equations:

$$D = R_{511_{ref}} - R_{511_s} = 2 \times \varepsilon_1 \times P_{3\gamma} \times A \qquad (8.6)$$

$$P_{3\gamma} = \frac{D}{2 \times \varepsilon_1 \times A} \qquad (8.7)$$

The difference D is attributed to the increase of the three photon positron annihilation in the tested sample and the relative yield of three-to-two photon annihilation is:

$$\frac{Y_{3\gamma}}{Y_{2\gamma}} = \frac{\left(R_{511_{ref}} - \left(R_{511_s} + \frac{R_{511_s}}{372} \right) \right)}{R_{511_s}} \qquad (8.8)$$

Where $(R_{511})_{ref}$ and $(R_{511})_s$ are the number of counts in the 511keV full energy photopeak area obtained in the reference material and in the sample, respectively. Aluminum was used as the reference material because positronium cannot form in metals [Dau81] and the probability of three gamma events is known, not to exceed that for a free annihilation, typically quoted as 1/372 [Ore49].

8.2.2 Peak-to-valley method

The peak-to-valley method is based on the principle that three gamma events cause the shift of counts from the full-energy photopeak at 511keV to lower energies. Thus the relative yields of the three photon positron annihilation to two photon positron annihilation is obtained by measuring the ratio of the counts of gamma rays in the spectrum lower than 511keV (valley region) emitted from three photon positron annihilation to the counts in the full-energy photopeak area at 511keV gamma peak. Compared to two-gamma emissions, three-gamma emissions are less energetic due to the sharing of the initial energy by three instead of two gammas. The reduced counts in the full-energy photopeak therefore reflect a change in competition between two-gamma and three-gamma events. Then the relative yields of 3γ/2γ annihilation photons can be calculated by the counts of the valley and the peak [Hey61, Bus64, Tan82].

$$\frac{Y_{3\gamma}}{Y_{2\gamma}} = \frac{\left(R_{vs} - KR_{ps}\right)}{\mu\xi R_{ps}} \qquad (8.9)$$

where R_v and R_p are the number of counts in the selected valley region and the photopeak area at 511keV gamma peak, for the sample under investigation, respectively. μ is the ratio of the valley to the peak regions detection efficiencies ($\varepsilon_3/\varepsilon_2$) multiplied by the factor (3/2) which accounts for the counts emitted in three and two gamma events. The term K can be obtained by measuring the reference material, K= $R_{v_{ref}} / R_{p_{ref}}$, where $R_{v_{ref}}$ and $R_{p_{ref}}$ are the counts in the valley and peak regions in the reference material, respectively. ξ is the theoretical correction for the selected region of the valley to the whole theoretical spectrum of 3γ annihilation.

Due to the presence of Compton background at low energies, in the 0-340keV region, part of the valley region is generally chosen to be between the Compton edge and the 511keV. This part is corrected by the factor ξ to derive the total 3γ counts for the whole theoretical 3γ annihilation predictions of the continuous spectrum of the γ-rays

from orthopositronium 3γ decay [Tan82, Cha85, Jin95]. Originally Ore and Powell [Ore49] calculated the lowest-order energy spectrum which was expressed as:

$$F(k)=\frac{1}{3}\left\{\frac{k(m-k)}{(2m-k)^2}-\frac{2m(m-k)^2}{(2m-k)^3}\ln\frac{m-k}{m}+\frac{2m-k}{k}+\frac{2m(m-k)}{k^2}\ln\frac{m-k}{m}\right\} \quad (8.10)$$

Where k is the γ-ray energy and m is the rest mass of the electron. It is a continuously rising distribution in the energy range from 0–511keV.

8.3 Experimental comparison between semiconductor and scintillation detectors using ^{22}Na with Teflon and silica samples

8.3.1 Materials and Methods

Four detectors were used in this study. $LaBr_3$:Ce and $LaCl_3$:Ce scintillators, doped with 5% and 10% of cerium respectively were supplied by Saint-Gobain™. The $LaCl_3$:Ce and $LaBr_3$:Ce crystals were directly coupled to Hamamatsu R6231 photomultiplier tube (PMT) and XP2060 respectively. The NaI(Tl) crystal, doped with approximately 0.5% of thallium, was directly coupled to a PMT (SCIONX 51 B 51/2). The High-purity Germanium (HPGe) detector was by EG&G Ortec, Model GEM-50P4. The size and operating voltages for the $LaBr_3$:Ce, $LaCl_3$:Ce, NaI(Tl) and HPGe detectors respectively were as follows: Ø 25.0 × 25.0 mm, 478 V; Ø 44.4 × 50.8 mm, 737 V; Ø 50.8 × 50.8 mm, 540 V and Ø 66.5 × 66.5 mm, 2200 V. The crystals were irradiated by a wide range of γ-ray point sources (^{133}Ba, ^{60}Co, ^{137}Cs and ^{22}Na). These isotopes cover the energy range of approximately 81 keV to 1332 keV. Gamma-ray spectra for each source were recorded with these detectors under identical operation conditions, such as acquisition time and surrounding shielding material.

Aluminium foils of 0.25 mm thickness were used as reference materials because in the presence of free electrons, positronium cannot form. The samples under investigation were Silica and Teflon©. Silica was supplied by Griffin & George Limited and used as a sample material to form ortho-positronium into the free volume between the silica grains [Bra68]. Teflon© (polytetrafluoroethylene, PTFE) of 0.05 mm thickness is a paraffin based material which has some or all of its hydrogen replaced by fluoride. It was used because it favours the formation of triplet-positronium since quenching is

low [Cha67]. In order to reduce the different gamma-ray absorption effects, the sample, the reference material and the ^{22}Na source were prepared in a five layer sandwich. The sample rate was obtained by placing the sample next to the source and the reference material on the outside; the reference rate was obtained by interchanging the position of Aluminium and Teflon© as shown (Figure 8.1).

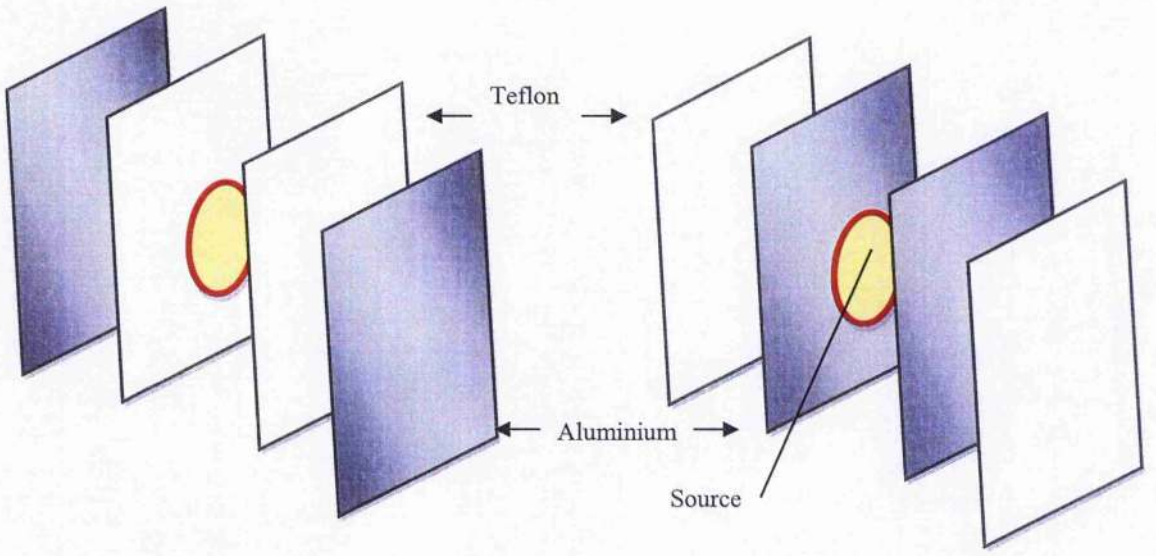

Fig. 8.1: Sandwich arrangement of aluminium, Teflon and the radiation source.

8.3.2 Results and Discussion

The characterisation of the gamma-ray detection properties of $LaBr_3$:Ce, $LaCl_3$:Ce, NaI(Tl) and HPGe detectors was obtained by using the Genie™ 2000 spectroscopy system software. The study involved recording of detected spectra and measurement of energy resolution and intrinsic photopeak efficiency (Figures 8.2, 8.3 and 8.4). The crystals of these detectors are of different sizes and densities, namely 5.29 g/cm^3, 3.79 g/cm^3, 3.67 g/cm^3 and 5.35 g/cm^3 respectively. In order to allow comparison, the solid angle subtended of the detectors was set at 0.22 steradian subtended between source and detectors for all measurements.

8.3.2.1 Energy resolution and intrinsic photopeak efficiency

Figure 8.2 shows the measured energy resolution for the four detectors with the gains set to encompass all energies of interest (i.e. up to 1332 keV). The HPGe detector shows its superior energy resolution over the scintillation detectors. The energy resolution figures achieved for the lanthanum based crystals are twice as good as that

of NaI(Tl). For instance, for the ^{22}Na 511 keV γ-ray, energy resolutions of (3.37±0.08)%, (4.11±0.03)%, (6.91±0.17)% and (0.50±0.01)% were measured for $LaBr_3$:Ce, $LaCl_3$:Ce, NaI(Tl) and HPGe, respectively (Figure 8.3).

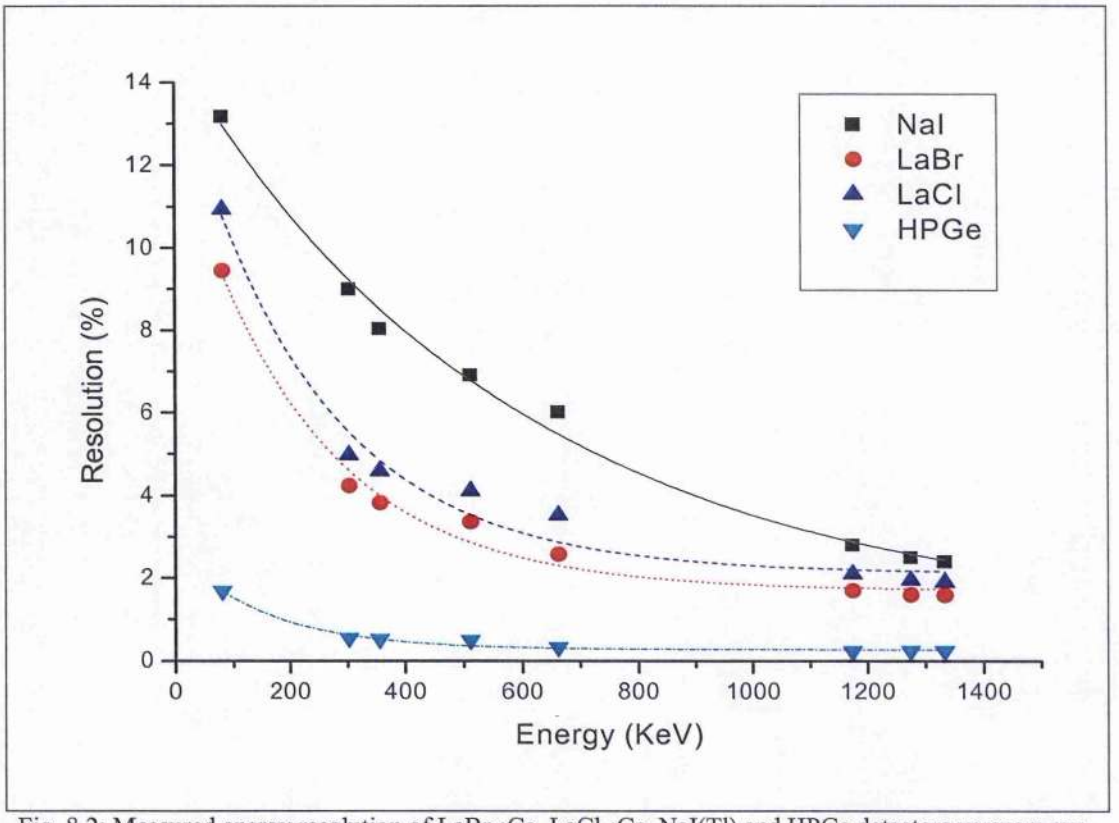

Fig. 8.2: Measured energy resolution of $LaBr_3$:Ce, $LaCl_3$:Ce, NaI(Tl) and HPGe detectors versus γ-ray energy.

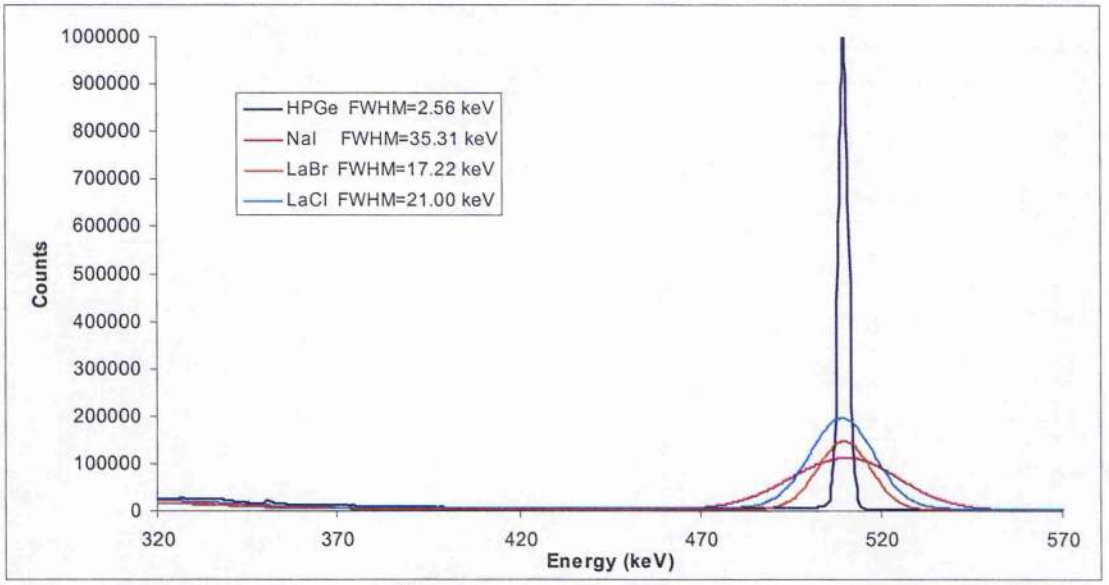

Fig. 8.3: Measured FWHM for the ^{22}Na 511 keV γ-ray of LaBr3:Ce, $LaCl_3$:Ce, NaI(Tl) and HPGe detectors.

Figure 8.4 shows the percentage of intrinsic photopeak efficiency for all detectors. It shows the high detection efficiency of NaI(Tl) is comparable to that of $LaBr_3$:Ce. For instance, for the ^{22}Na 511 keV γ-ray, intrinsic photopeak efficiency of (29.1±0.8)%, (22.2±0.5)%, (29.9±0.6)% and (12.8±0.9)% were measured for $LaBr_3$:Ce, $LaCl_3$:Ce, NaI(Tl) and HPGe, respectively. $LaBr_3$:Ce and $LaCl_3$:Ce have drawn significant interest due to their high scintillation yield and superior energy resolution which make them very valuable alternatives to most of the conventional scintillators and semiconductors.

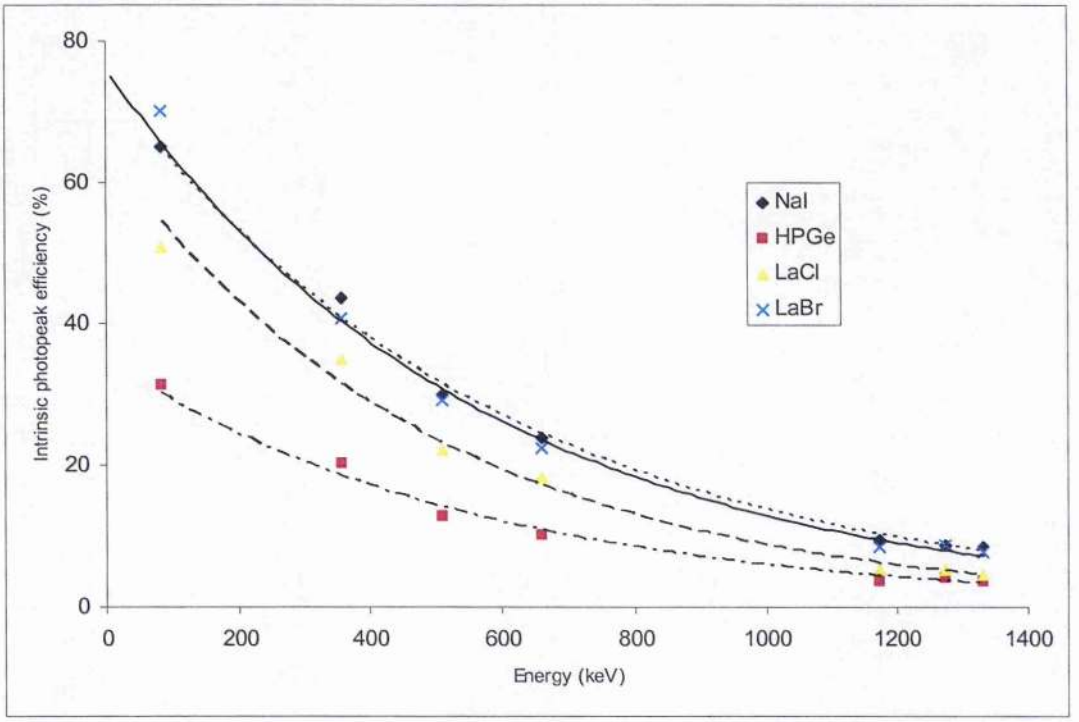

Fig. 8.4: Measured intrinsic photopeak efficiency of $LaBr_3$:Ce, $LaCl_3$:Ce, NaI(Tl) and HPGe detectors versus γ-ray energy.

8.3.2.2 The relative yield of 3γ annihilation

The relative 3γ/2γ yield was measured for a positron emitter ^{22}Na with the new scintillator detectors $LaCl_3$:Ce and $LaBr_3$:Ce, which had been characterised together with NaI(Tl) and HpGe detector. Table 8.2 shows the measured ratios of the relative yield of 3γ/2γ positron annihilation for the four different detectors by the peak-to-peak method for Teflon© and silica samples. It is clear that the 3γ/2γ value of both samples

shows the highest ratio when using the NaI(Tl) detector. This is due to the high detection efficiency of 3γ annihilation to be detected by NaI(Tl) detector. On the other hand, the HPGe detector shows the lowest value of 3γ/2γ due to relatively poor detection efficiency. For the lanthanum based crystals the 3γ/2γ values obtained were in between the values of the NaI(Tl) and HPGe detectors. Lanthanum based crystals have the advantage of excellent energy resolution and good efficiency among the scintillation detectors which makes them valuable alternatives to most of the conventional scintillators and semiconductors for investigating the 3γ yield .

Table 8.2: The measured result of 3γ/2γ positron annihilation by the peak-to-peak method.

Relative yield 3γ/2γ (10^{-2})		
Type of detector	Teflon	Silica
NaI(Tl)	3.26±0.10	4.01±0.16
$LaBr_3$:Ce	3.04±0.11	3.41±0.18
$LaCl_3$:Ce	2.17±0.11	2.98±0.13
HPGe	2.03±0.11	2.12±0.14

Table 8.3 illustrates the measured ratios of the relative yield of 3γ/2γ positron annihilation for the four different detectors by the peak-to-valley method for Teflon© and silica samples. Different parts of the valley region were chosen to be between the Compton edge and the 511keV for each detector. Figure 8.5 shows the selected valley region and the photopeak area at 511keV gamma peak for the NaI(Tl) detector. The results of table 8.3 show variation in the relative yields, the broader the valley region selected the higher is the relative yield of 3γ/2γ positron annihilation obtained.

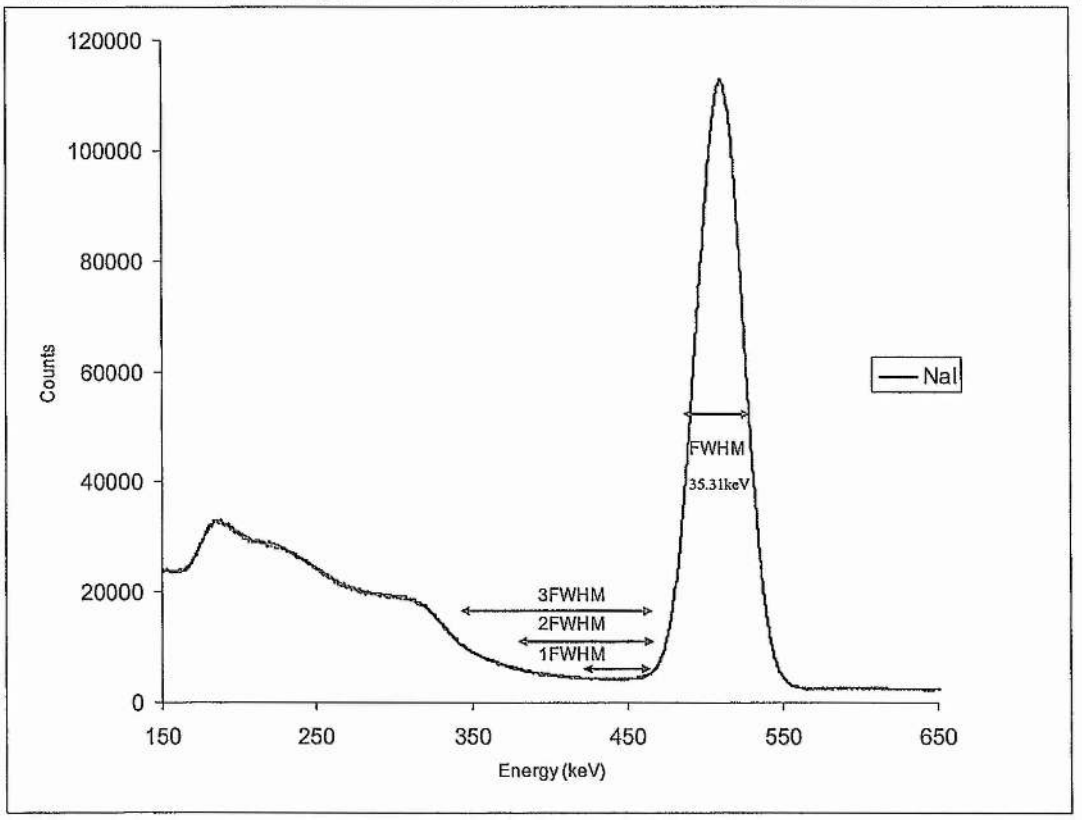

Fig. 8.5: selected valley region and the photopeak area at 511keV gamma peak for NaI(Tl) detector.

As expected, the relative yield of 3γ/2γ measured for the silica samples was higher than that of Teflon© sample in both peak-to-peak and peak-to-valley methods. This result agrees with the theory of positronium formation. In principle the precision of the peak-to-peak method only depends on the counts in the peak region. The precision can be improved by increasing the accumulated counts in the peak region. The results of the peak-to-peak method neither depend on the valley region where the counts are relatively low, nor are related to the correction factors ξ and μ values (equation 8.9). However, in the peak-to-valley method these factors must bring about errors, therefore the possible improvement of the precision is limited even if the time of measurement is increased. Thus the experimental precision of the peak-to-peak method is certainly better than the peak-to-valley method. The only limitation of using the peak-to-peak method is when the positron emitting source has only one peak as in the case of ^{18}F. The relatively longer lived positron emitter zirconium-89 (^{89}Zr), with a half-life about 78.4 hours, has recently drawn significant interest in the detection of lymph node metastases in head and neck cancers using PET imaging [Dij09, Nag07, Don07]. The ^{89}Zr source has a positron yield of 44.2% as well as a gamma-ray energy at 908 keV

of relative intensity 100% which is emitted almost simultaneously. Therefore peak-to-peak method can be clinically applied. Table 8.4 shows the main characteristics of positron emitters used in preclinical and laboratory studies.

Table 8.3: The measured result of 3γ/2γ positron annihilation by the peak-to-valley method.

NaI(Tl)		Valley Region			
		1FWHM	2FWHM	3FWHM	400-470 keV
		428.69-464 keV	393.38-464 keV	358.07-464 keV	
Relative 3γ/2γ (10^{-2})	Teflon	1.55±0.07	3.16±0.11	4.53±0.15	2.93±0.12
	Silica	1.92±0.11	3.59±0.16	4.90±0.22	3.99±0.16

HPGe		Valley Region					
		1FWHM	2FWHM	3FWHM	4FWHM	5FWHM	400-470 keV
		504.4-507 keV	501.8-507 keV	499.3-507 keV	496.7-507 keV	494.2-507 keV	
Relative 3γ/2γ (10^{-2})	Teflon	0.38±0.02	0.44±0.02	0.50±0.03	0.56±0.03	0.60±0.03	2.02±0.07
	Silica	0.63±0.04	0.74±0.06	0.83±0.06	0.98±0.07	1.07±0.08	2.66±0.20

$LaBr_3$:Ce		Valley Region					
		1FWHM	2FWHM	3FWHM	4FWHM	5FWHM	400-470 keV
		462.78-480 keV	445.56-480 keV	428.34-480 keV	411.12-480 keV	393.9-480 keV	
Relative 3γ/2γ (10^{-2})	Teflon	1.03±0.06	1.50±0.08	1.98±0.10	2.80±0.12	3.65±0.14	2.96±0.12
	Silica	1.29±0.09	1.92±0.13	2.69±0.16	3.30±0.18	4.37±0.21	3.59±0.19

$LaCl_3$:Ce		Valley Region					
		1FWHM	2FWHM	3FWHM	4FWHM	5FWHM	400-470 keV
		454-475 keV	433-475 keV	412-475 keV	391-475 keV	370-475 keV	
Relative 3γ/2γ (10^{-2})	Teflon	0.84±0.06	1.22±0.08	1.76±0.10	2.48±0.13	3.19±0.15	2.09±0.11
	Silica	1.11±0.06	1.59±0.09	2.26±0.11	3.11±0.13	3.93±0.15	2.75±0.11

The uncertainty in the peak-to-peak and peak-to-valley methods, respectively were calculated using the equations as quoted in reference [Tan82] (Appendix A). The associated uncertainties if calculated using error propagation analysis will give significantly greater errors than those quoted in Tables 8.2 and 8.3. It is recommended that further analysis of the errors for both methods should be calculated by taking into account the various factors in the experiments, such as the geometry of the different samples.

Table 8.4: The main characteristics of positron emitters used in preclinical and laboratory studies

Positron Emitter	Production	Half-life $T_{1/2}$	Main β+ energies (keV)	(%)	Intrinsic spatial resolution loss (mm)	Main γ energies (keV)	(%)
^{18}F	$^{18}O(p,n)$ $^{20}Ne(d,\alpha)$	1.83 hr.	633	(96.7)	0.7	511	(194)
^{64}Cu	$^{64}Ni(d,2n)$ $^{64}Ni(p,n)$	12.7 hr.	653	(17.4)	0.7	511 1345	(38) (0.5)
^{89}Zr	$^{80}Y(p,n)$	78.4 hr.	897	(22.7)	1.0	511 908	(44.2) (100)
^{22}Na	$^{19}F(\alpha,n)$ $^{24}Mg(d,\alpha)$	2.62 yr.	546	(90.4)	0.6	511 1274	(180) (99.9)

8.4 Gammasphere experiment using ^{18}F in blood samples of different oxygenation levels

8.4.1 Materials and Methods

The potential of incorporating 3γ annihilation into PET to detect oxygenation levels in biological samples was greatly accelerated by investigation using the Gammasphere facility at Argonne National Laboratory, Chicago, USA. The contract was awarded to Spyrou and the experiment carried out by Kacperski in November 2005. The data analysis was reported by Spyrou's group in September 2007 and February 2009 [Pre07, Chi09]. The Gammasphere is a spherical array of 110 HPGe detectors, each enclosed in a bismuth germanate (BGO) Compton-suppression shield. This provides a unique combination of high sensitivity and high resolution for gamma-ray spectroscopy.

^{18}F in the form of fluorodeoxyglucose (FDG) was used as the radiation source within each sample. With a short half-life (110min), this is the positron source most commonly used in PET for tracking body glucose metabolism. As a pure positron emitter, this clinical source creates additional challenges compared to laboratory sources typically used for three-gamma studies, e.g. ^{22}Na. In ^{22}Na, positron emissions are accompanied by 1.274MeV gamma rays, which provide the reference time trigger and the reference peak count in positronium lifetime and peak-to-peak analyses, respectively; both are useful methods of analysis for estimating 3γ ratios.

The haematological samples from sheep were aseptically collected and supplied by Hemostat Laboratories in the USA; whole blood, haemolysed blood, serum and cell concentrate. The whole blood had been treated with the anticoagulant sodium citrate. The haemolysed blood had been lysed by three complete freeze–thaw cycles. The serum had been sterile-filtered. For each measurement, a vial containing about 5ml of the sample, either oxygenated or deoxygenated, was placed at the centre of the detector assembly. About 1MBq of ^{18}F-FDG had been injected into the sample. During the measurements of oxygenated and deoxygenated samples a continuous flow of a varying mixture of O_2 and N_2 gas was blown over the sample. Measurements with

aluminium were carried out by sandwiching between two aluminium foils of 1.5 mm thickness on which a few drops of ^{18}F-FDG had been dried.

8.4.2 Results and Discussion

The ratios of the relative yield of 3γ/2γ positron annihilation was calculated by using the peak-to-valley method as the ratio of the counts summed over the FWTM of the full-energy photopeak to the counts summed over the 400–500keV range in the gamma spectrum. The FWHM and the FWTM of the 511 keV peak were 3.0 and 6.1 keV, respectively.

Figure 8.6 shows that the relative yield of 3γ/2γ, from the haematological samples, varied as much as 11% between haemolysed blood in an environment of with 2% O_2 and deoxygenated cell concentrate in an environment of N_2 gas. This variation suggests that the measurement of the relative yield of 3γ/2γ is sensitive to the chemical composition of the biological samples. Haemolysed blood, where haemoglobin had been liberated from red blood cells, and serum, where haemoglobin was absent, samples exposed to air were not differentiable. The similarity in the relative 3γ/2γ yield between the two confirms that bound O_2 did not cause changes in 3γ yields. Both samples have different levels of bound O_2 but similar levels of free (dissolved) O_2 due to their contact with the atmosphere. Table 8.5 shows the approximation of dissolved oxygen concentration in the haematological samples

The deoxygenation of serum produced an increased 3γ ratio, consistent with the reduced effects from O_2, which is known to quench ortho-positronium as well as to inhibit positronium formation [Coo67, Kak90]. Whole blood and haemolysed blood, both containing haemoglobin, appear to have little change in 3γ ratio after deoxygenation. Cell concentrate was found to have a reduced 3γ ratio after deoxygenation. It is relatable to the paramagnetic properties of haemoglobin, which may act as a quenching agent for ortho-positronium. The findings that the deoxygenation of serum increased 3γ ratio whereas the deoxygenation of cell concentrate reduced 3γ ratio support the suggestion that free haemoglobin might have played a quenching role.

These results which were analysed by the peak-to-valley method suggest that the behaviour of the samples on oxygenation and deoxygenation does not only depend on O_2 solubility alone but also depend on the sample containing haemoglobin, whether free, bound, or in venous blood, free O_2, free CO_2, oxyhaemoglobin, carboxyhaemoglobin, other chemical species that could have contributed to insensitivity in in-vitro samples. However, the blood components used here served only as biological samples. The choice by no means suggests the restriction of 3γ PET to the detection of blood chemistry. In tissue hypoxia applications, for example, 3γ PET is aimed at detecting in-vivo the local chemistry of the tissue itself, not the blood. This is important because measuring blood oxygen pressure (free oxygen in the blood) would not provide information on the oxygen available to the tissues; a highly hypoxic patient could have a distorted oxygen dissociation curve and/or a poor haemoglobin count but a normal blood oxygen pressure [Hoc01, Chi09].

Table 8.5: The approximation of dissolved oxygen concentration in the haematological samples

sample	Time (hour)	Oxygen concentration	
		ppm	%
Haemolysed blood (N_2)	10	0.3	5
Haemolysed blood (2%O_2)	2	3	35
Haemolysed blood (10%O_2)	2	4	50
Serum (N_2)	10	0.3	5
Serum (10%O_2)	2	4	50
Cell concentrate (N_2)	2	1	10
Whole blood (N_2)	2	0.5	7

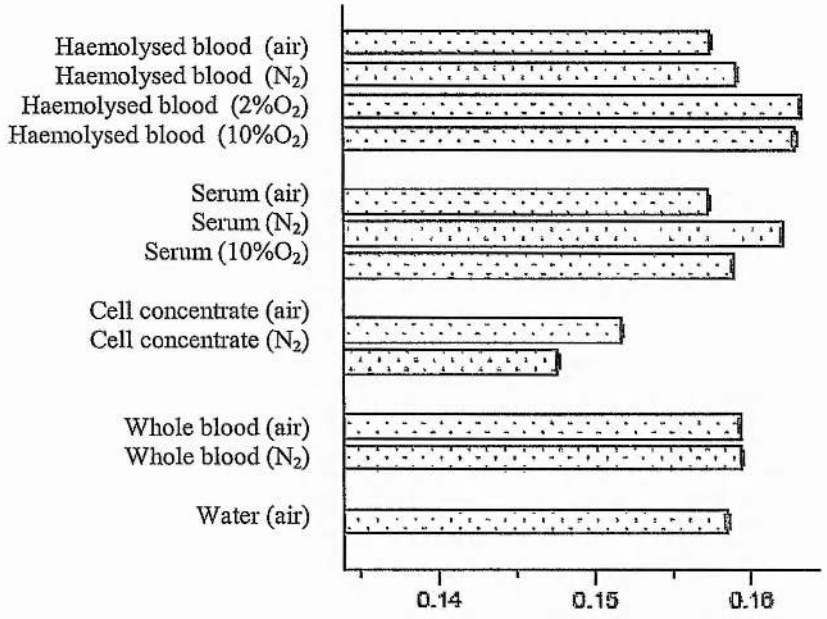

Figure 8.6: The relative yield of 3γ/2γ for the haematological samples

8.5 Conclusion

In this study, the relative yield of 3γ/2γ positron annihilation for investigating the formation and quenching processes of positronium in the Teflon© and silica samples was measured. A comparison between semiconductor and scintillation detectors was carried out in terms of the relative 3γ/2γ yield using the peak-to-peak and peak-to-valley methods. The peak-to-peak method can only be applied when the positron emission source is accompanied by radiative transition gamma ray (e.g. ^{22}Na, ^{64}Cu, ^{89}Zr) which provides the reference peak count in the peak-to-peak analysis. The experimental precision of the peak-to-peak method is better than the peak-to-valley method. This is due to the fact that the peak-to-peak method only depends on the counts in the peak region and the precision can be improved by increasing the accumulated counts in the peak region. From the results, the lanthanum based crystals ($LaBr_3$:Ce and $LaCl_3$:Ce) have the potential to replace NaI(Tl) and HPGe due to good energy resolution and good detection efficiency and can be the scintillators of choice for determining the yield of 3γ positron annihilation. The energy of three gamma rays

must fulfil the condition that $E_1 + E_2 + E_3 = 1022keV$ and therefore the detector must be able to resolve these three energies.

The peak-to-valley method was applied to measure the relative yield of 3γ/2γ positron annihilation using ^{18}F in 11 haematological samples of different oxygenation levels. The relative 3γ/2γ yield was found to vary as much as 11% between the components investigated. The sensitivity of this technique in differentiating the biological samples is encouraging. Interpretation of the variation in the 3γ yield in terms of the presence of free O_2, free haemoglobin and carboxyhaemoglobin was attempted. The paramagnetic properties of haemoglobin found in whole blood, haemolysed blood and cell concentrate acts as a quenching agent for ortho-positronium. The deoxygenation of serum produced an increased 3γ ratio, consistent with the reduced effects from O_2, which is known to quench ortho-positronium. We do not rule out additional modes of positronium quenching, quenching by other biochemical species as well as the inhibition of positronium formation. The results should encourage further studies on the different confounding factors contributing to the change in 3γ yields in biological tissues.

Chapter 9

Conclusion and future directions

Positron emission tomography (PET) is a functional imaging modality which is at present the most sensitive technique for cancer detection. Today, research and clinical work is concentrating on the use of PET as a multimodality system for more specific oncology areas such as responses to therapy applications and radiotherapy treatment planning. PET with the advent of new labelled positron emitting pharmaceuticals agents as cellular markers for detection of tumour hypoxia have demonstrated a certain amount of success in these areas and are expected to be in the forefront of these new imaging applications. In this thesis, however, the work is an approach to the new addition of a novel modality of 3γ PET to conventional 2γ PET as the positronium and its annihilation, could serve as an oxygen-sensitive marker.

Three photon positron annihilation as a new imaging modality can be developed as a non-invasive method for detection of tumour hypoxia. Changes in 3γ yield in matter are mainly due to changes in o-Ps quenching. One can predict that as the oxygen has highly quenched ortho-positronium (o–Ps), the low oxygen level in hypoxic cells may give higher three gamma yield events than in more oxygenated cells. Therefore if the work is continued to obtain images of samples with varying oxygen levels, it may be possible that hypoxic (or necrotic) tissue can be imaged directly as 'hot spots'. Also the image of 2γ can be mapped with that of 3γ and new valuable information can be extracted.

Follow-up research and more precisely measurements of three-photon positron annihilation in biological samples ('in-vitro' non-human) are required before taking any further steps to construct a new scanner. Are the differences in 3γ yields, in tissues, in relation to the oxygen measurable and with what sensitivity? The answers to these questions depend on the precision of the measurements of three

photon events and the accuracy of the oxygen concentrations in biological samples. It also depends on the ability of the system to determine the variation of quenching rate of the other molecules in tissues, e.g. either high quenching rate of oxygen or low quenching rate of carbon dioxide, which may provide valuable information not only of the location, but also the state of oxygenation of tumours.

Study of oxygen measurements in biological samples initially were examined experimentally, in Chapter 5. Efforts have been made to highlight the advantages of the polarography over colorimetery techniques for measuring different levels of dissolved oxygen in biological samples. In Chapter 6, further work for understanding and establishing the main factors that affect oxygen measurements under various conditions in defibrinated horse blood, plasma and mineral water were carried out by the introduction of controlled quantities of nitrogen and carbon dioxide through samples as well as AnearoGen to reduce oxygen, in preparation for hypoxia investigations. Study of the effect of variation of these values with temperature and pH is critical in translation from in-vitro to in-vivo. Based on the oxyhaemoglobin dissociation curve for understanding the factors that influence haemoglobin attraction to oxygen; a decrease of haemoglobin affinity to oxygen is caused by a decrease in pH, an increase in carbon dioxide concentration and an increase in temperature. From the experimental results obtained, bubbling nitrogen is not the method of choice for preparing hypoxic samples due to the conflicting effects of decreasing temperature and increasing pH values in all samples during the reduction of oxygen concentration. Bubbling carbon dioxide in all samples causes an increase in their acidity as in the case of hypoxic tumours, due to the formation of carbonic acid, however the temperature is reduced. On the other hand, using AnaeroGen is the choice for preparing in-vitro hypoxic samples due to the easy handling the AnaeroGen sachet as well as the good agreement with the factors that affect oxygen reduction. The next step ought to be in testing this with cultured cells. It would also be interesting to extend the work further by carrying out a similar study with gelatine, a soft tissue equivalent medium, and AnaeroGen reducing agent.

Determination of the relative oxygenation of samples by ortho-positronium 3γ decay for future application in oncology as a new analytical method to detect hypoxic tumour in oncology was investigated in Chapter 7. Three high-purity germanium

(HPGe) detectors were connected in coincidence and arranged in a plane with angles of about 120° to each other to form a simple three photon positron annihilation scanner. The 3γ yield was measured in normoxic and hypoxic environments, where AnaeroGen was used to generate the hypoxic environment. The percentage of the triple coincidence events qualified as 3γ was found to be 26.5% higher in the hypoxic environment. A laboratory source, ^{22}Na, is a positron emitter (90.4%), followed by a gamma energy of 1274 keV (99.9%) almost simultaneously. The latter may contribute false 3γ events when partially detected. Using a clinical pure positron emitter, ^{18}F, for the triple coincidence experiments is certainly worth further exploration in the variation of quenching processes between samples and therefore determine oxygen content and concentration.

The potential use of the new scintillator detectors, e.g. lanthanum chloride ($LaCl_3$:Ce) and lanthanum bromide ($LaBr_3$:Ce), was investigated in Chapter 8. The experimental part focused on measuring the relative 3γ/2γ yield in different samples by using a single detector. A comparison between the peak-to-peak and the peak-to-valley methods was examined. The peak-to-peak method can only be applied when the positron emissions source are accompanied by a radiative transition gamma ray (e.g. ^{22}Na, ^{64}Cu, ^{89}Zr) which provide the reference peak count in the peak-to-peak analyses. The experimental precision of the peak-to-peak method is better than the peak-to-valley method. This is due to the following; the peak-to-peak method only depends on the counts in the peak region and the precision can be improved by increasing the accumulated counts in the peak region. However, in the peak-to-valley method part of the spectrum is selected as the counts of the valley region, therefore it is necessary to correct the ratio of the 3γ counts in the selected part with the total 3γ counts in the whole theoretical spectrum of 3γ annihilation. Furthermore the average detection efficiency of the detector for 2γ and 3γ should be corrected by considering the ratio of gamma rays emitted from 2γ and 3γ annihilation. The results of the peak-to-peak method neither depend on the valley region where the counts are relatively low, nor are related to the correction factors mentioned above. The possible improvement of the precision of the peak-to-valley method is limited even if the time of measurement is increased. The only limitation of using the peak-to-peak method is when the positron emitting source has only one peak as in the case of ^{18}F i.e. a pure positron emitter.

The peak-to-valley method was applied to measure the relative yield of 3γ/2γ positron annihilation using ^{18}F in 11 haematological samples of different oxygenation levels. The experiments were carried out at the Argonne National Laboratory using the gammasphere instrument, USA. The relative 3γ/2γ yield was found to vary as much as 11% between these components investigated. The sensitivity of this technique in differentiating the biological samples is encouraging. Interpretation the variation in the 3γ yield in terms of the presence of free O_2, free haemoglobin and carboxyhaemoglobin was attempted. The paramagnetic properties of haemoglobin found in whole blood, haemolysed blood and cell concentrate acts as a quenching agent for ortho-positronium. The deoxygenation of serum produced an increased 3γ ratio, consistent with the reduced effects from O_2, which is known to quench ortho-positronium. These results should encourage further studies on the different confounding factors contributing to the change in 3γ yields in biological tissues.

In order to introduce the 3γ technique as complementary to conventional 2γ PET, high-energy resolution detectors are needed to improve the quality of the image and reduce the noise due to scattered events arising from Compton scattering which do not correspond to 3γ events. In addition, the detector should have high detection efficiency at energies of interest, as well as fast timing response. Characterisation of semiconductor and scintillation detectors was performed in this thesis in order to obtain good functional response and to evaluate the suitability of the detectors in a three photon positron annihilation detection system. Use of the new scintillator detectors $LaBr_3$:Ce and $LaCl_3$:Ce, indicates that their high scintillation yield and good energy resolution makes them valuable alternatives to most of the conventional scintillators and semiconductors for investigating the formation and quenching processes of positronium in different samples. They will also provide a more effective means of resolving the 3γ annihilation photon energies for coincidence measurements. A series of experiments should be carried with different geometrical configurations using single and three coincidence detectors, comparing measurements with the different type of detectors including CdZnTe semiconductor. The ideal clinical radioisotopes to carry out these experiments are ^{89}Zr and ^{18}F for the single and triple coincidence detectors, respectively.

References

[Abu07] Abuelhia E, Kacperski K and Spyrou NM (2007) Three-photon annihilation in PET: 2D imaging experiments. Journal of Radioanalytical and Nuclear Chemistry, 271(2):489-495

[Ada90] Adachi S. et al., (1990) "Measurement of e+ e- annihilation at rest into four gamma-rays," Phys. Rev. Lett., 65: 2634–2637

[Alk09] Alkhorayef M, Spyrou NM, (2009) Measurement of 3γ/2γ Positron Annihilation Ratios in Selection of Scintillation and Semiconductor Detectors, Transaction American Nuclear Society, 101: 111

[Amr01] Amrami R. et al. (2001) Timing performance of pixelated CdZnTe detectors, Nucl. Instrum. Meth. A. 458: 772–781

[Ana05] Anaerogen™ Anaerobic Atmosphere Generation System [Internet] Available from: <http://www.scientificdevice.com/intl_product_pages/ianaerogen.htm> [Accessed 20 Oct, 2005]

[And01] Andrukhovich SK, Berestov AV, Antovich NM, Metelitsa O N (2001) To the measurements of 2γ /3γ ratio for positron annihilation in matter using annihilation energy spectrum, Acta Physica Polonica A, No 3-4, Vol 99

[Ass01] Assaad SI, Powell SN, Slanetz P, Yeh E , Kopans D and Taghian AG, (2001) Taxol decreases the nterstitial fluid pressure and increases PO2 after neoadjuvant chemotherapy in patients with palpable breast cancer. International Journal of Radiation Oncology, 51: (3) 160-161.

[Bad06] Badawi R., "Introduction to PET Physics" [Internet] Available from: http://depts.washington.edu/nucmed/IRL/pet_intro/intro_src/section2.html [Accessed 16 Aug, 2006]

[Bas54] Basson J. K., (1954) "Direct quantitative observation of the three-photon annihilation of a positron-negatron pair," Phys. Rev., 96: 691–696

[Bel 65] Bell J., Celitans G. J., Green J. H., Tao S. J. (1965) Three-photon coincidence and lifetime apparatus for positronium in gases, Nuclear instruments and methods 37: 51-57

[Bel53] Bell R.E. and Graham R.L., (1953) "Time Distribution of Positron Annihilation in Liquids ad Solids", Physical Review, (4), 90

[Ben01] Benjamin M, Chapman J, Donald D, Halton, Alexandra L, Horwitz, Eric M, Pinover and Wayne H (2001). Hypoxia in Human Prostate Carcinoma: An Eppendorf Po2 Study. American Journal of Clinical Oncology.

[Ben03] Bentzen L, Keiding S, Nordsmark M, Falborg L, Hansen S.B, Keller J, Nielsen O.S, Overgaard J., (2003) Tumour oxygenation assessed by 18F-fluoromisonidazole PET and polarographic needle electrodes in human soft tissue tumours. Radiotherapy and Oncology; 67: 339-344

[Ber65] Bertolaccini M., Bussolati C., and Zappa L., (1965) "Three-quantum annihilation of positrons in metals and insulators," Phys. Rev., 139: A696–699

[Bin10] Binderup T, et al (2010) 18-F-Fluorodexyglucose positron emission tomography predicts survival of patients with neuroendocrine tumours, clin Cancer Res, 16(3) 978-985

[Bor03] Borden EC, Baker LH, Bell RS, Bramwell V, Demetri GD, et al. (2003) Soft tissue sarcomas of adults: state of the translational science. Clinical Cancer Res. 9(6):1941-56.

[Bow99] Bowers C. J., Freedman S. J., Fujikawa B., Macchiavelli A. O., MacLeod R. W., Reich J., Shang S. Q., Vetter P. A., Wasserman E., (1999) New measurement of the β-γ directional correlation in 22Na, Phys. Rev. C. 29 (2): 1113–1118

[Bra68] Brandt W. and Paulin R. (1968) Positronium diffusion in solids, Physical Review Letters, 21(4), 193-195

[Bra99] Brandt Tobias J.P. (1999) A Gamma-Ray Spectroscopy Experiment,< http://www.mth.uct.ac.za/~tbrandt/things/gamma-ray.html#tth_sEc1.2>. [Internet, Access on 18/12/2004]

[Bri95] Brizel DM, Rosner GL, Prosnitz LR, Dewhirst MW (1995) Patterns and variability of tumor oxygenation in human soft tissue sarcomas, cervical carcinomas, and lymph node metastases. International Journal Radiation Oncology Biology Physics 32:1121-1125

[Bri96] Brizel DM, Scully SP, Harrelson JM, et al. (1996) Tumour oxygenation predicts for the likelihood of distant metastases in human soft tissue sarcoma. Cancer Res 56:941–943.

[Bri99] Brizel DM, Dodge RK, Clough RW, Dewhirst MW. (1999) Oxygenation of head and neck cancer: changes during radiotherapy and impact on treatment outcome. Radiother Oncol. 53(2):113-7.

[Bru04] Brurberg KG, Graff BA, Olsen DR, Rofstad EK. (2004) Tumor-line specific PO2 fluctuations in human melanoma xenografts. Int J Radiat Oncol Biol Phys.58: 403-9.

[Bus64] Bussolati C, Zappa L, (1964) Anomalous three-quantum decay of positrons in alkaline earth oxides, Phys. Rev. 136: 657–659

[Bus94] Busch H. von et al., (1994) "Measurement of the decay e+ e- -- 4 at rest," Phys. Lett. B,325: 300–307

[Cav99] Cavalli F., Hansen H. and Kaye S. (1999). Textbook of Medical Oncology. 2nd Edition, Martin Dunitz Ltd, London.

[Cel64a] Celitans G. J. and Green J. H. (1964) Fomation and quenching of positronium in gases I. Results obtained with the three-photon coincidence method. Proc. Phys. Soc. 83: 823-831

[Cel64b] Celitans G. J., Tao S. J. and Green J. H. (1964) Formation and quenching of positronium in gases II. Results obtained with the positron Lifetime method Proc. Phys. Soc. 83: 833-842

[Cha01] Charlton M. and Humberston J.(2001) Positron Physics. Cambridge University Press.

[Cha67] Chandra G., Kulkarni V. G., Lagu R. G., Thosar B. V., (1967) Ph. Let., Vol 25A, 5: 368-369.

[Cha83] Chapman J.D., Franko A.J., Koch C.J. (1983) The fraction of hypoxic clonogenic cells in tumor populations, in Biological Bases and Clinical Implications of Tumor Radioresistance, 61–73.

[Cha85] Chang T, Tang H, Li Y, (1985) Gamma-ray energy spectrum from orthopositronium three-gamma decay. Physics letters B, 157 (5): 357-360

[Che03] Cherry S.R. et al, (2003) Physics in Nuclear Medicine, 3rd edition, Philadelphia: Saunders.

[Che04] Chen Y, Shi G, Xia W, Kong C, Zhao S, Gaw AF, Chen EY, Yang GP, Giaccia AJ, Le QT, Koong AC. (2004) Identification of hypoxia-regulated proteins in head and neck cancer by proteomic and tissue array profiling. Cancer Res; 64(20): 7302-10.

[Chi09] Chin MPW, Seweryniak D, Alkhorayef M, Spyrou NM, (2009) Variation of 3γ-to-2γ ratio from 18F in haematological components measured using the

GAMMASPHERE, Nuclear Instruments and Methods in Physics Research Section A: 604 (1): 331-334

[Con94] Consolati G., Quasso F., (1994) Magnetic quenching of the three-photon annihilation rate in some molecular solids, Phys. Rev. B 50 5848 - 5853

[Coo67] Cooper A.M., Laidlaw G. J., Hogg B.G. (1967) Oxygen quenching of positron lifetimes in liquids, Journal of Chemical Physics, 46 : 2441

[Cru03] Crundell M and Proctor K (2003) Medical Physics. John Murray, Bookprint Spain..

[Dam06] D'ambrosio C., De Notaristefani F., Hull G., Cencelli V. O., Pani R. (2006) Study of LaCl3:Ce light yield proportionality with a hybrid photomultiplier tube Nucl. Instr. and Meth. A 556: 187–191

[Dau81] Dauwe C. (1981) The accurate measurement of weak three-photon annihilation by a simple triple coincidence technique. Appl. Phys. 24: 279-285.

[Dav99] Davidson (1999) The Oxygen Dissociation Curve. [Internet] Available from: <http://www.bio.davidson.edu/Courses/anphys/1999/Dickens/Oxygendissociation.htm> [Accessed 26 Oct, 2005]

[Deb54] De Benedetti S. and Siegel R., (1954) "The three-photon annihilation of positrons and electrons," Physical Review, 94 (4): 955–959

[Dij09] Dijkers Eli C.F., Kosterink Jos G.W., Rademaker Anna P. (2009) Development and Characterization of Clinical-Grade 89Zr-Trastuzumab for HER2/neu ImmunoPET Imaging, Journal of Nuclear Medicine, 50:(6) 974-981

[Don07] Dongen Guus A.M.S. Van, Visser Gerard W.M., Hooge Marjolijn N. Lub-De, et al. (2007) Immuno-PET: A Navigator in Monoclonal Antibody Development and Applications, The Oncologist 12: 1379–1389

[Eis99] Eisen Y, Sihor A, and Mardor I. (1999) CdTe and CdZnTe gamma ray detectors for medical and industrial imaging systems, Nucl. Instrum. Meth. A. 428: 158–170

[Eva55] Evans RD. (1955) The Atomic Nucleus, McGraw-Hill, New York, LCCCN 55-7275.

[Fuk01] Fukumura D., Xu L., Chen Y., Gohongi T., Seed B., and Jain R. (2001) Hypoxia and Acidosis Independently Up-Regulate Vascular Endothelial Growth Factor Transcription in Brain Tumours in Vivo. Cancer Research (61) 6020–6024

[Fyl02] Fyles A, Milosevic M et al., (2002) Tumour hypoxia has independent predictor impact only in patients with node-negative cervix cancer. J Clinical Oncology 20: 680–687.

[Gag04] Gagel B, Reinartz P, DiMartino E, Zimny M, Pinkawa M, Maneschi P, Stanzel S, Hamacher K, Coenen HH, Westhofen M, Bull U, Eble MJ. (2004) PO2 Polarography versus positron emission tomography ([18F] Fluoromisonidazole, [18F]-2-fluoro-2'-deoxyglucose): an appraisal of radiotherapeutic relevant hypoxia. Strahlenther Onkol, 180:616-622.

[Gai64] Gainotti A, E Germagnolli, G Schianchi, and L Zecchina, (1964) Three-quantum annihilation of positrons in alkali halides, Phys. Lett. 13: 9-10

[Gia90] Giardina, B., Brix, O., Clementi, M. E., Scatena, R., Nicoletti, B., Cicchetti, R., Argentin, G. and Condo, S. G. (1990) Differences between horse and human haemoglobins in effects of organic and inorganic anions on oxygen binding. Biochem. J. , 266 (3): 897-900.

[Gil01] Gillies, R. J. (2001) Causes and Consequences of Acidic pH in Tumours. John Eiley & Sons, Ltd. West Sussex, United Kingdom

[Gil95] Gilmore G. and Hemingway J D. (1995) Practical Gamma-Ray Spectrometry. John Wiley and Sons. 2nd edition.

[Gre64] Green J. and Lee J. (1964) Positronium Chemistry. New York and London Academic Press.

[Gro04] Grönroos T, Bentzen L, Marjamäki P, Murata R, Horsman M, Keiding S, Eskola O, Haaparanta M, Minn H, Solin O., (2004) Comparison of the biodistribution of two hypoxia markers [18F]FETNIM and [18F]FMISO in an experimental mammary carcinoma, Eur J Nucl Med Mol Imaging 31: 513–520.

[Guy06] Guyton C. and Hall J. (2006) Textbook of Medical Physiology, Elsevier Saunders Inc.,

[Hac05] Hach Company, Instruction Manual, Pocket Colorimeter Analysis System Dissolved Oxygen. [Internet] Available from: <http://www.hach.com > [Accessed 26 Oct, 2005]

[Han05] Hanna Company, Instruction Manual, Dissolved Oxygen Meters. [Internet] Available from: <http://www.hannainst.com> [Accessed 26 Oct, 2005]

[Har02] Harris A. (2002) Hypoxia – a key regulatory factor in tumour growth. Nat. Rev. Cancer 2 : 38–47.

[Har04] Harrison L, Blackwell K. (2004) Hypoxia and anemia: factors in decreased sensitivity to radiation therapy and chemotherapy? Oncologist 9: 31-40.

[Haw98] Hawighorst H, Knapstein PG, Knopp MV, Weikel W, Brix G, Zuna I, et al. (1998) Uterine cervical carcinoma: comparison of standard and pharmacokinetic analysis of time–intensity curves for assessment of tumor angiogenesis and patient survival. Cancer Res 58: 3598–3602.

[Hei57] Heinberg M, Page L. (1957) Annihilation of positron in gases, Physical Review 107 (6): 1589-1600

[Hel97] Helmlinger, G., Yuan, F., Dellian, M., and Jain, R. K. (1997) Interstitial PH and PO2

[Hey61] Heymann FF, Osmon PE, Veit JJ, Williams WF (1961) Measurements of Quenching of Ortho-positronium in Gases Proc. Phys. Soc. 78: 1038-1047

[Hil04] Hillel P. (2004) Basic of Gamma Camera Positron Emission Tomography, IPEM Report 87

[Hit78] Hitchman, M. L. (1978) Measurement of dissolved oxygen; Chemical Analysis; Vol. 49.

[Hoc01a] Höckel M and Vaupel P. (2001) Tumour Hypoxia: definitions and current clinical, biological, and molecular aspects. J. Natl. Cancer Inst. 93: 266–276.

[Hoc01b] Höckel, M and Vaupel, P. (2001) Prognostic significance of tissue hypoxia in cervical cancer. J Gynecol Oncol 6: 216–225.

[Hoc93] Höckel M, Vorndran B, Schlenger K, Baußmann E & Knapstein PG., (1993) Tumor oxygenation A new predictive parameter in locally advanced cancer of the uterine cervix, Gynecol Oncol 51: 141–149.

[Hop90] Hopkins B, and Zerda T. (1990) Oxygen quenching of positronium in silica gels. Physics Letters A Vol 145 number 2,3.

[Hum03] Humm J L, Rosenfeld A, Guerra A D, (2003) From PET detectors to PET scanners, Eur J Nuc Med Mol Imag. 30 (11): 1574-1597

[Hus89] Hsu F. H., Shao M. J., Hulett L. D., Rosseel T. M., and Dale J. M., (1989) "Three-photon yield of positron annihilation in Cab-O-Sil (SiO)," J. Phys. Condens. Matter, 1: 7453–7456

[Iva02] Ivanov I. A. and Mitroy J., (2002) "Pick-off annihilation in positronium scattering from alkali-metal ions", Physical Review A, 65

[Jin95] Jinrong C. et al, (1995) Computer Simulation Study of the Properties of ortho-positronium 3 Gamma Decay, Journal of Computational Physics, 118: 396-400

[Kac04a] Kacperski K, Spyrou NM (2004). Three-gamma annihilation as a new modality in PET, Nuclear Science Symposium Conference Record IEEE. 6: 3752- 3756

[Kac04b] Kacperski K, Spyrou NM, and Smith FA (2004) Three-gamma annihilation imaging in positron emission tomography. IEEE Transactions on Medical Imaging. 23(4):525-529

[Kac05] Kacperski K. and Spyrou N. M., (2005) Performance of three-photon PET imaging: Monte Carlo simulations, Phys. Med. Biol. 50: 5679-5695

[Kak90] Kakimoto M, Hyodo T, Chang TB, (1990) Conversion of ortho-positronium in low density oxygen gas, Journal of Physics B-Atomic Molecular and Optical Physics, 23: 589-597

[Kan65] Kanazawa H., Ohtsuki Y.H., Yanagawa S., (1965) Phys. Rev. A 138: 1155

[Kha98] Khalili A., Basu A. J., and Pietrzyk U., "Flow visualization in porous media via positron emission tomography," (1998) Phys. Fluids, 10: 1031–1033,

[Kin06] King R. and Robins M. (2006) Cancer Biology, Pearson Prentice Hall, Harlow, England.

[Kno00] Knoll G. F., Radiation detection and measurement (2000) New York: John Wiley and Sons, Inc.

[Koh92] Koh WJ, Rasey JS, Evans ML, et al. (1992) Imaging of hypoxia in human tumors with F-18 fluoromisonidazole. Int J Radiat Oncol Biol Phys;22:199–212.

[Koh95] Koh WJ, Bergman KS, Rasey JS, et al. (1995)Evaluation of oxygenation status during fractionated radiotherapy in human nonsmall cell lung cancers using [F18]fluoromisonidazole positron emission tomography. Int J Radiat Oncol Biol Phys;33:391–8.

[Koo00] Koong, A, Mehta, V, Le, Q, Giaccia, A, Ibrahim, H, and Terris, D (2000). Tumor Hypoxia in Human Pancreatic and Peripancreatic Cancers. Proc Am Soc Clin Oncol 19

[Koo03] Koong, L, Mitchell, J, Whyte, R, Cannon, W, Morasca, A, and Giaccia, A. (2003). In-vivo measurements of tumor oxygenation (pO2) in patients undergoing surgical resection for early stage non-small cell lung cancers (NSCLC). Proc Am Soc Clin Oncol 22

[Kou82] Kouris K, Spyrou NM, Jackson DF, (1982) Imaging with Ionizing Radiations – Progress in medical and environmental physics, Surrey University Press, UK

[Kuh04] Kuhn A., Surti S., Karp J. S., Raby P. S., Shah K. S., Perkins A. E., Muehllehner G. (2004) Design of a Lanthanum Bromide detector for TOF PET, IEEE Trans. Nucl. Sci. 51 2550-2557.

[Kup03] Kuper M. and Soni N. (2003). Oxygen transfer: cascade or whirlpool?. Current Anaesthesia & Critical Care, 14(2) 58-65.

[Lar97] Lartigau E, Randrianarivelo H, Avril MF et al. (1997) Intratumoral oxygen tension in metastatic melanoma. Melanoma Res; 7: 400–406.

[Lee65] Lee J, Celitans G. (1965) Oxygen and nitric oxide quenching of positronium in liquids. Journal of Chemical Physics 44 (6): 2506-2511.

[Leh01] Lehtio K, Oikonen V, Gronroos T, et al. (2001) Imaging of blood flow and hypoxia in head and neck cancer: initial evaluation with [15O]H2O and [18F] fluoroerythronitroimidazole PET. J Nucl Med;42:1643–52.

[Leh04] Lehti K, Eskola O, Viljanen T, Oikonen V, Gronroos T, Sillanmaki L, Grenman R, Minn H. (2004) Imaging perfusion and hypoxia with PET to

predict radiotherapy response in head-and-neck cancer. Int J Radiat Oncol Biol Phys 59(4):971-982

[Leo04] Leonard I. Wiebe. (2004) PET radiopharmaceuticals for metabolic imaging in oncology. International Congress Series, 1264: 53-76.

[Ler01] Lerch MLF, Rosenfeld AB, Taylor GN, Meikle SR, Perevertailo VL. (2001) Spectral characterization of blue-enhanced silicon photodiode. IEEE Trans Nucl Sci, 48: 1220–1224.

[Lew01] Lewis J.S., Sharp T.L. and Laforest R. et al., (2001) Tumor uptake of copper-diacetyl-bis(N(4)-methylthiosemicarbazone) Effect of changes in tissue oxygenation, J Nucl Med 42: 655–661.

[Lew99] Lewis J.S., McCarthy DW, McCarthy TJ, Fujibayashi Y and Welch MJ., (1999) Evaluation of 64Cu-ATSM in vitro and in vivo in a hypoxic tumor model, J Nucl Med 40: 177–183.

[Lon02] Loncaster JA, Carrington BM, Sykes JR, Jones AP, Todd SM, Cooper RA, et al. (2002) Prediction of radiotherapy outcome using dynamic contrast enhanced magnetic resonance imaging of carcinoma of the cervix.Int. J. Radiation Oncology Biol Phys, 54(3): 759-767

[Mad92] Mader S. (1992) Human Biology, Wm.C.Brown Publishers.

[Man70] Mankamo T. and Jauho P., (1970) "Measurements of the momentum correlation inn the three-photon annihilation of positronium," Nucl. Phys. A, 158: 487–496

[Mar94] Marieb E. (1994) Essentials of human anatomy & physiology. The Benjamin/ Cummings

[Mat96] Matsumoto T. et al., (1996) "Measurement of five-photon decay in orthopositronium," Phys. Rev. A, 54: 1947–1951

[Mel00] Melcher C L (2000) Scintillation crystals for PET. J Nuc Med 41 (6): 1051-1055

[Men05] Menon, C and Fraker, D (2005). Tumor oxygenation status as a prognostic marker. Cancer Letters, 221 (2): 225-235

[Mos05] Moses W. W., Shah K. S. (2005) Potential for RbGd2Br7:Ce, LaBr3:Ce, LaBr3:Ce, and LuI3:Ce in nuclear medical imaging, Nucl. Instr. and Meth. A 537: 317–320

[Mou84] Moulder J.E., Martin D.F. (1984) Hypoxic fraction determinations in the BA1112 rat sarcoma: variations within and among assay techniques, Radiat. Res. 99.

[Mou87] Moulder JE and Rockwell S. (1987) Tumor hypoxia: its impact on cancer therapy. Cancer Metastasis Rev. 5, 313–341.

[Mov00] Movsas B, Chapman JD, Greenberg RE et al. (2000) Increasing levels of hypoxia in prostate carcinoma correlate significantly with increasing clinical stage and patient age: an Eppendorf pO(2) study. Cancer; 89:2018–2024.

[Mov99] Movsas B, Chapman JD, Horwitz EM et al. (1999) Hypoxic regions exist in human prostate carcinoma. Urology;53:11–18.

[Mur06] Murtagh D.J., Arcidiacono C., Pesic Z.D., Laricchia G., (2006) Positronium formation from CO2 and H2O, Nuclear Instruments and Methods in Physics Research B 247: 92-97

[Nag07] Nagengast Wouter B., Vries1 Elisabeth G. de, Hospers1 Geke A., (2007) In Vivo VEGF Imaging with Radiolabeled Bevacizumab in a Human Ovarian Tumor Xenograft, Journal of Nuclear Medicine, 48: (8) 1314-1319

[Nat10] National statistics. Focus on health report, Cancer [Internet] Available from: http://www.statistics.gov.uk/CCI/nugget.asp?ID=1332&Pos=1&ColRank=1&Rank=294 [Accessed 18 Jan, 2010]

[Nor01] Nordsmark M, Loncaster J, Chou SC, et al. (2001) Invasive oxygen measurements and pimonidazole labeling in human cervix carcinoma. Int J Radiat Oncol Biol Phys;49:581–6.

[Nor03] Nordsmark M, Loncaster J, Aquino-Parsons C, Chou SC, Ladekarl M, Havsteen H, Lindegaard JC, Davidson SE, Varia M, West C, Hunter R, Overgaard J, Raleigh JA, (2003) Measurements of hypoxia using pimonidazole and polarographic oxygen-sensitive electrodes in human cervix carcinomas, Radiotherapy and Oncology : Journal of the European Society for Therapeutic Radiology and Oncology., 67(1) 35-44

[Nor94] Nordsmark M, Bentzen SM, Overgaard J., (1994) Measurement of human tumour oxygenation status by a polarographic needle electrode. An analysis of inter- and intratumour heterogeneity, Acta Oncol 33: 383–389.

[Nor96] Nordsmark M, Hoyer M, Keller J, et al (1996) The relationship between tumor oxygenation and cell proliferation in human soft tissue sarcomas. Int J Radiat Oncol Biol Phys, 35: 701-708

[Ore 49] Ore A., Powell J. L. (1949) Three photon annihilation of an electron-positron pair. Phys. Rev., 75: 1696-1699

[Pad05] Padhani (2005) Where are we with imaging oxygenation in human tumours? Cancer Imaging, 5, 128-130.

[Pad07] Padhani, A, Krohn, K, Lewis, J, and Alber, M. (2007). Imaging oxygenation of human tumours. European Radiology 17(4): 861–872

[Par04] Parker C, Milosevic M, Toi A, Sweet J, Panzarella T, Bristow R, Catton C, Catton P, Crook J, Gospodarowicz M, McLean M, Warde P, Hill RP. (2004) Polarographic electrode study of tumor oxygenation in clinically localized prostate cancer, Int J Radiat Oncol Biol Phys 58: 750–757.

[Pec05] Pecorino L. (2005), Molecular Biology of Cancer, Oxford University Press, Oxford, UK

[Phe06] Phelps M E, (2006) PET Physics, Instrumentation, and Scanners, Springer, USA

[Pot01] Potger K. C. (2001) Blood gas electrodes, notes in clinical perfusion, a multinational cardiac educational resource centre [Internet] Available from: <http://www.perfusion.com.au/CCP/ccp> [Accessed 23 Oct, 2005]

[Pre07] Prekas G., Jones G., Kacperski K., Alkhorayef M. and Spyrou N.M. (2007) Determination of 3γ photon yields in biological samples. Analysis of results obtained from experiment using the 'Gammsphere' at Argonne National Laboratory (Chicago, USA), Proceedings of MTAA-12- The 12th International Conference Modern Trends in Activation Analysis, Tokyo, Japan, 75: 114

[Rao72] Rao M Rama, Sen P, Patro AP. (1972) Three-quantum annihilations in silicone fluids, J. Phys. A: Gen. Phys. 5: 763-766

[Ras00] Rasey JS, Casciari JJ, Hofstrand PD, Muzi M, Graham MM, Chin LK., (2000) Determining hypoxic fraction in a rat glioma by uptake of radiolabeled fluoromisonidazole. Radiat Res 153: 84–92.

[Ras87] Rasey JS, Grunbaum Z, Magee S, Nelson NJ, Olive PL, Durand RE, Krohn KA, (1987) Characterization of radiolabeled fluoromisonidazole as a probe for hypoxic cells. Radiat. Res. 111: 292–304.

[Ras96] Rasey JS, Koh WJ, Evans ML, Peterson LM, Lewellen TK, Graham MM, Krohn KA. (1996) Quantifying regional hypoxia in human tumors with positron emission tomography of [18F]fluoromisonidazole A pretherapy study of 37 patients, Int J Radiat Oncol Biol Phys 36: 417–428.

[Rei07] Reischl, G, Dorow, D, Cullinane, C, Katsifis, A, Roselt, P, Binns, D, and Hicks, R. (2007). Imaging of tumor hypoxia with [124I] IAZA in comparison

with [18F] FMISO and [18F] FAZA – first small animal PET results. Journal of pharmaceutical science 10 (2): 203-211

[Res 01] Reske SN, Kotzerke J. (2001) FDG-PET for clinical use. Results of the 3rd German Interdisciplinary Consensus Conference, Eur J Nucl Med 28: 1707–1723.

[Rob99] Robinson SP, Collingridge DR, Howe FA, Rodrigues LM, Chaplin DJ,Griffiths JR. (1999) Tumour response to hypercapnia and hyperoxia monitored by FLOOD magnetic resonance imaging. NMR Biomed 12: 98–106.

[Sal07] Salvador S, Guyonnet JL. (2007) Study of 4 inorganic scintillating crystals for an operative gamma probe in radioguided surgery, Journal of Institute of Physics (JINST) (2) 8003

[Saw94] Sawyer C., McCarty P. and Parkin G. (1994) Chemistry for environmental engineering.

[Sea07] Seam1Pamela, Juweid Malik E., and Cheson Bruce D. (2007) The role of FDG-PET scans in patients with lymphoma, Review in translational hematology, 110, No. (10): 3507-351

[Sem02] Semenza GL. (2002) HIF-1 and tumour progression: pathophysiology and therapeutics. Trends Mol Med, 8: 62-67.

[Sha04] Shannon AM, Bouchier-Hayes DJ, Condron CM, and Toomey D. (2003) Tumour hypoxia, chemotherapeutic resistance and hypoxia-related therapies. Cancer Treat. Rev. 29, 297-307.

[Sha05] Sharp P. F., Gemmell H. G. and Murray A. D. (2005) Practical Nuclear Medicine. 3rd edition, Birkhäuser

[Sha94] Shapiro B., Peruzzi W. and Templin R. (1994) Clinical Application of Blood Gases. 5th edition, Georg Stamathis, Mosby Inc.

[Sha96] Shantarovich V. P., (1996) On the role of free volume in pick-off annihilation and positronium chemical reactions, J. Rad. Nuc. Chem. 210 357-369

[Sil98] Silverman D. H., Hoh C. K., Seltzer M. A., Schiepers C., Cuan G. S., Gambhir S. S., Zheng L., Czernin J. & Phelps M. E. (1998) Evaluating tumor biology and oncological disease with positron-emission tomography. Seminars in Radiation Oncology, 8(3): 183-196.

[Sin99] Sinex J. (1999) Pulse Oximetry: Principles and limitations. American Journal of Emergency 17(1) 59-65

[Sor03] Sorger D, Patt M, Kumar P, Wiebe LI, Barthel H, Seese A, Dannenberg C, Tannapfel A, Kluge R, Sabri O., (2003) [18F]fluoroazomycinarabinofuranoside (18FAZA) and [18F]fluoromisonidazole (18FMISO) A comparative study of their selective uptake in hypoxic cells and PET imaging in experimental rat tumors, Nucl Med Biol 30: 317–326.

[Spy04] Spyrou NM (2004) Physics of positron annihilation, plenary lecture, Proceedings of Nuclear Medicine Society, Greece.

[Spy05] Spyrou NM, Kacperski K, Kafala S, Abuelhia E (2005) A prototype Semiconductor-based Scanner using Three-photon Coincidence Technique. International Journal of Scientific Research. Vol. 16.

[Sto93] Stone HB, Brown JM, Phillips TL. Sutherland RM. (1993) Oxygen in human tumors: correlations between methods of measurement and response to therapy. Summary of a workshop held November 19–20, 1992, at the National Cancer Institute, Bethesda, MD. Radiat Res 136: 422–434.

[Str97] Strauss L. G. (1997). PET in clinical oncology: current role for diagnosis and therapy monitoring in oncology. J. Nucl. Med., 32: 623-648.

[Sue00] Sueoka O., Kawada M.K., Kimura M., (2000) Nuclear Instruments and Methods in Physics Research B 171: 96.

[Suk93] Sukker M., El-Munshid H. and Ardawi M. (1993) Concise Human Physiology. Blackwell

[Tan82] Tang X. W., Liu G. H., Wang Y. Y. (1982) Positron Annihilation, Measurement of 3γ annihilation using a Ge(Li) detector. Eds., P. G. Coleman, S. C. Sharma, L. M. Diana. 880-882.

[Tei95] Teicher BA. (1995) Physiologic mechanisms of therapeutic resistance: blood flow and hypoxia. Hematol. Oncol. Clin. North America 9: 475–506.

[Ter82] Ter-Pogossian M.M.(1982) Positron Emission Tomography. Journal of Medical System 8: 569-577

[Tho90] Thompson C. J. (1990) The effects of detector material and structure on PET spatial resolution and efficiency. IEEE Transactions on Nuclear Science, 37: 718-724.

[Too95] Toole G. & Toole S. (1995) Understanding Biology for Advanced Level, 3rd edition, Cheltenham : Stanley Thornes,.

[Tor03] Tortora G. and Grabowsk S. (2003) Principle of Anatomy and Physiology. John Wiley & sons, Inc.

[Tre98] Treacher D. F. and Leach R. M. (1998) Clinical review: ABC of oxygen, British Medical Journal, 317:1302-1306.

[Val03] Valk P E, Bailey D L, Townsend D W, et al, (2003) Positron emission tomography, Basic science and clinical practice. Spinger-Verlag, New York.

[Van88] Van den Bergen E. A. and Jonkers G., "Industrial applications of positron emission computerized tomography," (1988) Trans. Amer. Nucl. Soc., 56: 10–11

[Vau01] Vaupel P, Thews O, Höckel M. (2001) Treatment resistance of solid tumours: role of hypoxia and anemia. Med. Oncol. 18: 243–259.

[Vau03] Vaupel, P, Mayer, A, Briest, S, and Höckel, M. (2003) Oxygenation Gain Factor. Cancer Research 63: 7634-7637

[Vau04] Vaupel P. and Harrison L. (2004) Tumour Hypoxia: Causative Factors, Compensatory Mechanisms, and Cellular Response. The Oncologist, 9: 4-9

[Vau91] Vaupel P, Schlenger K, Knoop C, Hockel M. (1991) Oxygenation of human tumors: evaluation of tissue oxygen distribution in breast cancers by computerized O2 tension measurements. Cancer Res. 51:3316–3322.

[Vuj03] Vujaskovic Z, Rosen EL, Blackwell KL, Jones EL, Brizel DM, Prosnitz LR, Samulski TV, Dewhirst MW. (2003) Ultrasound guided PO2 measurement of breast cancer reoxygenation after neoadjuvant chemotherapy and hyperthermia treatment. Int. J Hyperthermia. 19(5):498-506.

[Won97] Wong RK, Fyles A, Milosevic M, Pintilie M and Hill RP. (1997) Heterogeneity of polarographic oxygen tension measurements in cervix cancer: an evaluation of within and between tumor variability, probe position, and track depth. Int.J. Radiat. Oncol. Biol. Phys. 39: 405-412.

[Wre51] Wernn F, Good M, Handler P. (1951) The use of positron emitting radioisotopes for the localization of brain tumours, Science 113: 525-527.

Appendix A: Definitions and formulas

Disintegration rate of a source: $D_S = D_0 \cdot e^{-\lambda t}$

Where D_0 is the number of disintegrations at time t=0 and λ is the disintegration constant.

The number of photons of energy E emitted per disintegration: I_γ^E

Number of photons of energy E emitted by a source per unit time: $N_\gamma^{'} = D_S \cdot I_\gamma^E$

Number of photons of energy E that are incident on a detector per unit time:

$$N_\gamma^{''} = \frac{\Omega}{4\pi} \cdot D_S \cdot I_\gamma^E$$

Absolute full-energy photopeak efficiency: $\varepsilon_{abs,p} = \frac{C_p}{N_\gamma^{'}} \times 100\%$

Error in absolute full-energy photopeak efficiency:

$$\sigma_{Eabs,p} = \sqrt{\left(\frac{1}{D_S \cdot I_\gamma^E}\right)^2 \cdot \sigma_{Cp}^2 + \left(\frac{C_p}{D_S^2 \cdot I_\gamma^E}\right)^2 \cdot \sigma_{Ds}^2 + \left(\frac{C_p}{D_S \cdot I_\gamma^{E2}}\right)^2 \cdot \sigma_{I_\gamma^E}^2}$$

Intrinsic full-energy photopeak efficiency: $\varepsilon_{\text{int},p} = \frac{C_p}{N_\gamma^{''}} \times 100\%$

Error in intrinsic full-energy photopeak efficiency:

$$\sigma_{E\text{int},p} = \sqrt{\left(\frac{1}{\Omega/4\pi}\right)^2 \cdot \sigma_{Eabs,p}^2 + \left(\frac{\varepsilon_{abs,p}}{(\Omega/4\pi)^2}\right) \cdot \sigma_{\Omega/4\pi}^2}$$

Solid angle subtended by a cylindrical detector at a point source:

$$\Omega = 2\pi\left(1 - \frac{d}{\sqrt{d^2 + a^2}}\right)$$

Where d is the distance source-detector crystal and α is the radius of the detector crystal.

Error in the solid angle factor: $\sigma_{\Omega/4\pi} = \frac{1}{\pi} \cdot \left[\frac{1}{\sqrt{d^2 + a^2}} - \frac{d^2}{\sqrt[3]{d^2 + a^2}}\right] \cdot \sigma_d$

Solid angle subtended by a rectangular detector at a point source:

$$\Omega = 4 \cdot \arctan \frac{\frac{a}{2} \cdot \frac{b}{2}}{d\left(\left(\frac{a}{2}\right)^2 + \left(\frac{b}{2}\right)^2 + d^2\right)^{1/2}}$$

Where a, b are the sides of the rectangle, and d is the distance source-detector crystal.

Error in the solid angle factor:

$$\sigma_{\Omega/4\pi} = \frac{\frac{a}{2} \cdot \frac{b}{2}}{\pi} \cdot \left[\frac{\frac{1}{d^2 \cdot \sqrt{\left(\frac{a}{2}\right)^2 + \left(\frac{b}{2}\right)^2 + d^2}} + \frac{1}{\sqrt[3]{\left(\frac{a}{2}\right)^2 + \left(\frac{b}{2}\right)^2 + d^2}}}{1 + \frac{\left(\left(\frac{a}{2}\right)^2 + \left(\frac{b}{2}\right)^2\right)^2}{d^2 \cdot \left(\left(\frac{a}{2}\right)^2 + \left(\frac{b}{2}\right)^2 + d^2\right)}} \right] \cdot \sigma_d$$

Errors calculation in the peak-to-peak method

$$Error_{\frac{3\gamma}{2\gamma}} = \left(\frac{R_{511ref} - \left(R_{511_S} - \frac{R_{511_S}}{372} \right)}{R_{511_S}} \right) \pm \frac{1}{R_{511_S}} \sqrt{\frac{R^2{}_{511_{ref}}}{R_{511_S}} + R_{511_S}}$$

Errors calculation in the peak-to-valley method

$$Error_{\frac{3\gamma}{2\gamma}} = \frac{\left(R_{vs} - kR_{ps}\right)}{\mu \xi R_{ps}} \pm \frac{k + \sqrt{k} + \sqrt{k + k^2}}{\mu \xi \sqrt{I_{ps}}} + \frac{\Delta\mu}{\mu} \times \frac{Y_{3\gamma}}{Y_{2\gamma}}$$

Appendix B: Detectors specifications

HPGe detectors

Detector (A) was a p-Type High Purity Ge detector, model #GEM 10175-p, serial # 31-TP 20644 A and bias volt +3000V (Positive). Its crystal diameter was 42.4mm, its crystal length 44.1mm while the gap between crystal and end cap of the detector was 3mm.

Detector (B) was an n-Type High Purity Ge detector, model #GMX 20190, serial # 32-TN 10846 A (R-2431) and bias volt -2500V (Negative). Its crystal diameter was 55mm, its crystal length 51mm while the gap between crystal and end cap of the detector was 3mm.

Detector (C) was a p-Type High Purity Ge detector, model #GEM 50P4, serial # 44-TP 12070 A and bias volt +2200V (Positive). Its crystal diameter was 66.5mm, its crystal length 66.5mm while the gap between crystal and end cap of the detector was 4mm.

CZT detectors

All three detectors had a rectangular crystal of 10mm x 10mm x 7.5mm dimensions, while the gap between crystal and end cap of the detector was 5.5mm. Also, all three detectors had a bias volt of -1000V (Negative). Detector's A model# was B1591, detector's B model# was B1592 while detector's C model# was B1590.

NaI(Tl)

Dimension 50.8×50.8mm, 540V, Scionix Holland

$LaBr_3$:Ce

25.0×25.0mm, 478V, Saint-Gobain

$LaCl_3$:Ce

44.4×50.8mm 737V Saint-Gobain

Appendix C: Peak-to-peak and peak-to-valley methods

Peak-to-peak method with Teflon

Teflon NaI(Tl)

Peak-to-peak	Counts	Time	counts/sec	Correction factor	Corrected c/s
R511 Teflon sample	1.14E+07	86400	1.32E+02	1.01E+00	1.34E+02
R1274	2.21E+06	86400	2.56E+01		2.59E+01
R511 Al reference	1.19E+07	86400	1.38E+02		1.38E+02
R1274	2.24E+06	86400	2.59E+01		2.59E+01
				Yield	3.26E-02
				Error	1.02E-03

Teflon HPGe

Peak-to-peak	Counts	Time	counts/sec	Correction factor	Corrected c/s
R511 Teflon sample	8.74E+06	86400	1.01E+02	1.01E+00	1.02E+02
R1274	2.52E+06	86400	2.92E+01		2.95E+01
R511 Al reference	9.00E+06	86400	1.04E+02		1.04E+02
R1274	2.55E+06	86400	2.95E+01		2.95E+01
				Yield	2.03E-02
				Error	1.08E-03

Teflon $LaCl_3$:Ce

Peak-to-peak	Counts	Time	counts/sec	Correction factor	Corrected c/s
R511 Teflon sample	1.03E+07	86400	1.19E+02	1.01E+00	1.20E+02
R1274	2.02E+06	86400	2.34E+01		2.36E+01
R511 Al reference	1.06E+07	86400	1.23E+02		1.23E+02
R1274	2.04E+06	86400	2.36E+01		2.36E+01
				Yield	2.17E-02
				Error	1.05E-03

Teflon $LaBr_3$:Ce

Peak-to-peak	Counts	Time	counts/sec	Correction factor	Corrected c/s
R511 Teflon sample	6.81E+06	86400	7.88E+01	9.82E-01	7.74E+01
R1274	1.09E+06	86400	1.26E+01		1.24E+01
R511 Al reference	6.87E+06	86400	7.95E+01		7.95E+01
R1274	1.07E+06	86400	1.24E+01		1.24E+01
				Yield	3.04E-02
				Error	1.14E-03

Peak-to-peak method with silica

Silica NaI(Tl)

Peak-to-peak	Counts	Time	counts/sec	Correction factor	Corrected c/s
R511 Silica sample	1.88E+06	86400	2.18E+01	1.07E+00	2.34E+01
R1274	4.16E+05	86400	4.81E+00		5.17E+00
R511 Al reference	2.10E+06	86400	2.43E+01		2.43E+01
R1274	4.47E+05	86400	5.17E+00		5.17E+00
				Yield	4.01E-02
				error	1.61E-03

Silica HPGe

Peak-to-peak	Counts	Time	counts/sec	Correction factor	Corrected c/s
R511 Silica sample	3.49E+06	86400	4.04E+01	1.03E+00	4.15E+01
R1274	1.14E+06	86400	1.32E+01		1.35E+01
R511 Al reference	3.65E+06	86400	4.22E+01		4.22E+01
R1274	1.17E+06	86400	1.35E+01		1.35E+01
				Yield	2.12E-02
				error	1.35E-03

Silica $LaCl_3$:Ce

Peak-to-peak	Counts	Time	counts/sec	Correction factor	Corrected c/s
R511 Silica sample	4.39E+06	86400	5.08E+01	9.80E-01	4.98E+01
R1274	9.78E+05	86400	1.13E+01		1.11E+01
R511 Al reference	4.42E+06	86400	5.12E+01		5.12E+01
R1274	9.59E+05	86400	1.11E+01		1.11E+01
				Yield	2.98E-02
				error	1.29E-03

Silica $LaBr_3$:Ce

Peak-to-peak	Counts	Time	counts/sec	Correction factor	Corrected c/s
R511 Silica sample	1.21E+06	86400	1.40E+01	1.08E+00	1.51E+01
R1274	2.22E+05	86400	2.57E+00		2.77E+00
R511 Al reference	1.34E+06	86400	1.56E+01		1.56E+01
R1274	2.39E+05	86400	2.77E+00		2.77E+00
				Yield	3.41E-02
				error	1.82E-03

Peak-to-valley method with NaI(Tl)

Teflon
NaI(Tl)

	Valley Region keV	Rvref	Rpref	Rvs	Rps	k	μ	ξ	yield	Error
1FWHM	428.69-464	402726	3644545	408535	3486797	0.1105	1.7508	0.2456	0.01550	0.00072
2FWHM	393.38-464	831842	3644545	842596	3486797	0.2282	1.801	0.2359	0.03156	0.0011
3FWHM	358.07-464	1396616	3644545	1402890	3486797	0.3832	1.8612	0.2271	0.04527	0.00149

Silica NaI

	Valley Region keV	Rvref	Rpref	Rvs	Rps	k	μ	ξ	yield	Error
1FWHM	428.69-464	204722	1787045	210651	1715087	0.1146	1.7508	0.2456	0.01922	0.00105
2FWHM	393.38-464	423550	1787045	432632	1715087	0.2370	1.801	0.2359	0.03587	0.00160
3FWHM	358.07-464	707864	1787045	714891	1715087	0.3961	1.8612	0.2271	0.04901	0.00216

Peak-to-valley method with HPGe

Teflon HPGe

	Valley Region keV	Rvref	Rpref	Rvs	Rps	k	μ	ξ	yield	Error
1FWHM	504.4-507	125872	7258068	134043	6962020	0.0173	1.6289	0.3098	0.00379	0.00020
2FWHM	501.8-507	193172	7258068	200889	6962020	0.0266	1.6406	0.3072	0.00444	0.00024
3FWHM	499.3-507	248254	7258068	255636	6962020	0.0342	1.6523	0.303	0.00502	0.00028
4FWHM	496.7-507	307688	7258068	314637	6962020	0.0424	1.6528	0.3003	0.00564	0.00031
5FWHM	494.2-507	359369	7258068	365174	6962020	0.0495	1.6573	0.297	0.00597	0.00034

Silica HPGe

	Valley Region keV	Rvref	Rpref	Rvs	Rps	k	μ	ξ	yield	Error
1FWHM	504.4-507	53645	2293918	58472	2200180	0.0234	1.6289	0.3098	0.00632	0.00041
2FWHM	501.8-507	93098	2293918	97487	2200180	0.0406	1.6406	0.3072	0.00739	0.00055
3FWHM	499.3-507	126581	2293918	130495	2200180	0.0552	1.6523	0.303	0.00825	0.00064
4FWHM	496.7-507	162833	2293918	166821	2200180	0.0710	1.6528	0.3003	0.00975	0.00074
5FWHM	494.2-507	194665	2293918	198331	2200180	0.0849	1.6573	0.297	0.01073	0.00082

Peak-to-valley method with $LaCl_3$:Ce

Teflon LaCl

	Valley Region keV	Rvref	Rpref	Rvs	Rps	k	μ	ξ	yield	Error
1FWHM	454-475	289810	3823218	294387	3702231	0.0758	1.71	0.2578	0.00842	0.00057
2FWHM	433-475	553989	3823218	556195	3702231	0.1449	1.7463	0.2504	0.01219	0.00082
3FWHM	412-475	835751	3823218	837602	3702231	0.2186	1.7834	0.244	0.01757	0.00104
4FWHM	391-475	1151900	3823218	1155294	3702231	0.3013	1.8213	0.2385	0.02478	0.00125
5FWHM	370-475	1544737	3823218	1547103	3702231	0.4040	1.8599	0.233	0.03194	0.00149

Silica LaCl

	Valley Region keV	Rvref	Rpref	Rvs	Rps	k	μ	ξ	yield	Error
1FWHM	454-475	323160	3878289	331157	3754701	0.0833	1.71	0.2578	0.01105	0.00060
2FWHM	433-475	619467	3878289	625878	3754701	0.1597	1.7463	0.2504	0.01593	0.00087
3FWHM	412-475	906282	3878289	914270	3754701	0.2337	1.7834	0.244	0.02257	0.00108
4FWHM	391-475	1212411	3878289	1224565	3754701	0.3126	1.8213	0.2385	0.03114	0.00128
5FWHM	370-475	1543346	3878289	1558070	3754701	0.3979	1.8599	0.233	0.03927	0.00147

Peak-to-valley method with $LaBr_3$:Ce

Teflon LaBr

	Valley Region keV	Rvref	Rpref	Rvs	Rps	k	μ	ξ	yield	Error
1FWHM	462.78-480	124458	2339837	133844	2302728	0.0532	1.8229	0.2624	0.01031	0.00056
2FWHM	445.56-480	233242	2339837	245939	2302728	0.0997	1.8511	0.2563	0.01501	0.00079
3FWHM	428.34-480	348905	2339837	364878	2302728	0.1491	1.8796	0.2504	0.01984	0.00099
4FWHM	411.12-480	465106	2339837	487985	2302728	0.1988	1.9086	0.2456	0.02803	0.00117
5FWHM	393.9-480	608623	2339837	638107	2302728	0.2601	1.938	0.2406	0.03645	0.00136

Silica LaBr

	Valley Region keV	Rvref	Rpref	Rvs	Rps	k	μ	ξ	yield	Error
1FWHM	462.78-480	61264	1056423	63976	997481	0.0580	1.8229	0.2624	0.01285	0.00088
2FWHM	445.56-480	116712	1056423	119272	997481	0.1105	1.8511	0.2563	0.01917	0.00126
3FWHM	428.34-480	171593	1056423	174629	997481	0.1624	1.8796	0.2504	0.02686	0.00157
4FWHM	411.12-480	227877	1056423	230584	997481	0.2157	1.9086	0.2456	0.03298	0.00184
5FWHM	393.9-480	287277	1056423	291561	997481	0.2719	1.938	0.2406	0.04367	0.00210

Peak-to-valley method -- valley range 400-470keV

Teflon NaI(Tl)

Valley Region keV	Rvref	Rpref	Rvs	Rps	k	μ	ξ	yield	Error
400-470	919658	3644545	923462	3486797	0.2523	1.7839	0.2395	0.02927	0.00118

Silica NaI(Tl)

Valley Region keV	Rvref	Rpref	Rvs	Rps	k	μ	ξ	yield	Error
400-470	404605	1787045	417554	1715087	0.2264	1.7839	0.2395	0.03991	0.00155

Teflon HPGe

Valley Region keV	Rvref	Rpref	Rvs	Rps	k	μ	ξ	yield	Error
400-470	1296533	7258068	1306508	6962020	0.1786	1.8614	0.2395	0.02024	0.00065

Silica HPGe

Valley Region keV	Rvref	Rpref	Rvs	Rps	k	μ	ξ	yield	Error
400-470	992815	2293918	978388	2200180	0.4328	1.8614	0.2395	0.02664	0.00202

Teflon $LaCl_3$:Ce

Valley Region keV	Rvref	Rpref	Rvs	Rps	k	μ	ξ	yield	Error
400-470	922952	3823218	927423	3702231	0.2414	1.814	0.2395	0.02094	0.00109

Silica $LaCl_3$:Ce

Valley Region keV	Rvref	Rpref	Rvs	Rps	k	μ	ξ	yield	Error
400-470	994088	3878289	1007224	3754701	0.2563	1.814	0.2395	0.02747	0.00113

Teflon $LaBr_3$:Ce

Valley Region keV	Rvref	Rpref	Rvs	Rps	k	μ	ξ	yield	Error
400-470	475097	2339837	499387	2302728	0.2030	1.9467	0.2395	0.02964	0.00116

Silica $LaBr_3$:Ce

Valley Region keV	Rvref	Rpref	Rvs	Rps	k	μ	ξ	yield	Error
400-470	236671	1056423	240167	997481	0.2240	1.9467	0.2395	0.03591	0.00185

Appendix D: Publications

- **M. Alkhorayef**, E. Abuelhia, M.P.W. Chin, N.M. Spyrou. Determination of the relative oxygenation of samples by ortho-positronium 3γ decay for future application in oncology, Journal of Radioanalytical and Nuclear Chemistry, 281: (2) 171–174 (2009)
- **M. Alkhorayef**, E. Abuelhia, K. Alzimami, M. Marouli, M.P.W. Chin and N.M. Spyrou. Experimental comparison of the relative yield of 3γ/2γ positron annihilation using semiconductor and scintillation detectors, Journal of Radioanalytical and Nuclear Chemistry, 280: (2) 315–318 (2009).
- **M. Alkhorayef** and N.M. Spyrou. Measurement of 3γ/2γ positron annihilation ratios in selection of scintillation and semiconductor detectors, Nuclear Analytical Methods for the 21st Century, Trans. American Nuclear Society, 101: 111 (2009).
- **M. Alkhorayef** and N.M. Spyrou. Can we extract useful information from three-gamma decay in positron emission tomography for tumour hypoxia imaging?, Proceedings of SiC09 - The 3rd Saudi International Conference, Guildford, UK, 1:40 (2009).
- **M. Alkhorayef**, A. Tziakouris, K. Alzimami, M.P.W. Chin and N.M. Spyrou. Measurement of the relative yield of 3γ to 2γ positron annihilation using peak-to-peak and peak-to-valley methods. Abstracts' proceeding of MARC VIII - The 8th International Conference on Methods and Applications of Radioanalytical Chemistry, Kailua-Kona, Hawai'i, USA, 389:140 (2009)
- M.P.W. Chin, D. Seweryniak, **M. Alkhorayef** and N.M. Spyrou. Variation of 3γ-to-2γ ratio from F-18 in haematological components measured using the GAMMASPHERE, Nuclear Instruments and Methods in Physics Research A 604: (2) 331–334 (2009).
- K. Alzimami, S. Sassi, **M. Alkhorayef**, A.J. Britten, N.M. Spyrou, Optimisation of computed radiography systems for chest imaging, Nuclear Instruments and Methods in Physics Research Section A 600: (2) 513-518 (2009).
- N.M. Spyrou, K. Alsafi, **M. Alkhorayef** , Comparison of Radiation Exposure to Staff in Mobile and Static PET/CT Units, Trans. American Nuclear Society, 100: 31(2009).
- **M. Alkhorayef** and N.M. Spyrou. Factors that affect dissolved oxygen in biological samples in the imaging of tumour hypoxia using three gamma positron emission tomography. Proceedings of SiiC08 - The 2nd Saudi International Innovation Conference, Leeds, UK, 1:46 (2008).
- E. Abuelhia, K. Alzimami, **M. Alkhorayef**, Z. Podolyák and N.M. Spyrou. Measurement of coincidence timing resolution of scintillation detectors compared to semiconductor detectors to image three-photon positron annihilation, Journal of Radioanalytical and Nuclear Chemistry, 278: (3) 767-771(2008).
- K. Alzimami, S. Sassi, **M. Alkhorayef**, N.M. Spyrou, Optimisation of FBP with using Butterworth, Metz and Weiner reconstruction filtering in ^{99m}Tc SPECT images, Proceedings of SiiC08 – The 2nd Saudi International Innovation Conference, Leeds UK, 1:36 (2008).
- **M. Alkhorayef** and N.M. Spyrou. Study of oxygen measurement in relation to three photon positron annihilation yield in biological samples. Proceedings of SiC07 - The 1st Saudi Innovation Conference, Newcastle, UK, 1: 33-39 (2007).
- G. Prekas, G. Jones, K. Kacperski, **M. Alkhorayef** and N.M. Spyrou. Determination of 3γ photon yields in biological samples. Analysis of results obtained from experiment using the 'Gammsphere' at Argonne National Laboratory (Chicago, USA)

Proceedings of MTAA-12- The 12th International Conference Modern Trends in Activation Analysis, Tokyo, Japan, 75: 114 (2007)

Prizes

- The first prize for the best student paper at the 9th International Conference on Nuclear Analytical Methods in the Life Sciences (NAMLS-9), 7th -12th September 2008, Lisbon, Portugal.
- Distinguished achievement prize at the 3rd Saudi International Conference (SiC09), 5th- 6th June 2009, University of Surrey, Guildford, UK.

Co-supervised MSc & BSc Medical Physics & Medical Imaging Dissertations

- Marshad Alzeer, Investigation of oxygen measurement of biological samples in relation to three-gamma yield. MSc. Medical Physics dissertation, University of Surrey, 2006. Co-supervised with Prof NM Spyrou.
- Georgios Prekas, Determination of 3-gamma photon yields in biological samples: analysis of results obtained from experiment using the Gammasphere at Argonne National Physical Laboratory (Chicago, USA). MSc. Medical Physics dissertation, University of Surrey, 2006. Co-supervised with Prof NM Spyrou.
- Demetrius Kaolis, Optimisation of the spatial resolution of a 3γPET system configuration. MSc.Medical Physics dissertation, University of Surrey, 2006. Co-supervised with Dr. E. Abuelhia and Prof NM Spyrou.
- Faten Aldhafeeri, Investigation of oxygen measurement in relation to three-gamma yield in biological samples. MSc. Medical Physics dissertation, University of Surrey, 2007. Co-supervised with Prof NM Spyrou.
- Andreas Tziakouris, The effect of collimation on precise measurement of the three gamma annihilation rates of positrons –a novel PET imaging method. BSc.Medical Physics dissertation, University of Surrey, 2007. Co-supervised with Dr. E. Abuelhia and Prof NM Spyrou.
- Andreas Tziakouris, Measuring the relative yield of 3γ/2γ annihilations using semiconductor and scintillation detectors. MSc. Medical Physics dissertation, University of Surrey, 2008. Co-supervised with Prof NM Spyrou.
- Efstratios Kamperidis, Measuring the relative yield of 3γ/2γ annihilations using CdZnTe, HPGe and NaI(Tl) detectors. MSc. Medical Physics dissertation, University of Surrey, 2009. Co-supervised with Prof NM Spyrou.
- Hanan Aldousari, Study of the factors that affect dissolved oxygen in biological samples in relation to three photon positron annihilation. MSc. Medical Imaging dissertation, University of Surrey, 2009. Co-supervised with Prof NM Spyrou.
- Ahmar Yaseen, Assessing of ^{64}Cu-ATSM Uptake in hypoxic tumour cell-lines of Glioma and Chinese hamster V79 using two different detectors - A preliminary study. MSc. Medical Physics dissertation, University of Surrey, 2009. Co-supervised with Dr. E Dalah and Prof NM Spyrou.